Report on the Fragility and Consequence Models for the Groningen Field (Version 7)

Helen Crowley and Rui Pinho

Date March 2020

Editors Jan van Elk & Dirk Doornhof

General Introduction

Crucially important for the assessment of seismic risk in the Groningen area are the fragility curves describing the response of the building stock and the consequence model describing the impact on life safety risk. The fragility curves describe the probability of exceedance of a given damage state for a building typology (structural system) in the Groningen field area depending on the ground motion.

These fragility curves have been developed based on an extensive experimental and modelling program. The experimental program incorporates in-situ and laboratory tests (to determine the properties of building materials, the behavior of wall elements and wall units) and tests on full-scale buildings. These tests were conducted at the facilities of TU Delft, TU Eindhoven, Eucentre (Pavia, Italy) and LNEC (Lisbon, Portugal). In these experiments much attention was given to masonry, but also pre-fab elements and pre-fab and cast-in-place concrete structures were tested.

The results of these experiments were used to model the seismic response of different structural systems (typologies) encountered in the Groningen building stock and further calibrate these models. Modelling was carried out by teams in ARUP, TU Delft, Mosayk and Eucentre.

Although much attention was given to unreinforced masonry buildings, cast-in-place concrete and pre-fab buildings have also been tested and modeled. Also, timber and steel frame buildings have been studied and modelled. The hazard and risk assessment has been updated regularly (Ref. 1 to 8). For the hazard and risk assessments of November 2015 (Ref. 1) and for Winningsplan 2016 (Ref. 2 to 4) the fragility curves and consequence model of version 2 were used (Ref. 9). For the hazard and risk assessments of November 2017 (Ref. 5) the hazard and risk assessment for production profile Basispad Kabinet of 2018 (Ref. 6) the fragility curves and consequence model version 5 (Ref. 10) were used.

The experimental and modelling program as well as the development of the fragility and consequence model based thereon have been assured by an international panel of experts in February 2018 (Ref. 12). Recommendations of the panel were addressed in the fragility curves and consequence model version 6, (Ref. 11). These models were used in the hazard and risk assessment for production profile GTS-raming 2019 of March 2019 (Ref. 7). The assurance panel reviewed the implementation of their recommendations in the fragility and consequence model in 2019 (Ref. 13). The table on the next age summarizes the fully probabilistic hazard and risk assessments prepared by NAM and the fragility and consequence models used in these assessments.

The current report contains an update of the fragility models for selected typologies; terraced masonry houses (URM3L and URM4L), three and more storey masonry buildings (URM3M_U and URM3M_B) and farm buildings (URM1_F). For the farm buildings three fragility models have been developed: 1 for houses that are an aggregate with the barn, 2 houses that have a continuous roof with the barn and 3 stand – alone barns. These have been used in the hazard and risk assessment for production profile GTS-raming 2020. Fragility models for the other typologies used in the HRA are described in the v6 report (Ref. 11).

Hazard and Risk Assessment	Ref	Fragility and Consequence Model	Ref
Hazard and Risk Assessment – November 2015	1	Fragility and Consequence Model (version 2)	9
Winningsplan 2016	2 to 4	Fragility and Consequence Model (version 2)	9
Hazard and Risk Assessment – November 2017	5	Fragility and Consequence Model (version 5)	10
Hazard and Risk Assessment – Basispad Kabinet (2018)	6	Fragility and Consequence Model (version 5)	10
Hazard and Risk Assessment – GTS-raming 2019	7	Fragility and Consequence Model (version 6)	11
Hazard and Risk Assessment – GTS-raming 2020	8	Fragility and Consequence Model (version 7)	11 and this report

The current report describes the fragility and consequence model for the hazard and risk assessment for production profile GTS-raming 2020 (Ref. 8).

References

1. Hazard and Risk Assessment for Induced Seismicity in Groningen Interim Update November 2015, Nederlandse Aardolie Maatschappij BV (Jan van Elk and Dirk Doornhof, eds), 1st November 2015.
2. Winningsplan Groningen 2016, Nederlandse Aardolie Maatschappij BV, 1st April 2016.
3. Technical Addendum to the Winningsplan Groningen 2016 - Production, Subsidence, Induced Earthquakes and Seismic Hazard and Risk Assessment in the Groningen Field, PART III - Hazard Assessment, Nederlandse Aardolie Maatschappij BV (Jan van Elk and Dirk Doornhof, eds), 1st April 2016.
4. Technical Addendum to the Winningsplan Groningen 2016 - Production, Subsidence, Induced Earthquakes and Seismic Hazard and Risk Assessment in the Groningen Field, PART IV - Risk Assessment, Nederlandse Aardolie Maatschappij BV (Jan van Elk and Dirk Doornhof, eds), 1st April 2016.
5. Induced Seismicity in Groningen – Assessment of Hazard, Building Damage and Risk, NAM, Jan van Elk and Dork Doornhof, NAM, November 2017.
6. Seismic Risk Assessment for Production Scenario “Basispad Kabinet” for the Groningen field (Addendum to: Induced Seismicity in Groningen Assessment of Hazard, Building Damage and Risk (November 2017), Nederlandse Aardolie Maatschappij BV (Jan van Elk and Dirk Doornhof, July 2018.
7. Hazard and Risk Assessment - GTS raming 2019, NAM, Jan van Elk and Dirk Doornhof, March 2019.
8. Hazard and Risk Assessment - GTS raming 2020, NAM, Jan van Elk and Dirk Doornhof, March 2020.
9. Development of v2 fragility and consequence functions for the Groningen Field, H. Crowley, R. Pinho, B. Polidoro, P. Stafford, October 2015.
10. Report on the v5 Fragility and Consequence Models for the Groningen Field, Helen Crowley and Rui Pinho, October 2017.
11. Report on the v6 Fragility and Consequence Models for the Groningen Field, Helen Crowley and Rui Pinho, March 2019.
12. Assurance Meeting on Exposure, Fragility and Fatality Models for the Groningen Building Stock (Long Version), Letter and Report Assurance Panel, March 2018.
13. Assurance Check on Exposure, Fragility and Fatality Models for the Groningen Building Stock, Assurance Panel Building Fragility, Typology and Exposure, Assurance Panel Building Fragility, Typology and Exposure, Dec 2019.

NAM

Title	**Report on the v7 Fragility and Consequence Models for the Groningen Field**	**Date**	March 2019
		Initiator	NAM
Autor(s)	**Helen Crowley and Rui Pinho**	**Editors**	Jan van Elk and Dirk Doornhof
Organisation	Independent Academics	**Organisation**	NAM
Place in the Study and Data Acquisition Plan	Study Theme: Development of Fragility Curves Comment: Crucially important for the assessment of seismic risk in the Groningen area are the fragility curves describing the response of the building stock and the consequence model describing the impact on life safety risk. The fragility curves describe the probability of exceedance of a given damage state for a building typology (structural system) in the Groningen field area depending on the ground motion. These fragility curves have been developed based on an extensive experimental and modelling program. The experimental program incorporates in-situ and laboratory tests (to determine the properties of building materials, the behavior of wall elements and wall units) and tests on full-scale buildings. These tests were conducted at the facilities of TU Delft, TU Eindhoven, Eucentre (Pavia, Italy) and LNEC (Lisbon, Portugal). In these experiments much attention was given to masonry, but also pre-fab elements and pre-fab and cast-in-place concrete structures were tested. The results of these experiments were used to model the seismic response of different structural systems (typologies) encountered in the Groningen building stock and further calibrate these models. Modelling was carried out by teams in ARUP, TU Delft, Mosayk and Eucentre. Although much attention was given to unreinforced masonry buildings, cast-in-place concrete and pre-fab buildings have also been tested and modeled. Also, timber and steel frame buildings have been studied and modelled. The hazard and risk assessment has been updated regularly. For the hazard and risk assessments of November 2015 and for Winningsplan 2016 the fragility curves and consequence model of version 2 were used. For the hazard and risk assessments of November 2017 the hazard and risk assessment for production profile Basispad Kabinet of 2018 the fragility curves and consequence model version 5 were used. The experimental and modelling program as well as the development of the fragility and consequence model based thereon have been assured by an international panel of experts in February 2018. Recommendations of the panel were addressed in the fragility curves and consequence model version 6. These models were used in the hazard and risk assessment for production profile GTS-raming 2019 of March 2019. The assurance panel		

	reviewed the implementation of their recommendations in the fragility and consequence model in 2019. The current report describes the fragility and consequence model for the hazard and risk assessment for production profile GTS-raming 2020.
Directliy linked research	(1) Building Material properties (2) Shake table tests (3) Seismic Response of Buildings (URM and non-URM) (4) Risk Assessment
Used data	Full experimental and Modelling program into seismic response URM & non-URM buildings.
Associated organisation	NAM
Assurance	Independent Assurance Panel carried out aa assurance review in2018. This was followed-up by a implementation assessment in 2019.

GRONINGEN FIELD SEISMIC HAZARD AND RISK ASSESSMENT

Report on the v7 Fragility and Consequence Models for the Groningen Field

---

Authors:

Helen CROWLEY and Rui PINHO

March, 2020

Contents

Acknowledgements

The authors would like to express their gratitude to Jan van Elk who has provided the support, guidance and conditions that have allowed this study to be carried out and completed within the necessary timeframe. Particular acknowledgment is due also to Jeroen Uilenreef for his crucial role in the management of the numerical modelling, exposure model development and experimental testing campaign.

The work presented herein has benefitted greatly from discussions and feedback from Julian Bommer, who is responsible for the development of the ground-motion prediction equations for the region. The important interface between ground shaking and building damage has been ensured through this strong collaboration with Julian. Peter Stafford is also acknowledged for his useful feedback and for the scripts he provided for correlating significant duration with AvgSa (for the selection of hazard consistant records). Thanks are also due to Roy Scheefhals for generating hazard and risk results and history checks that have provided useful insights into the performance of the models.

There is a large team working on modelling and testing of components and structures for calibration of the numerical models used herein, with the main contributions coming from collaborators at Arup, Eucentre, and Mosayk. Not all of those involved can be mentioned and acknowledged here, but particular thanks is given to Francesco Graziotti, Stelios Kallioras, Umberto Tomassetti, Luca Grottoli, Filippo Dacarro, Rinke Kluwer, Alex Christodoulou, Damian Grant, Daniele Malomo, Barbara Polidoro, Francesco Cavalieri and Antonio Correia are gratefully acknowledged .

A significant part of the strong-motion database used for the derivation of all fragility functions was provided by Julian Bommer. The Groningen recordings were provided to Julian by Bernard Dost of KNMI. The European database was made available to Julian by Sinan Akkar from Bogazici University, Istanbul. In addition, the authors are also particularly grateful to Pauline Kruiver, who kindly provided access to the soil mechanical characterisation data and response analysis results for the Groningen region.

Finally, the methodology to develop the fragility and consequence models has benefitted greatly from the review comments and report provided by an international review panel, comprising experts in structural engineering, earthquake engineering and risk analysis, namely Jack Baker, Ihsan Engin Bal, Matjaz Dolsek, Paolo Franchin, Ronald Hamburger, Nicolas Luco, Marko Schotanus and Dimitrios Vamvatsikos (see Baker et al., 2018; 2019 for more details).

Chapter 1

Introduction

1.1 Overview

Gas production in the Groningen field in the northern Netherlands is inducing earthquakes, the largest of which to date was the magnitude M_L 3.6 (**M** 3.4) Huizinge event of August 2012. In response to this induced seismicity, NAM has been developing a comprehensive seismic hazard and risk model for the region (van Elk et al., 2019), which comprises the entire gas field plus a 5 km buffer zone onshore.

A key component of the risk assessment involves the definition of fragility functions (which provide the probability of reaching or exceeding a given damage or collapse state, conditional on a level of input ground motion) for each structural system that has been identified within the region, and included within the exposure model. Although many fragility functions have been developed over the years (see e.g. Calvi et al., 2006; D'Ayala et al., 2014; Yepes et al., 2016), the vast majority are not appropriate for use in Groningen, where many of the buildings feature details and charateristics not typically seen in tectonic seismically active areas. A predominantly analytical approach, which also includes elements of expert judgment and empirical and experimental data calibration, is thus being employed for developing new Groningen-specific fragility and consequence functions.

An iterative approach to the development of these new functions has been followed, with functions being updated every 6-12 months (from v0 in October 2014 to v6 in March 2018), to allow the lessons learned from these intermediate development phases to be fed back into the methodology. The v2 fragility and consequence models were used for the risk assessment underlying the 2016 Winningsplan, as documented in Crowley et al. (2015), and were reviewed by an international panel of experts. Developments to the methodology during the v3 and v4 phases have been published in peer-reviewed literature (Crowley et al., 2017). The v5 fragility and consequence models have been used in NAM's v5 risk assessment of November 2017 (Crowley and Pinho, 2017; Crowley et al., 2019a) and were again reviewed by an international review panel in March 2018 (Baker et al., 2018). The v6 models (Crowley et al., 2019b) successfully incorporated the recommendations of the aforementioned review panel (see Baker et al., 2019), and were used in NAM's March 2019 hazard and risk assessment. This report describes the v7 fragility and consequence models which are being used in NAM's Hazard and Risk Assessment (HRA) 2020.

In order to optimise the v7 model development efforts a decision was made to focus on those vulnerability classes that were seen to be contributing most to the risk results, i.e. URM3L, URM4L, URM1_F, URM3M_U and URM3M_B. For the remaining vulnerability classes the models do not

differ from v6 and thus it is recommended that interested readers review first the v6 report (Crowley et al., 2019).

In v7, as described in the present report, the classes URM3L, URM4L, URM1_F, URM3M_U and URM3M_B have thus been updated in the following ways:

- Hazard-consistent duration has been considered when selecting the records for the nonlinear dynamic analysis of both the MDOF and SDOF models. (It was found that this new set of records has a minimal impact on the fragility functions and thus there was not a need for the other building classes to be updated using this new set of records).
- Negative slopes have been added to the backbones of URM3L and URM4L to better match the MDOF analyses for these typologies (see Arup 2019f).
- The URM1_F class, which comprised both the house and barn in v6, has been separated into three fragility/vulnerability models: i) houses that are part of an aggregate together with the barn (URM1F_HA), ii) houses that have a continuous roof with the barn (URM1F_HC), and iii) the barn alone (URM1F_B).
- Additional MDOF LS-DYNA index buildings for URM3L, URM4L and URM1_F have been produced (see Arup, 2019c).
- The material model used in the LS-DYNA models of URM3M_U and URM3M_B has been updated (see Arup, 2019d) and hence new backbone SDOF models have been produced and calibrated for these classes.

Although this report only covers the above vulnerability classes that have been updated/added since v6, the complete set of fragility and fatality models used in the HRA2020 is nonetheless included in Chapter 6.

1.2 Outline of Methodology

The initial focus of NAM's risk assessment has been on the safety of the population exposed to induced earthquakes. Methodologies for estimating fatalities from earthquakes range from those that directly attempt to predict the number of casualties from the magnitude of the earthquake (e.g. Samardjieva and Badal, 2002) or a level of ground shaking such as macroseismic intensity (e.g. Jaiswal et al., 2009), to those that propose ratios between the mean number of casualties (or injured persons) and the number of people exposed to a building with a given level of damage, so-called mean fatality ratios (e.g. So and Pomonis, 2012). An approach that estimates the fatality risk from the probability of collapse of the buildings has been selected for the Groningen gas field risk model, given that it has been observed in past earthquakes that the number of earthquake shaking casualties is driven by the number of buildings that fully or partially collapse (e.g. Coburn and Spence 2002). Furthermore, by estimating in this manner the fatality risk for different typologies of buildings, additional knowledge on the structural defects of the buildings is obtained, which can then be used to guide the strengthening efforts to be applied to the buildings in the region.

As mentioned previously, the probability of collapse of the buildings is assessed through an analytical, rather than an empirical, approach due to the particular details and characteristics of the buildings in the Groningen region. Further, there are drawbacks to using empirical data to derive fragility and fatality models, as during post-earthquake reconnaissance missions buildings are often

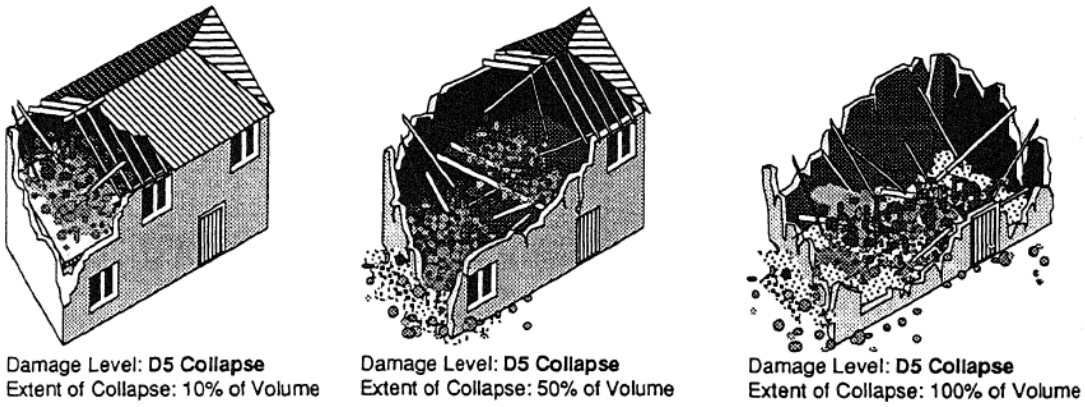

Figure 1.1 Varying volumetric reduction of a building defined as having "total destruction" or D5 damage level (from Coburn et al., 1992)

defined as having the same 'damage state' despite having very different volumes of collapsed debris, which would imply very different fatality risks (see Figure 1.1). This limitation can be overcome by using analytical structural models that allow different collapse mechanisms and associated collapsed debris to be estimated.

Hence, the methodology presented herein attempts to use a predominantly analytical approach, that is augmented where possible with empirical and experimental data, to estimate both fragility and consequence models for damage estimation and local personal risk. The main causal pathways for loss of life that are currently being considered include the following: being hit by the collapse of a chimney outside of the building, or being hit by the debris caused by different structural collapse states of the building (both inside and outside) brought about by the global dynamic response of the structure to an input acceleration.

In order to model the dynamic response of a large population of buildings in a given region, it is common practice to first classify the buildings into classes or types, which have similar structural and architectural characteristics (see e.g. FEMA, 2004). Once these classes have been identified, at least one real representative building from the region is found for each vulnerability class (so-called index building) and the structural drawings are used to develop a multi-degree-of-freedom (MDOF) numerical model of the structural system including the predominant non-structural elements (such as partition and external façade walls). However, the computational effort associated with running nonlinear dynamic analyses of many such numerical models (35 different vulnerability classes have been defined for the region of Groningen), each subjected to tens of records, was too high to allow fragility functions to be directly developed from these analyses (though, as presented in Chapter 7, this has been undertaken for some classes for validation purposes). Therefore, a simplified single-degree-of-freedom (SDOF) equivalent system approach has been used instead to analytically represent each index building (Figure 1.2).

Figure 1.3 shows the equivalent SDOF model that is used to represent each index building. This model requires the definition of the effective mass, a hysteretic force displacement model to describe the dynamic response of the system, and an equivalent macro-element to represent the soil-structure interaction (SSI). Chapters 2 and 3 describe the calibration of this SDOF model for the new or updated index buildings considered herein.

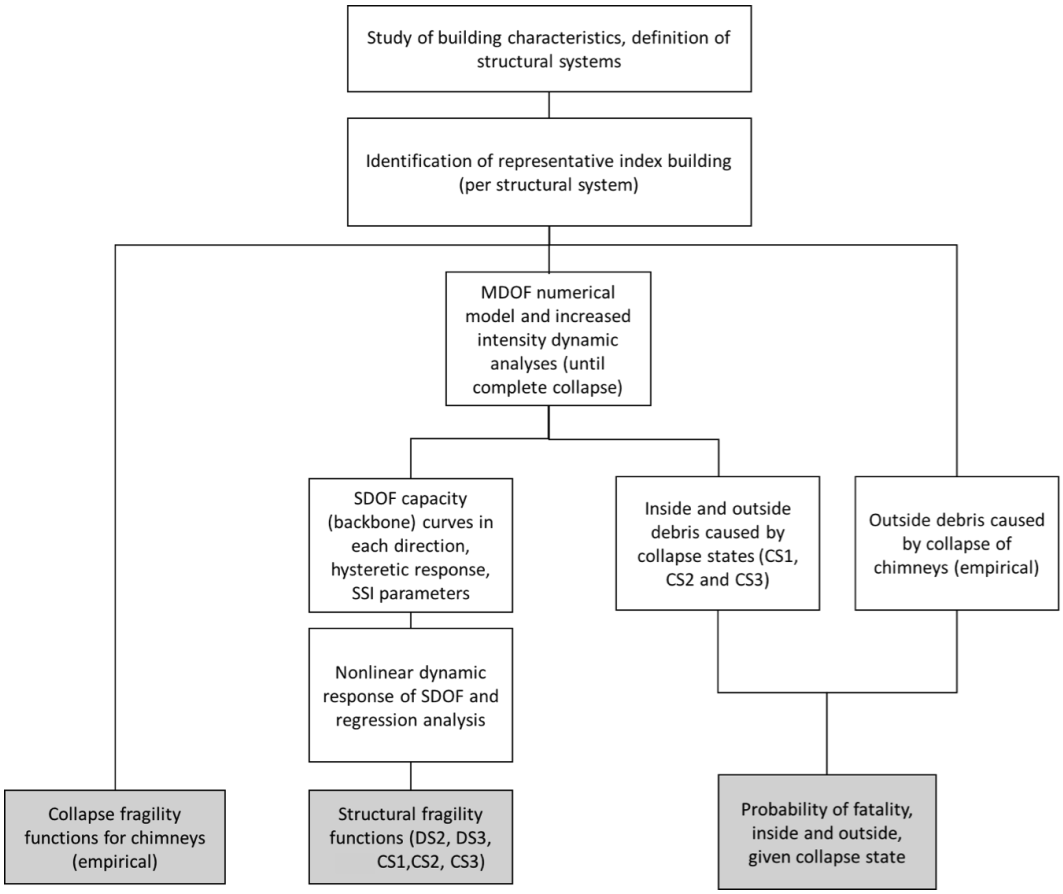

Figure 1.2 Flowchart of the main steps of the methodology used to develop the fragility and consequence models. The grey boxes illustrate the three main models that are input into the risk engine.

For the global response, nonlinear dynamic analysis of the MDOF numerical models using records with increasing intensity has been employed to produce the SDOF backbone capacity curves and to identify the consequences of different collapse mechanisms. A large suite of hazard-consistent records was then utilised in the nonlinear dynamic analyses of these SDOF systems to model the record-to-record variability, and regression analysis is used to relate the average spectral acceleration (AvgSa) of each record to the nonlinear response in order to produce the fragility functions. Consequence models based on the extent of partial and complete collapse debris observed in the MDOF numerical analyses are then developed. A study of the collapse of chimneys of URM buildings from a number of earthquakes has been undertaken by Taig and Pickup (2016), in order to develop empirical fragility functions and consequence models that have been used in the v6 and v7 models. As the latter have not changed they are not presented in this report and readers are referred to (Crowley et al., 2019b) for more details.

1.3 Risk Metrics

In early 2015, an advisory committee (Commissie Meijdam) was established to advise on risk policy related to Groningen earthquakes, including the selection of risk metrics. Two individual risk metrics were introduced: Individual Risk (IR), defined as the annual risk that an individual is exposed to due to the potential collapse of the various structures in or near which this individual is

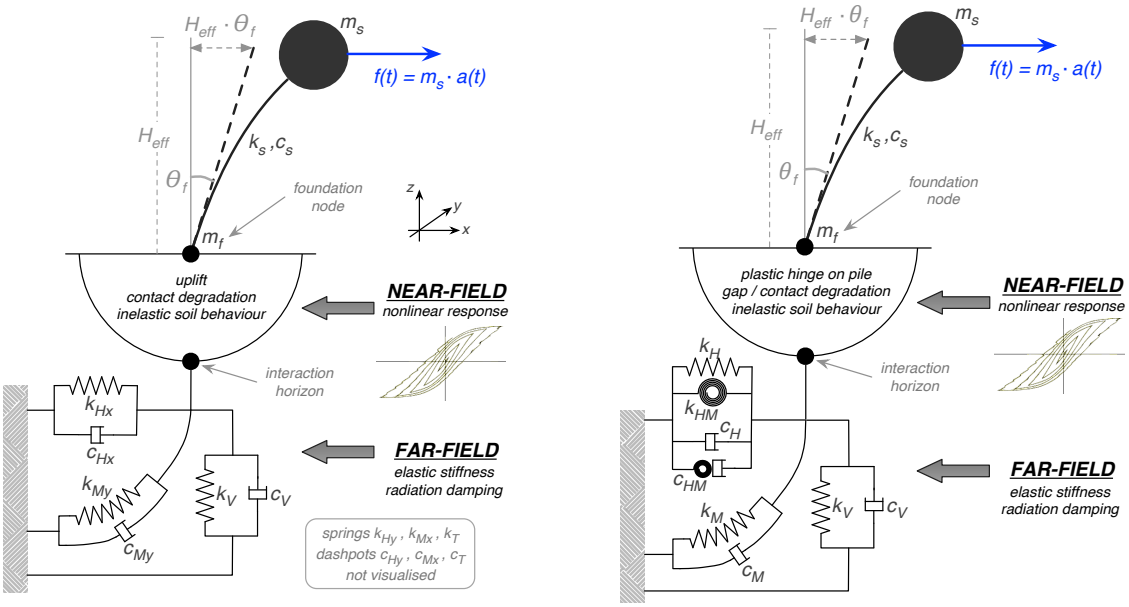

(a) Shallow foundation

(b) Piles foundation

Figure 1.3 SDOF model used to develop structural fragility functions (Cavalieri et al., 2020a; 2020b)

present, and Object-bound Individual Risk (OIR), defined as the probability that an individual dies in a year due to collapse of falling objects (as a result of an earthquake) of a building in which or in the direct vicinity of which this person is present. IR has not yet been calculated in the risk engine as in principle it would require knowledge of the buildings that each individual in the Groningen region visits over a 24 hour period. Instead, the calculations have focused to date on the local personal risk (LPR), defined as the annual probability of fatality for a hypothetical person who is continuously present without protection inside or outside (and nearby) a building. The v6 hazard and risk assessment calculated OIR for the first time by multiplying the LPR by residence times that have been estimated for each building in the exposure database as a function of their use.

In 2016 the Dutch Ministry of Economic Affairs (MEA) also requested the forecast of group risk for damage (so-called Maatschappelijk Risico (Schade)). To meet this request, F-N curves that present the annual frequency of exceedance against number of damaged buildings have been calculated using the fragility functions for damage states DS2 and DS3. It is noted that this is not standard practice, and it is more common to calculate loss exceedance curves for groups of buildings that report the annual frequency of exceedance of loss (e.g. due to the repair of damage or due to loss of life). Indeed, group risk for fatalities can also be calculated using the input models presented herein, by combining the inside and outside LPR by the average number of people present in and around the buildings during the day and night, as provided in the exposure model.

The estimation of group damage, group risk, LPR and OIR is undertaken within an engine (Figure 1.4) that uses Monte Carlo simulation to generate a catalogue of events from the seismicity model, and then correlated estimates of ground motion parameters at the location of the buildings in the exposure model are produced using the ground-motion prediction equation (GMPE) for the field (Bommer et al., 2016; Bommer et al., 2017). The probability of exceeding a given damage or collapse state, conditional on the aforementioned ground motion parameters, is then estimated for a

building type at a given location using the fragility functions described herein. The probability of loss of life both inside and outside the building, given that collapse occurs, is calculated from the consequence model for the building type (as also presented in this report), and the results are combined considering the relative probability of being inside or outside the building type (for LPR), or the relative number of people inside or outside the building (for group risk). By repeating these calculations for a large number of simulated events, the annual probability of fatality for the hypothetical person (i.e. the local personal risk) or F-N curves can be calculated.

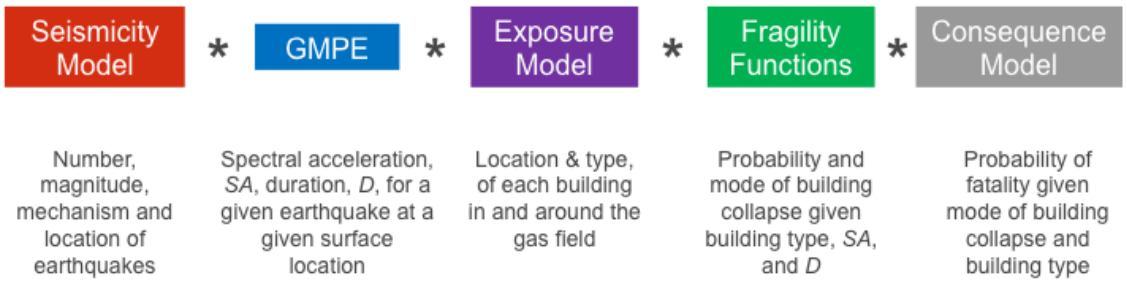

Figure 1.4 Components of the risk engine for the calculation of Local Personal Risk. For the calculation of group damage, fragility functions for damage states are required, and there is no consequence model. For group risk, the exposure model includes the number of people in and around buildings.

Chapter 2

HRA2020 Building Vulnerability Classes

2.1 HRA2020 Exposure Model

2.1.1 Summary of the v7 exposure database

The v7 exposure database (EDB v7) (Arup, 2019a) contains the location, structural characteristics and exposed population (inside and outside) of over 260,000 buildings inside and within 5km of the Groningen gas field (Figure 2.1). Each building is described using structural systems that combine 9 different attributes of the building, with the first related to the geometric layout (S-shed, U-unit, B-block, W-barn/warehouse, T-tower) and the following 8 attributes defined according to the GEM Building Taxonomy (Brzev et al., 2013): material and type of lateral load-resisting system in each direction of the building, presence of external walls, floor system, number of floors and irregularities. The structural system of each building in the exposure database has been assigned through various sources:

- Data-mining algorithms on the AHN (Actueel Hoogtebestand Nederland) height map and BAG (Basisregistratie Adressen en Gebouwen) building footprint outlines, to assign the most probable geometric layout.
- Inspection data (e.g. Rapid Visual Screening, structural drawings, Extended Visual Screening, Streetview image inspection): these data provided some or all of the attributes of the structural system.
- Data-driven and expert judgement-based inference rules that relate characteristics of the building (e.g. geometric layout and age of construction) to the structural system.

The HRA2020 risk assessment has been undertaken for all of the populated (or potentially populated) buildings, defined as those in the EDB v7 with $\geq$0 inside population during the day, unless their functional use is unknown or 'other', leading to a total of approximately 158k buildings, with around 431k daytime occupants and 412k night-time occupants. These buildings were probabilistically assigned to 497 different structural systems.

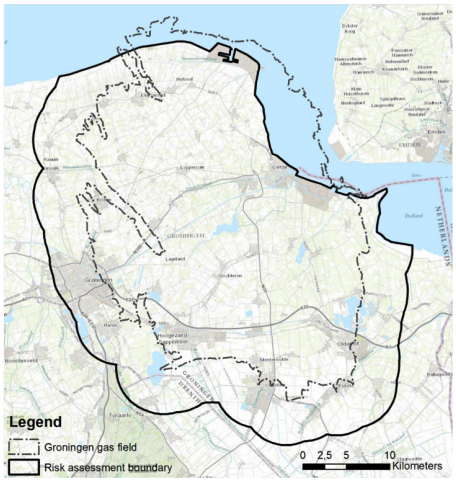

Figure 2.1 Extent of the v7 exposure model

2.1.2 Mapping structural systems to vulnerability classes

A vulnerability class represents a group of structures that are expected to have a similar performance under seismic action. Table 2.1 lists all of the vulnerability classes considered in the HRA2020 analyses, together with a brief description. A reference is made in this table to the vulnerability classes that have not changed since v6 (see Crowley et al., 2019b) and those that have been updated for v7, as described herein. The structural systems in the EDB v7 have initially been mapped to each of the 35 vulnerability classes based on the attributes in the taxonomy string, together with expert judgment.

Table 2.1 Vulnerability Classes considered in the HRA2020 analyses

Vulnerability Class	No. buildings	Description	Version
RC1L	3	Reinforced concrete moment frame, low-rise	v6
RC1M	0	Reinforced concrete moment frame, mid-rise	v6
RC1H	6	Reinforced concrete moment frame, high-rise	v6
RC2	216	Reinforced concrete (cast-in-place) post and beam	v6
PC2	124	Reinforced concrete (pre-cast) post and beam	v6
RC3L	7698	Reinforced concrete (cast-in-place) wall-slab-wall, low-rise	v6
RC3M	1002	Reinforced concrete (cast-in-place) wall-slab-wall, mid-rise	v6
RC3H	126	Reinforced concrete (cast-in-place) wall-slab-wall, high-rise	v6
PC3L	5215	Reinforced concrete (pre-cast) wall-slab-wall, low-rise	v6
PC3M	681	Reinforced concrete (pre-cast) wall-slab-wall, mid-rise	v6
PC3H	64	Reinforced concrete (pre-cast) wall-slab-wall, high-rise	v6
W2	495	Timber (glulam) portal frame	v6
W3	4039	Timber frame (with panels) detached house	v6
S1L	78	Steel portal frame, low-rise	v6
S1M	20	Steel portal frame, mid-rise	v6
S1H	8	Steel portal frame, high-rise	v6
S2L	983	Steel braced frame, low-rise	v6
S2M	60	Steel braced frame, mid-rise	v6
S2H	17	Steel braced frame, high-rise	v6
S3	1340	Lightly braced steel frame	v6
URM1F_B	4571	Timber barn of the barn/farmhouse building	v7
URM1F_HC	2192	URM house of a barn/farmhouse building with continuous roof with the barn	v7
URM1F_HA	1809	URM house of an aggregate barn/farmhouse building	v7
URM2L	7085	Unreinforced masonry aggregate unit with solid walls and timber floor	v6
URM3L	40775	Unreinforced masonry 1-2 storey terraced unit with cavity walls and concrete floor	v7
URM3M_U	9650	Unreinforced masonry 3+ storey aggregate unit with cavity walls and concrete floor	v7
URM3M_D	1075	Unreinforced masonry 3+ storey terraced unit with cavity walls and concrete floor and ground floor garage	v6
URM3M_B	3098	Unreinforced masonry 3+ storey block unit with cavity walls and concrete floor	v7
URM4L	8263	Unreinforced masonry 1-2 storey terraced unit with cavity walls and concrete floor	v7
URM5L	6355	Unreinforced masonry terraced unit with cavity walls and timber floor	v6
URM6L	15254	Unreinforced masonry detached unit with solid walls and timber floor	v6
URM7L	20913	Unreinforced masonry detached unit with cavity walls and concrete floor	v6
URM8L	11999	Unreinforced masonry detached unit with cavity walls and timber floor	v6
URM9L	2427	Unreinforced masonry aggregate unit with cavity walls and concrete floor and strengthened ground floor	v6
URM10	313	Small buildings with unknown lateral system	v6

This initial mapping was tested using a so-called 'distance-to-index' analysis (Arup, 2020), and this led to a refinement of the mapping table. The distance-to-index analysis compares the geometrical properties and age of the buildings of a given structural system in the exposure model against those parameters of the vulnerability classes in order to identify which class would best represent the structural system. Given that each vulnerability class is represented by one or more index buildings (as described in the next section), the parameters of the index buildings are used in this analysis. Appendix B presents the final mapping table that has been used in the HRA2020 risk assessment.

2.2 Index Buildings

A study of the characteristics of the buildings in the Groningen region in terms of age and geometry (e.g. height, volume, façade area, footprint area, shape in plan) has allowed a representative real building (so-called index building) to be identified for a number of the vulnerability classes. For these buildings, structural drawings have then been retrieved and used to develop numerical models with average material properties based on the data collected during an in-situ testing campaign (Eucentre et al., 2015). For some of the other less common building types, the index building is assumed to correspond to the model building types in HAZUS (FEMA, 2004), and numerical models have not been developed; instead, the capacity curves (presented in Chapter 4) have been directly obtained from HAZUS.

Table 2.2 presents the index buildings used for the v6/v7 fragility and consequence models, together with the GEM taxonomy string (see Appendix A for an explanation of each attribute). Each index building that has been modelled is presented in Figure 2.2. Further details on these models and the modelling assumptions are provided in Arup (2017; 2019b; 2019c) and Mosayk (2017d). It is noted that in some cases it has not yet been possible to model real buildings, and so generic structures with typical characteristics of the structural system have been modelled; these are identified with an asterix in Table 2.2.

One vulnerability class (URM6L) has been based on the LNEC-BUILD3 shake-table test (Kallioras et al., 2018) and so the backbone curve has been taken directly from the experimental test results. When an index building has '+ HAZUS' this means that the capacity curve of the index building has been adapted to account for an increase in number of storeys by applying the ratios between the stiffness, strength and ultimate displacement capacity of low, mid and high rise capacity curves for similar building types in HAZUS (FEMA, 2004). In some cases a vulnerability class is a combination of more than one index building, and the results of each index building are combined according to the percentages shown in the table (see Arup, 2019a), and as further described in Chapter 6. The principal characteristics of all the modelled index buildings are provided in Table 2.3.

Table 2.2 Structural systems and vulnerability classes of the index building models

Index Building Name	GEM Taxonomy String	Vulnerability Class
HAZUS C1L	B/CR+CIP/LFM/CR+CIP/LFM/EW/FC/HBET:2;1/IR99	RC1L
HAZUS C1M	B/CR+CIP/LFM/CR+CIP/LFM/EW/FC/HBET:20;3/IR99	RC1M
HAZUS C1H	T/CR+CIP/LFM/CR+CIP/LFM/EW/FC/HBET:20;1/IR99	RC1H
CIP RC post and beam*	W/CR+CIP/LPB/CR+CIP/LPB/EWN/FN/HBET:20;1/IR99	RC2
Precast RC post and beam*	W/CR+PC/LPB/CR+PC/LPB/EWN/FN/HBET:20;1/IR99	PC2
CIP RC wall-slab-wall*	U/CR+CIP/LWAL/CR+CIP/LN/EW/FC/HBET:2;1/IR99	RC3L
CIP RC wall-slab-wall + HAZUS	U/CR+CIP/LWAL/CR+CIP/LN/EW/FC/HBET:20;3/IR99	RC3M
CIP RC wall-slab-wall + HAZUS	T/CR+CIP/LWAL/CR+CIP/LN/EW/FC/HBET:20;1/IR99	RC3H
Welhaak	U/CR+PC/LWAL/CR+PC/LN/EW/FC/HBET:2;1/IR99	PC3L (50%)
Adamistraat	U/CR+PC/LWAL/CR+PC/LN/EW/FC/HBET:2;1/IR99	PC3L (50%)
Welhaak + HAZUS	U/CR+PC/LWAL/CR+PC/LN/EWN/FC/HBET:20;3/IR99	PC3M (50%)
Adamistraat + HAZUS	U/CR+PC/LWAL/CR+PC/LN/EWN/FC/BET:20;3/IR99	PC3M (50%)
Welhaak + HAZUS	T/CR+PC/LWAL/CR+PC/LN/EWN/FC/BET:20;1/IR99	PC3H (50%)
Adamistraat + HAZUS	T/CR+PC/LWAL/CR+PC/LN/EWN/FC/BET:20;1/IR99	PC3H (50%)
HAZUS W2	W/W/LPB/S/LFBR/EW/FN/HBET:20;1/IR99	W2
Kwelder 8	U/W/LWAL/W/LWAL/EW/FW/HBET:2;1/IR99	W3
Steenweg 19	B/S/LFM/S/LFM/EW/FC/HBET:2;1/IR99	S1L
Steenweg 19 + HAZUS	B/S/LFM/S/LFM/EW/FC/HBET:20;3/IR99	S1M
Steenweg 19 + HAZUS	T/S/LFM/S/LFM/EW/FC/HBET:20;1/IR99	S1H
HAZUS S2L	B/S/LFBR/S/LFBR/EW/FC/HBET:2;1/IR99	S2L
HAZUS S2M	B/S/LFBR/S/LFBR/EW/FC/HBET:20;3/IR99	S2M
HAZUS S2H	T/S/LFBR/S/LFBR/EW/FC/HBET:20;1/IR99	S2H
Beneluxweg 15	W/S/LPB/S/LFBR/EW/FN/HBET:20;1/IR99	S3
De Haver	WC/MUR/LH/MUR/LH/EWN/FW/HBET:20;1/IR99	URM1F_B (25%) and URM1F_HC (50%)
Molenweg 25	WC/MUR/LH/MUR/LH/EWN/FW/HBET:20;1/IR99	URM1F_B (34%) and URM1F_HC (50%)
Molenweg 29	WA/MUR/LH/MUR/LH/EW/FW/HBET:20;1/IR99	URM1F_B (23%) and URM1F_HA (50%)
Eestumerweg 51	WA/MUR/LH/MUR/LH/EWN/FW/HBET:20;1/IR99	URM1F_B (18%) and URM1F_HA (50%)
Solwerderstraat 55	U/MUR/LWAL/MUR/LN/EWN/FW/HBET:2;1/IR99	URM2L
Julianalaan 52	U/MUR/LWAL/MUR/LN/EW/FC/HBET:2;1/IR99	URM3L (25%)
E45 Schildwolde	U/MUR/LWAL/MUR/LN/EW/FC/HBET:2;1/IR99	URM3L (25%)
Wilgenbros	U/MUR/LWAL/MUR/LN/EW/FC/HBET:2;1/IR99	URM3L (25%)
Oostergoweg	U/MUR/LWAL/MUR/LN/EW/FC/HBET:2;1/IR99	URM3L (25%)
Koeriersterweg	U/MUR/LWAL/MUR/LN/EW/FC/HBET:20;3/IR99	URM3M_U
Drive-in	U/MUR/LWAL/MUR/LN/EW/FC/HBET:20;3/IRVP+DIB	URM3M_D
Schuitenzandflat 2-56	B/MUR/LWAL/MUR/LN/EW/FC/HBET:20;3/IR99	URM3M_B
Zijlvest 25	U/MUR/LWAL/MUR/LN/EW/FC/HBET:2;1/IRVP+OPL	URM4L (50%)
E45 Delfzijl	U/MUR/LWAL/MUR/LN/EW/FC/HBET:2;1/IRVP+OPL	URM4L (50%)
Patrimoniumstraat	U/MUR/LWAL/MUR/LN/EW/FW/HBET:2;1/IR99	URM5L
LNEC-BUILD3**	U/MUR/LWAL/MUR/LWAL/EWN/FW/HBET:2;1/IR99	URM6L and URM10
Kwelder 1	U/MUR/LWAL/MUR/LWAL/EW/FC/HBET:2;1/IR99	URM7L
Badweg 12	U/MUR/LWAL/MUR/LWAL/EW/FW/HBET:2;1/IR99	URM8L
Dijkstraat (building A)	U/MUR/LH/MUR/LH/EWN/FW/HBET:2;1/IR99	URM9L

* Generic model
** Shake table test

Table 2.3 Characteristics of index building models

Index Building Name	Vulnerability Class	Year of Construction	Geometric Layout	Gutter Height (m)	Footprint area (m^2)
Cast-in-place RC post and beam	RC2	N/A	W	6.5	1880
Precast RC post and beam	PC2	N/A	W	6.5	1880
CIP RC wall-slab-wall	RC3L	N/A	U	5.56	44 per unit
Welhaak	PC3L	1979	U	5.4	66 per unit
Adamistraat	PC3L	1979	U	2.85	90 per unit
De Haver barn	W1	1900's	W	3.7	1530
Kwelder 8	W3	1996	U	2.75	76
Steenweg 19	S1L	2005	W	6.5	432
Beneluxweg 15	S3	2001	W	3.8	300
De Haver barn	URM1F_B	1900's	WC	3.7	1530
De Haver house	URM1F_HC			2.9	194
Molenweg 25 barn	URM1F_B	1877	WC	2.49	140
Molenweg 25 house	URM1F_HC			3.16	243
Molenweg 29 barn	URM1F_B	1958	WA	2.85	443
Molenweg 29 house	URM1F_HA			2.65	95
Eestumerweg 51 barn	URM1F_B	1960	WA	2.1	220
Eestumerweg 51 house	URM1F_HA			2.75	69
Solwerderstraat 55	URM2L	<1945	U	6.1	113
Julianalaan 52	URM3L	1950's	U	5.4	45 per unit
E45 Schildwolde	URM3L	1971	U	6.17	59 per unit
Wilgenbros	URM3L	1963	U	5.35	47 per unit
Oostergoweg	URM3L	1961	U	5.25	59 per unit
Koeriersterweg	URM3M_U	1941	U	8.59	50 per unit
Drive in	URM3M_D	1972	U	8.1	47 per unit
Schuitenzandflat 2-56	URM3M_B	1964	B	13.8	720
Zijlvest 25	URM4L	1976	U	5.5	53 per unit
E45 Delfzijl	URM4L	1966	U	5.35	61 per unit
Patrimoniumstraat	URM5L	1940's	U	2.85	39 per unit
Kwelder 1	URM7L	1996	U	2.75	98
Badweg 12	URM8L	1940's	U	2.8	67
Dijkstraat (building A)	URM9L	<1945	U	7.5	170

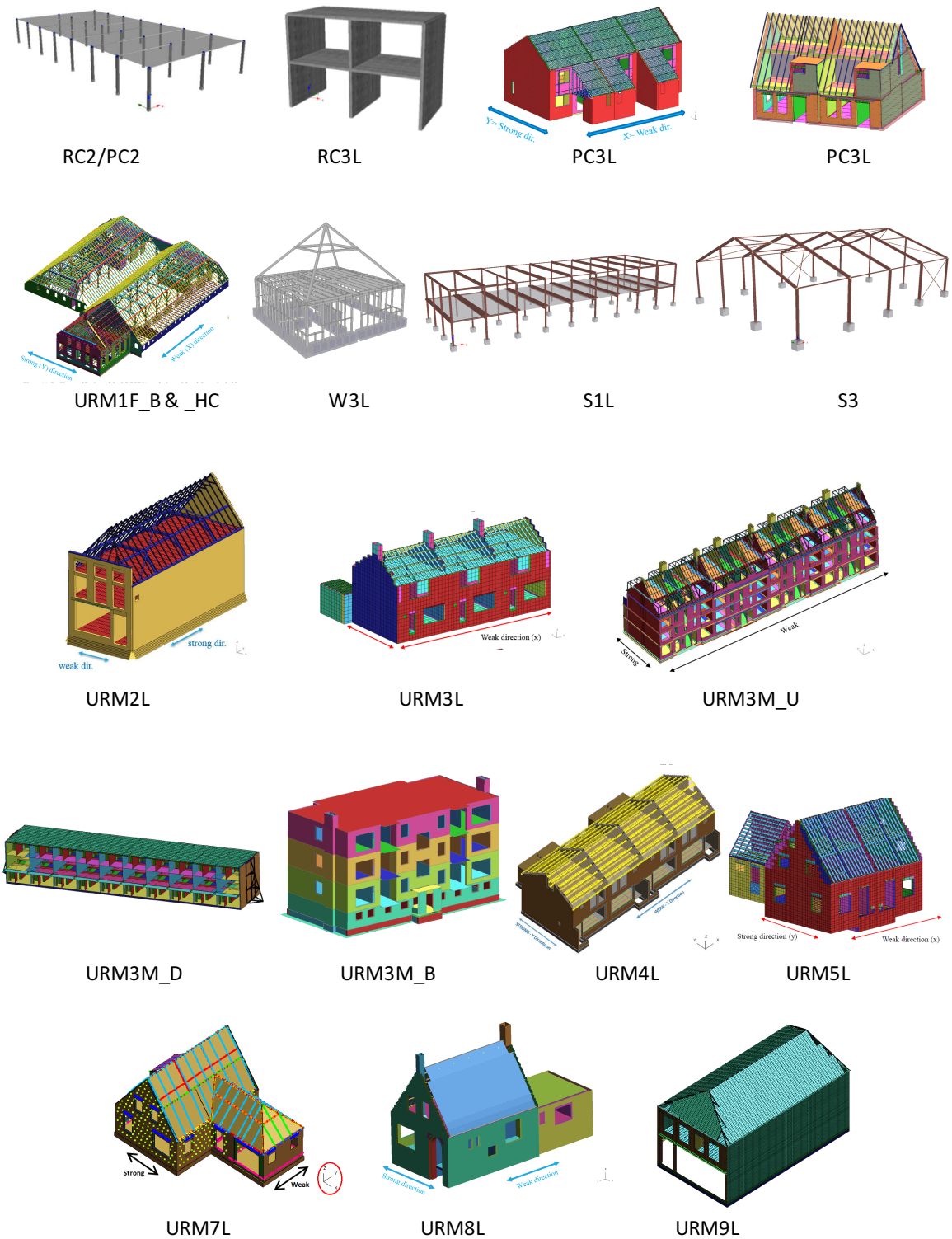

Figure 2.2 Screenshots of one index building model per vulnerability class

Chapter 3

SDOF Models for Updated/Additional Index Buildings

This chapter describes the calibration of SDOF models for those index buildings presented previously in Table 2.2 that have been updated or added since the completion of the v6 model. These index buildings are the following:

- URM3L: Julianalaan 52, E45 Schildwolde, Wilgenbros, and Oostergoweg.
- URM1_F: De Haver (barn and house), Molenweg 25 (barn and house), Molenweg 29 (barn and house), and Eestumerweg 51 (barn and house).
- URM3M_U: Koeriersterweg.
- URM3M_B: Schuitenzandflat 2-56.
- URM4L: Zijlvest 25 and E45 Delfzijl.

3.1 Results from MDOF Modelling

Nonlinear dynamic analyses (using a set of 11 triaxial "training ground motions") of the modelled index buildings have been undertaken using LS-DYNA (LSTC, 2013), and the results are presented in Arup (2019b, 2019c and 2019d). Figures 3.1 to 3.8 to show the hysteresis loops of all nonlinear dynamic analyses; only the weaker direction of each building (i.e. with lower base shear) has been plotted, as all consequences observed in the 3D models of the buildings have been associated with the displacements in the weaker direction of the building.

3.2 Fixed-Base SDOF Models

The points of peak base shear and corresponding attic (i.e. highest level in the building before the roof) displacement (after removal of the time lag with respect to the shear force response time-history, identified on a case-by-case basis from the dynamic analyses) from each nonlinear dynamic/static analysis presented above have been extracted and transformed to equivalent SDOF properties, using the methodology described in the next section.

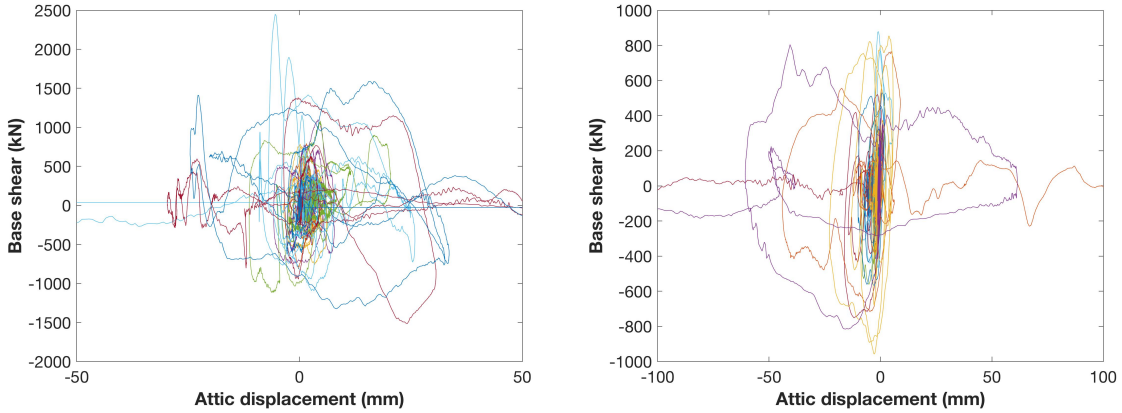

(a) De Haver barn (URM1F_B) **(b)** De Haver house (URM1F_HC)

Figure 3.1 Hysteretic plots of the LS-DYNA De Haver barn and house index building models

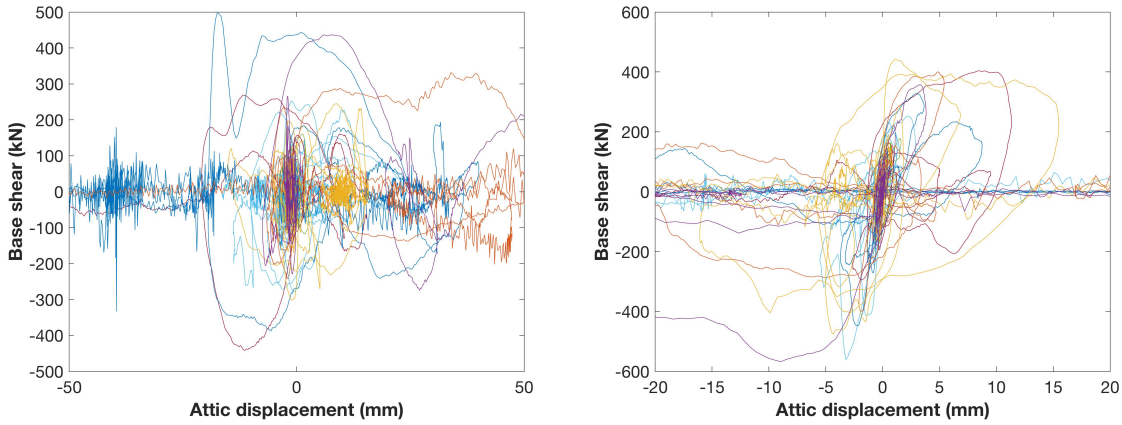

(a) Molenweg 25 barn (URM1F_B) **(b)** Molenweg 25 house (URM1F_HC)

Figure 3.2 Hysteretic plots of the LS-DYNA Molenweg 25 barn and house index building models

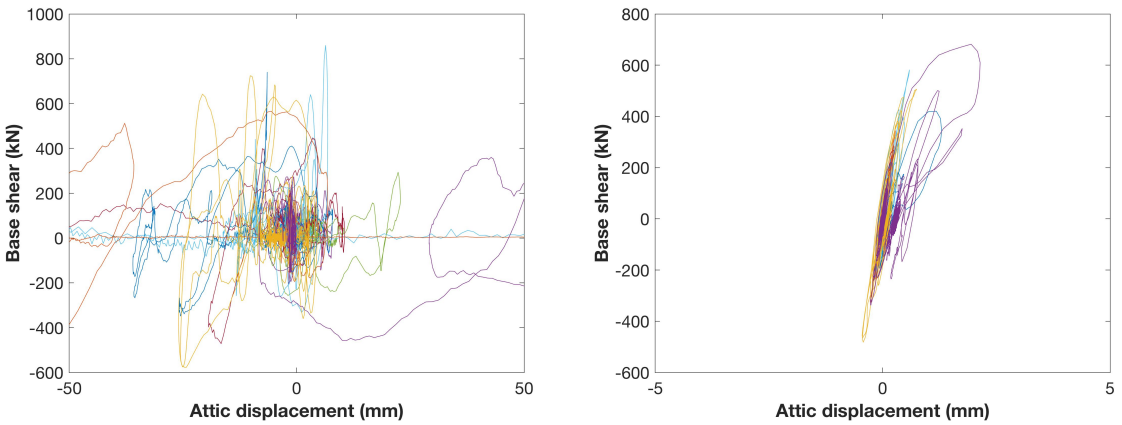

(a) Molenweg 29 barn (URM1F_B) **(b)** Molenweg 29 house (URM1F_HA)

Figure 3.3 Hysteretic plots of the LS-DYNA Molenweg 29 barn and house index building models

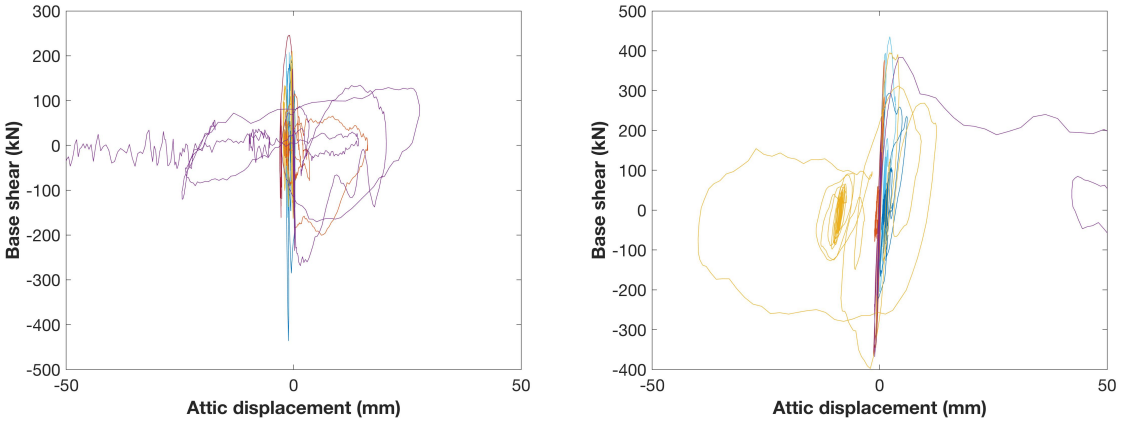

(a) Eestumerweg 51 barn (URM1F_B)

(b) Eestumerw. 51 house (URM1F_HA)

Figure 3.4 Hysteretic plots of the LS-DYNA Eestumerweg 51 barn and house index building models

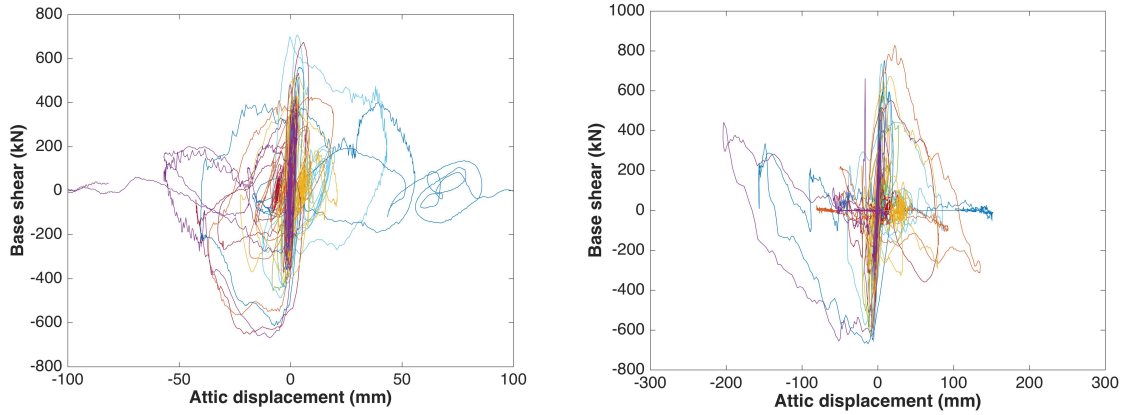

(a) Julianalaan 52 (URM3L)

(b) E45 Schildwolde (URM3L)

Figure 3.5 Hysteretic plot of the LS-DYNA Julianalaan 52 and E45 Schildwolde index building models

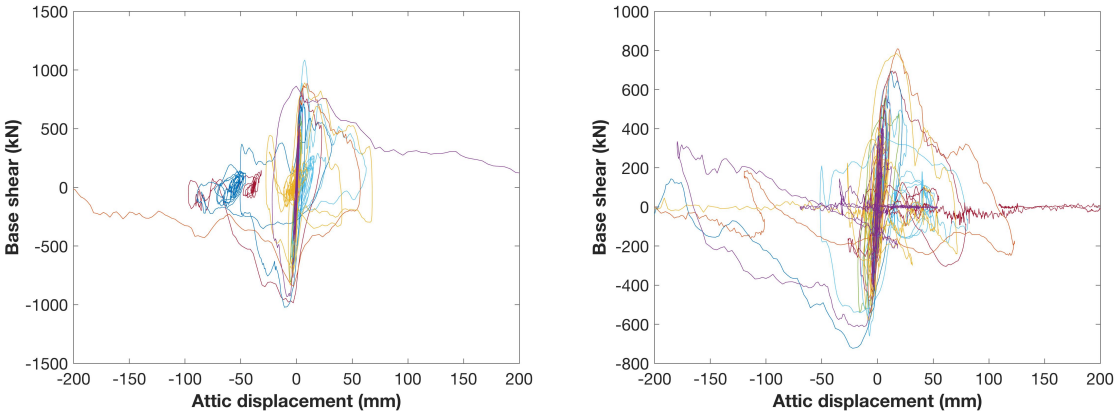

(a) Wilgenbros (URM3L)

(b) Oostergoweg (URM3L)

Figure 3.6 Hysteretic plots from the LS-DYNA Wilgenbros and Oostergoweg index building models

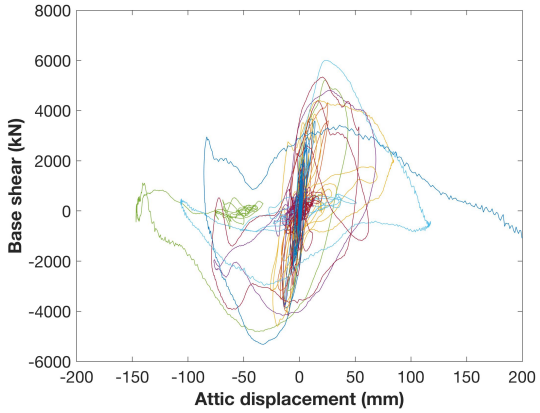

(a) Koeriersterweg (URM3M_U)

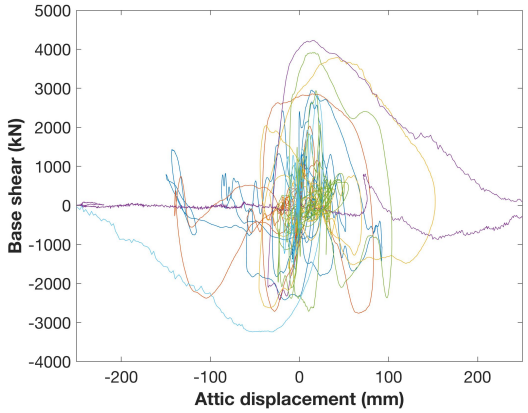

(b) Schuitenzandflat (URM3M_B)

Figure 3.7 Hysteretic plots from the LS-DYNA Koeriersterweg and Schuitenzandflat 2-56 index building models

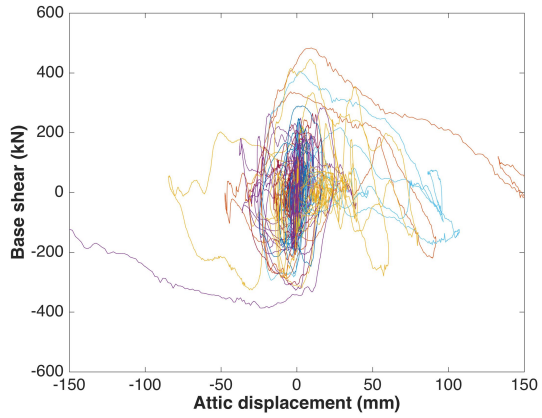

(a) Zijlvest 25 (URM4L)

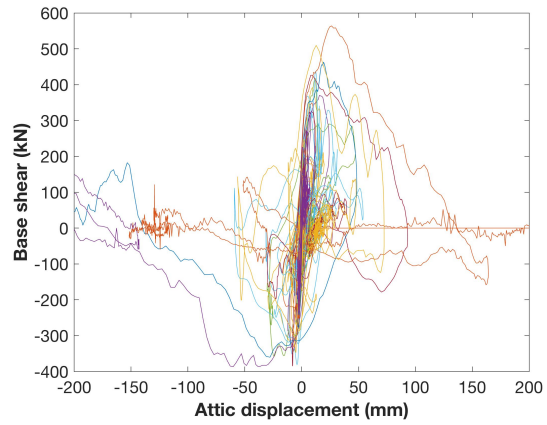

(b) E45 Delfzijl (URM4L)

Figure 3.8 Hysteretic plots from the LS-DYNA Zijlvest 25 and E45 Delfzijl index building models

3.2.1 Transformation to SDOF

Transformation to an equivalent SDOF system has been undertaken using the transformation methodology presented in Casarotti and Pinho (2007). The transformation factor, Γ_t, has been calculated using the results of the analysis that led to the maximum attic displacement (Δ_{max}) without global collapse. At the time step, t, of maximum displacement, the transformation factor Γ_t has been calculated as follows:

$$\Gamma_t = \frac{\sum m_i \phi_{it}}{\sum m_i \phi_{it}^2} \tag{3.1}$$

where m_i is the mass of each floor i of the model (noting that the roof mass is added to the attic/top floor), and ϕ_{it} are the displacements of each floor normalized by Δ_{max}. The spectral displacement (S_d) is calculated by dividing the attic/top floor displacement by Γ_t:

$$S_d = \frac{\Delta_{max}}{\Gamma_t} \tag{3.2}$$

and the base shear coefficient is estimated by dividing the base shear by the effective mass, m_{eff}, given by Equation 3.3:

$$m_{eff} = \sum m_i \phi_{it} \Gamma_t \tag{3.3}$$

The effective height (H_{eff}) of the SDOF can be calculated as follows:

$$H_{eff} = \frac{\sum m_i \phi_{it} h_i}{\sum m_i \phi_{it}} \tag{3.4}$$

where h_i is the height to each floor and m_i is the mass of each floor. The SDOF drift is calculated by dividing the spectral displacement (S_d) by the effective height (H_{eff}).

3.2.2 Backbone curves

The backbone curve of the SDOF model up until peak base shear has been obtained using the points of peak base shear and corresponding attic displacement from each dynamic analysis (or directly the pushover curve for those models for which static analysis was used). The base shear is assumed to be zero when the global collapse capacity is reached and in many cases a negative slope from peak base shear to zero force has been assumed, as this was found to lead to a better comparison with the MDOF models, as further validated in Chapter 7.

For a given model, the global collapse displacement capacity has been taken as the average of the lowest attic displacement when collapse occurs (in those records that lead to global collapse) and the highest attic displacement attained in the analyses that do not lead to global collapse. Further discussion on the identification of the displacement capacity at collapse for each model is provided in Chapter 5.

The backbone curves in terms of base shear and attic displacement obtained from the dynamic analyses are plotted in Figures 3.9 to 3.16 on top of the original hysteretic curves. Only the weaker direction of each building (i.e. with the lower base shear) has been plotted, as all consequences observed in the 3D models of the buildings have been associated with the displacements in the weaker direction of the building. The SDOF displacement is then calculated using the procedure described in the previous section, and the base shear versus SDOF displacement together with the effective mass is used to define the fixed-base SDOF model.

Shear and displacement response time-histories of MDOF structural systems are not necessarily fully in-phase, particularly when multiple modes of vibration or failure mechanisms are activated during the response of a given structure (a phenomenon that is further accentuated when the structure is pushed into the nonlinear inelastic response range). This effectively implies the presence of a time-lag between the time instant when the peak value of base-shear is observed and the instant at which the corresponding displacement is recorded; the latter typically arriving with a slight delay with respect to the former. In the definition of the SDOF backbone capacity curves, such time-lag obviously needs to be removed (since it has no physical meaning within a SDOF representation of the response), this being the reason why the black dots in the plots below (representing the max shear-displacement points with the time-lag removed) do not necessarily always appear on top of the hysteretic curves (where the time-lag is instead present).

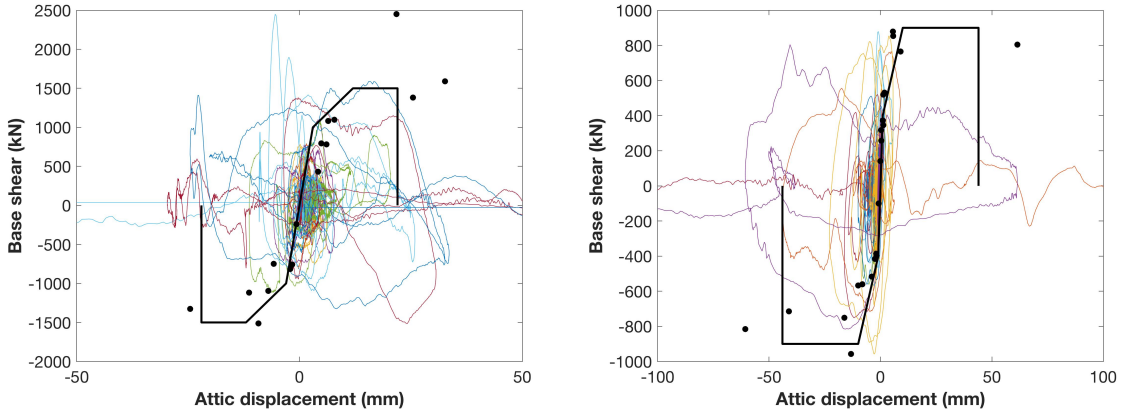

(a) De Haver barn (URM1F_B) **(b)** De Haver house (URM1F_HC)

Figure 3.9 Backbone plots for the De Haver barn and house index building models

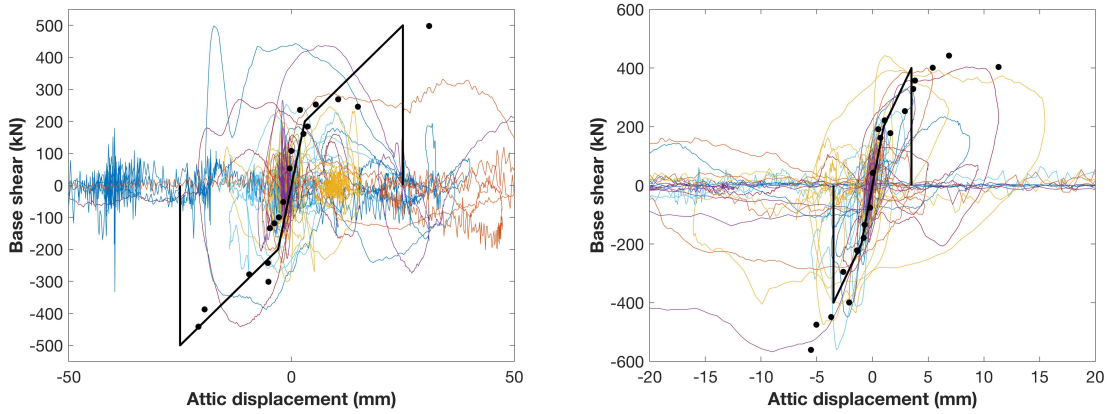

(a) Molenweg 25 barn (URM1F_B) **(b)** Molenw. 25 house (URM1F_HC)

Figure 3.10 Backbone plots for the Molenweg 25 barn and house index building models

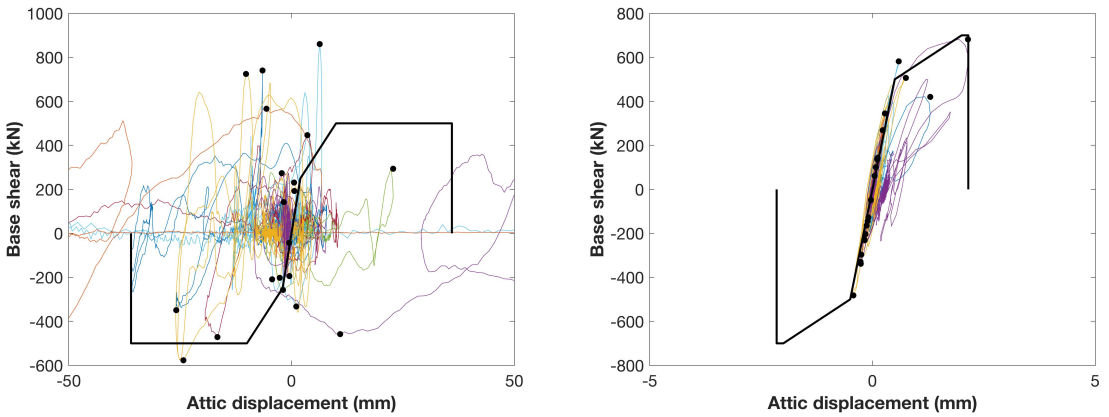

(a) Molenweg 29 barn (URM1F_B) **(b)** Molenw. 29 house (URM1F_HA)

Figure 3.11 Backbone plots for the Molenweg 29 barn and house index building models

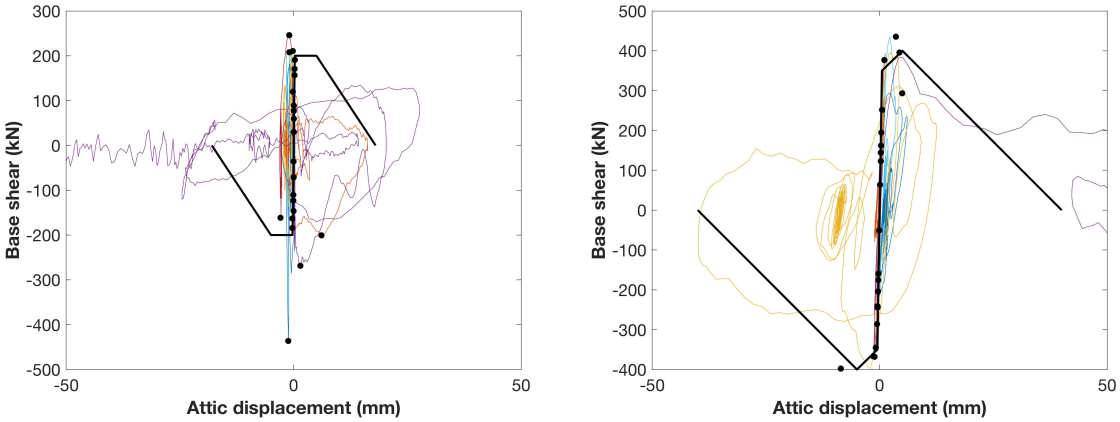

(a) Eestumerweg 51 barn (URM1F_B)

(b) Eestumerw. 51 house (URM1F_HA)

Figure 3.12 Backbone plots for the Eestumerweg 51 barn and house index building models

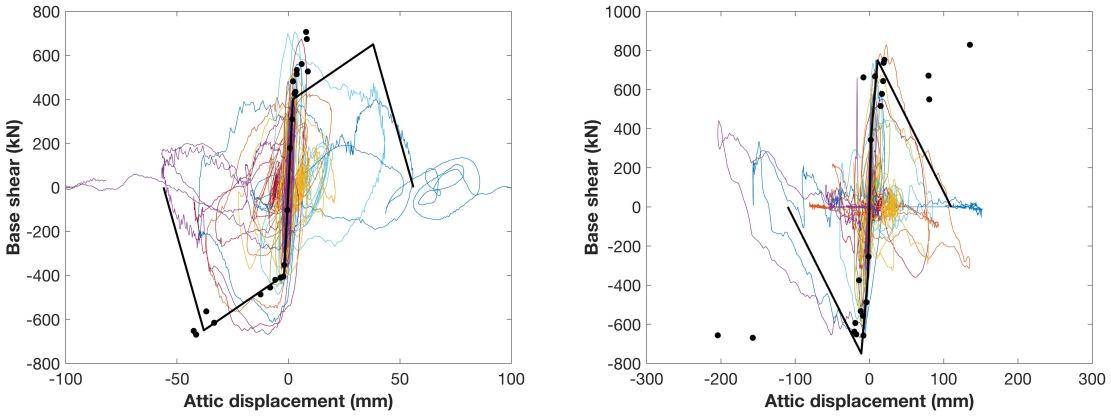

(a) Julianalaan 52 (URM3L)

(b) E45 Schildwolde (URM3L)

Figure 3.13 Backbone plots for the Julianalaan 52 and E45 Schildwolde index building models

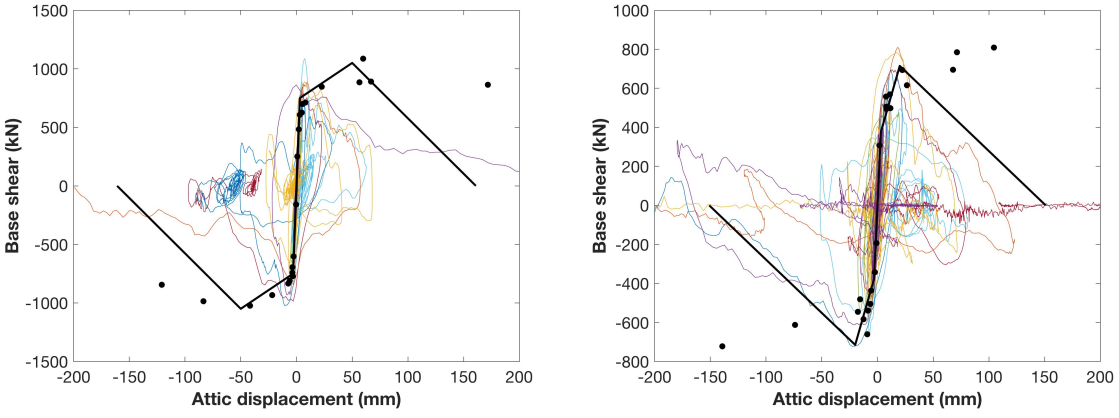

(a) Wilgenbros (URM3L)

(b) Oostergoweg (URM3L)

Figure 3.14 Backbone plots for the and Wilgenbros and Oostergoweg index building models

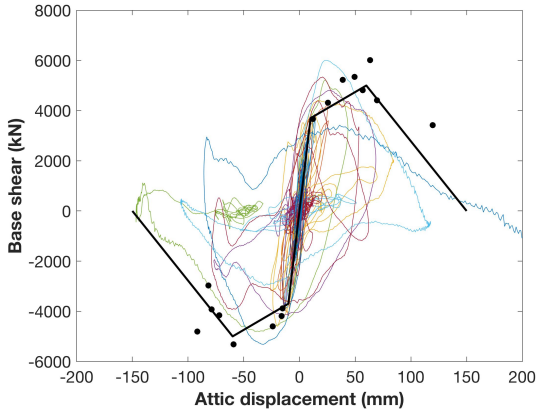

(a) Koeriersterweg (URM3M_U)

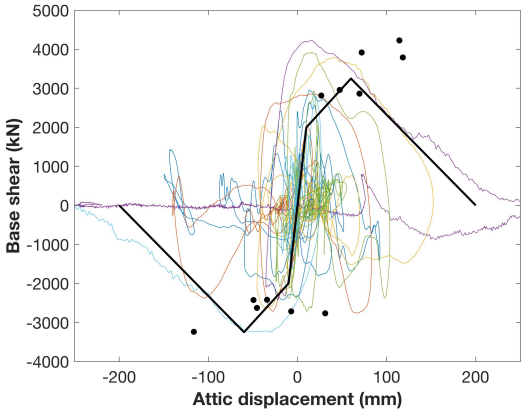

(b) Schuitenzandflat (URM3M_B)

Figure 3.15 Backbone plots for the Koeriersterweg and Schuitenzandflat 2-56 index building models

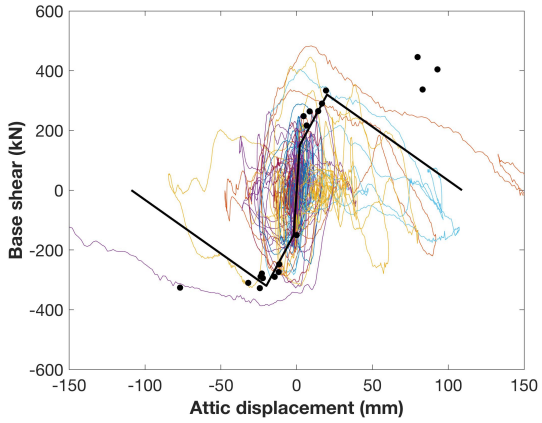

(a) Zijlvest 25 (URM4L)

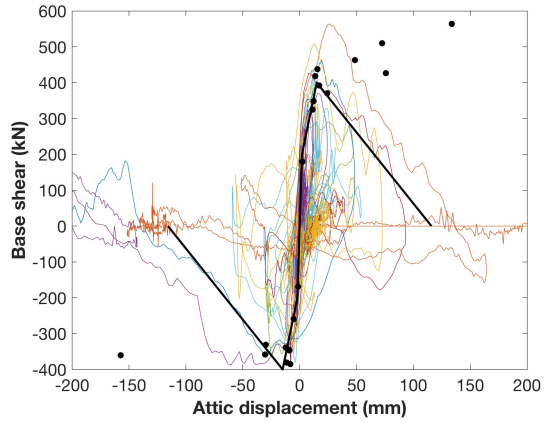

(b) E45 Delfzijl (URM4L)

Figure 3.16 Backbone plots for the Zijlvest 25 and E45 Delfzijl index building models

3.2.3 Structural response hysteretic model

The SDOF systems have been modelled in SeismoStruct (Seismosoft, 2019) using the polygonal hysteresis loop 'multi_lin' by Sivaselvan and Reinhorn (1999). With the exception of the tri-linear backbone curve parameters, all other default values of the model have been kept, except for those buildings with a negative post-peak backbone stiffness where the ductility-based strength decay parameter (HBD) takes a value of 1 and those for which a stiffness degrading parameter (HC) of 1 has been assigned.

Some iterations involving slight modifications to the backbone curves, damping percentages and the stiffness degrading parameter were carried out until a reasonable prediction of the response displacement under the training records used in MDOF nonlinear dynamic analyses was obtained, ensuring also that collapse was predicted under the same records (note that the backbone curves presented above correspond already to the final versions obtained at the end of this iterative process). Comparisons of the nonlinear response of the MDOF displacement (transformed to SDOF displacement) and the displacement of the SDOF models is shown in Figures 3.17 to 3.24. Linear regression of these displacement responses has been undertaken to ensure similar regressions are obtained, given that this is how the fragility functions are developed (see Chapter 4), and to also

make sure that the same number of collapses occurred in the MDOF and SDOF models.

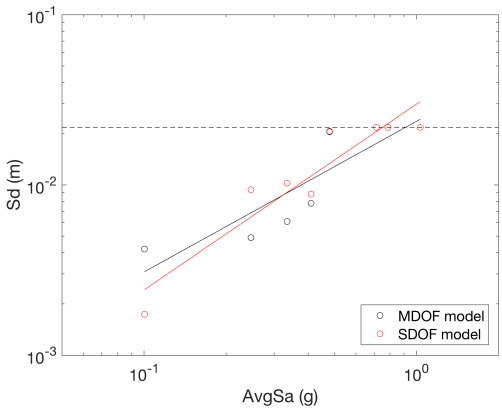

(a) De Haver barn (URM1F_B)

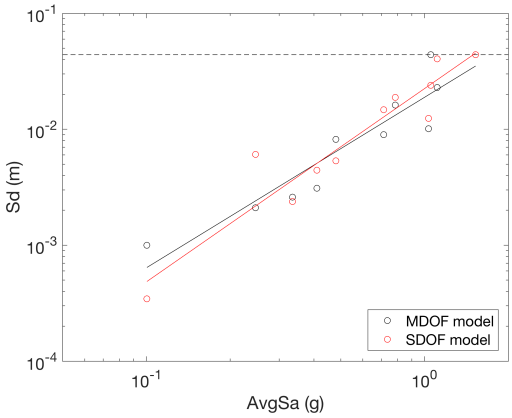

(b) De Haver house (URM1F_HC)

Figure 3.17 Comparison of observed and predicted effective height displacements for the De Haver barn and house index building models

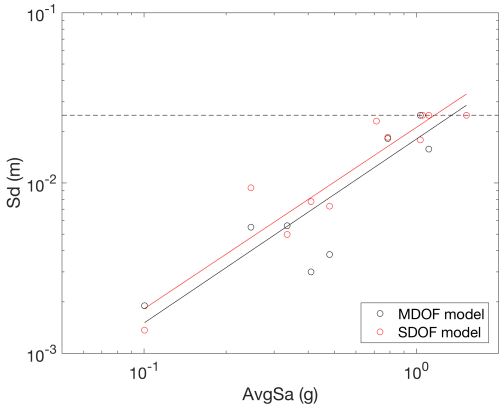

(a) Molenweg 25 barn (URM1F_B)

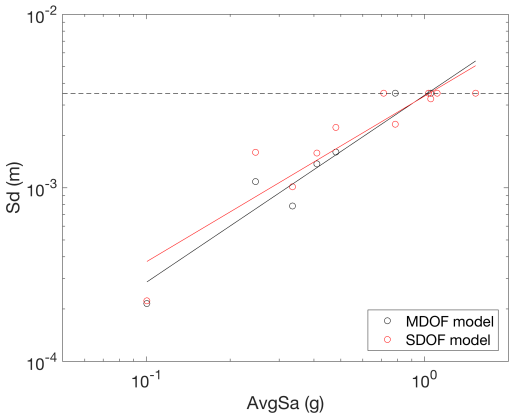

(b) Molenw. 25 house (URM1F_HC)

Figure 3.18 Comparison of observed and predicted effective height displacements for the Molenweg 25 barn and house index building models

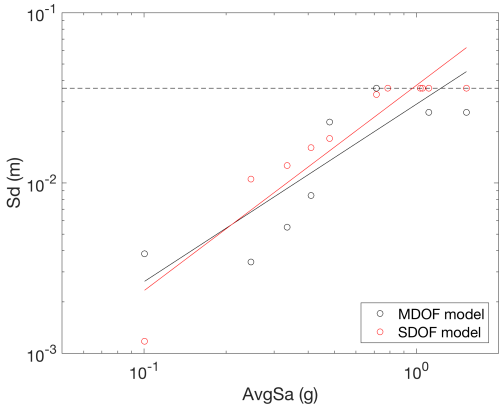

(a) Molenweg 29 barn (URM1F_B)

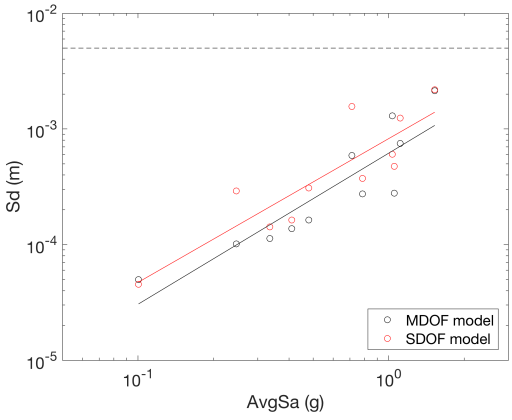

(b) Molenw. 29 house (URM1F_HA)

Figure 3.19 Comparison of observed and predicted effective height displacements for the Molenweg 29 barn and house index building models

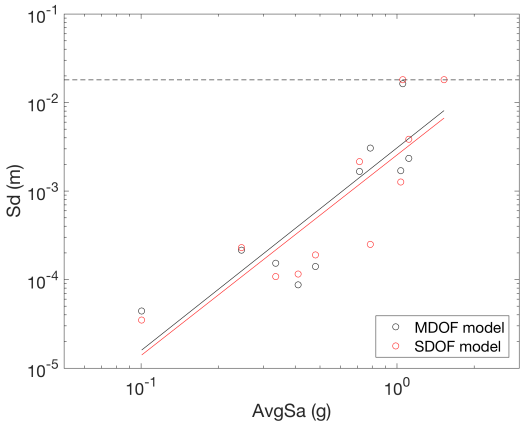

(a) Eestumerweg 51 barn (URM1F_B)

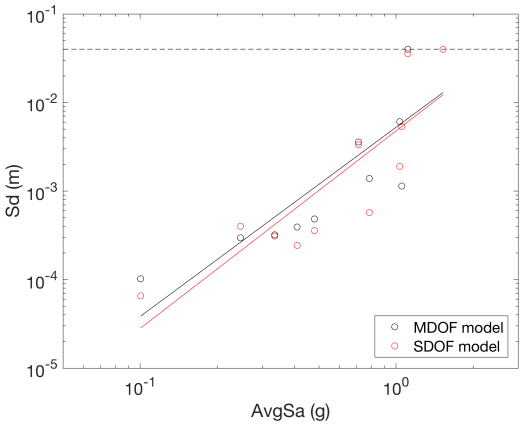

(b) Eestumerw. 51 house (URM1F_HA)

Figure 3.20 Comparison of observed and predicted effective height displacements for the Eestumerweg 51 barn and house index building models

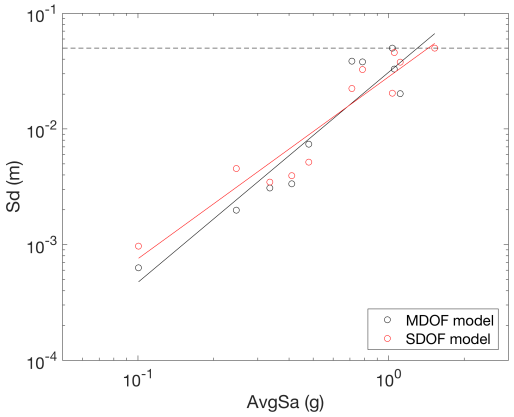

(a) Julianalaan 52 (URM3L)

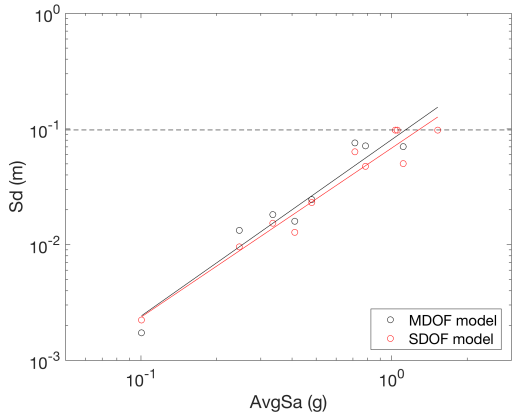

(b) E45 Schildwolde (URM3L)

Figure 3.21 Comparison of observed and predicted effective height displacements for the Julianalaan 52 and E45 Schildwolde index building models

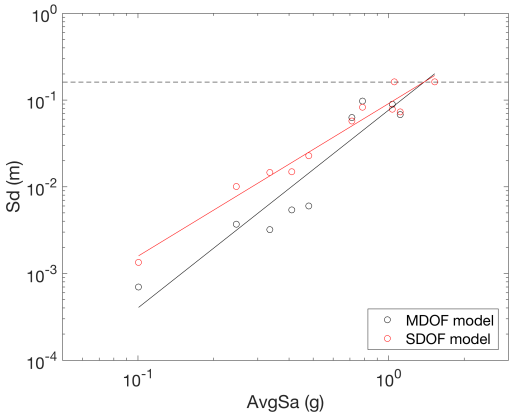

(a) Wilgenbros (URM3L)

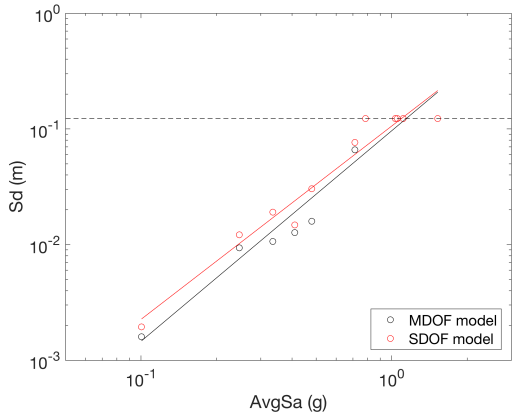

(b) Oostergoweg (URM3L)

Figure 3.22 Comparison of observed and predicted effective height displacements for the Wilgenbros and Oostergoweg index building models

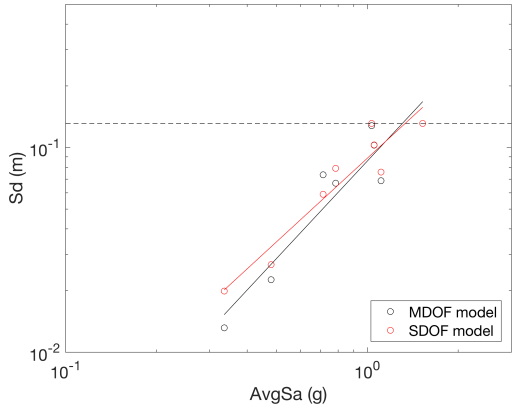

(a) Koeriersterweg (URM3M_U)

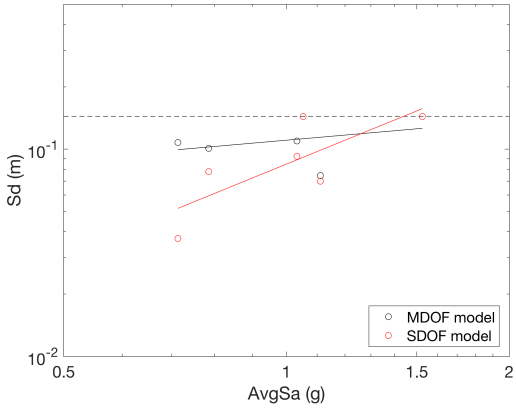

(b) Schuitenzandflat (URM3M_B)

Figure 3.23 Comparison of observed and predicted effective height displacements for the Koeriersterweg and Schuitenzandflat 2-56 index building models

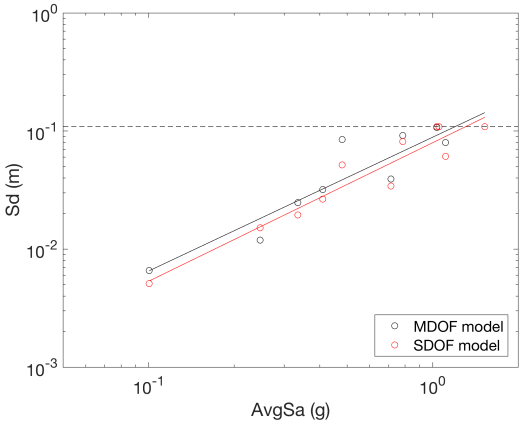

(a) Zijlvest 25 (URM4L)

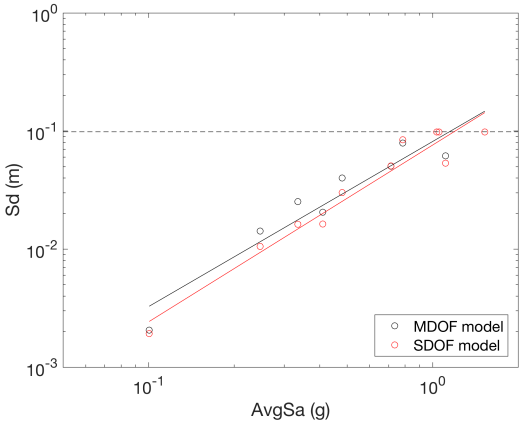

(b) E45 Delfzijl (URM4L)

Figure 3.24 Comparison of observed and predicted effective height displacements for the Zijlvest 25 and E45 Delfzijl index building models

3.2.4 Final fixed-base SDOF models

Tables 3.1 and 3.2 present the final properties of the fixed base SDOF models from all the index building models presented above.

Table 3.1 SDOF Properties of the Updated/Additional Index Buildings (Part 1)

Index Building	Vulnerability Class	Meff (t)	Heff (m)	T (s)	EI (kN/m)	Yield Disp (m)	Ult Disp (m)
De Haver barn	URM1F_B (25%)	576	3.30	0.261	333,333	0.012	0.022
De Haver house	URM1F_HC (50%)	159	3.70	0.125	400,000	0.010	0.044
Molenweg 25 barn	URM1F_B (25%)	65	2.49	0.196	66,667	0.025	0.025
Molenweg 25 house	URM1F_HC (50%)	50	3.16	0.099	200,000	0.0035	0.0035
Molenweg 29 barn	URM1F_B (25%)	139	2.85	0.209	125,000	0.010	0.036
Molenweg 29 house	URM1F_HA (50%)	64	2.65	0.050	1,000,000	0.002	0.005
Eestumerweg 51 barn	URM1F_B (25%)	37	2.10	0.042	800,000	0.005	0.018
Eestumerweg 51 house	URM1F_HA (50%)	64	2.75	0.060	700,000	0.005	0.040
Julianalaan 52	URM3L (25%)	124	4.01	0.148	224,000	0.034	0.050
E45 Schildwolde	URM3L (25%)	231	4.99	0.245	151,846	0.015	0.098
Wilgenbros	URM3L (25%)	288	3.83	0.213	250,000	0.050	0.161
Oostergoweg	URM3L (25%)	211	4.56	0.233	153,750	0.020	0.123
Koeriersterweg	URM3M_U	1390	6.83	0.359	424,760	0.052	0.131
Schuitenzandflat 2-56	URM3M_B	1670	10.72	0.487	278,000	0.043	0.145
Zijlvest 25	URM4L (50%)	219	3.75	0.340	75,000	0.020	0.109
E45 Delfzijl	URM4L (50%)	163	4.09	0.234	117,800	0.021	0.099

Table 3.2 SDOF Properties of the Updated/Additional Index Buildings (Part 2)

Index Building	Vulnerability Class	Cracking BS (kN)	Yield BS (kN)	Ultimate BS (kN)	Damping %	HC parameter	HBD
De Haver barn	URM1F_B (25%)	1000	1500	2500	2	200	0.001
De Haver house	URM1F_HC (50%)	400	900	900	2	1	0.001
Molenweg 25 barn	URM1F_B (25%)	200	500	500	2	1	0.001
Molenweg 25 house	URM1F_HC (50%)	200	400	400	2	1	0.001
Molenweg 29 barn	URM1F_B (25%)	250	500	500	2	1	0.001
Molenweg 29 house	URM1F_HA (50%)	500	700	700	2	1	0.001
Eestumerweg 51 barn	URM1F_B (25%)	200	200	0	2	1	1
Eestumerweg 51 house	URM1F_HA (50%)	350	400	0	2	1	1
Julianalaan 52	URM3L (25%)	400	650	0	1	200	1
E45 Schildwolde	URM3L (25%)	350	750	0	2	1	1
Wilgenbros	URM3L (25%)	750	1050	0	1	1	1
Oostergoweg	URM3L (25%)	375	713	0	1	1	1
Koeriersterweg	URM3M_U	3700	5000	0	2	1	1
Schuitenzandflat 2-56	URM3M_B	2000	3250	0	2	1	1
Zijlvest 25	URM4L (50%)	150	320	0	1	1	1
E45 Delfzijl	URM4L (50%)	200	400	0	1	1	1

3.3 Modelling of Soil-Structure Interaction

Given the very soft soils found in the Groningen region (with Vs30 values often less than 200 m/s), it was felt to be important to account for soil-structure interaction (SSI), which denotes the coupling between the structure and its supporting medium during an earthquake, in the derivation of the fragility functions.

The methodology used to model SSI in the development of fragility functions has not changed since the v6 model and is documented in reports by Mosayk (2019b) and Crowley et al. (2019b), as well as in the journal papers by Cavalieri et al. (2020a, 2020b). Tables 3.3 to 3.4 present the stiffness, capacity and damping input properties of the SSI macro-elements for shallow and pile foundations for the updated/additional index buildings (where the macroement is defined with local axis 1 in the global z direction, local axis 2 in the x direction and local axis 3 in the y direction).

Table 3.3 Stiffness, capacity and damping input properties of the SSI macro-element models for shallow foundations (units in metres, tonne, kN)

Parameters	Values
K_N1	1.52E+07
K_H2	1.17E+07
K_M3	8.51E+08
K_H3	1.10E+07
K_M2	1.57E+08
K_T	5.98E+07
Nmax	4.65E+03
Hmax2	6.63E+02
Mmax3	2.19E+04
Hmax3	6.35E+02
Mmax2	5.72E+03
Tmax	1.35E+05
Cx=C2	3.57E+04
Cy=C3	2.92E+04
Cz=C1	7.37E+04
Cxx=C22	3.61E+03
Cyy=C33	7.36E+02
Czz=C11	3.41E+03
Foundation mass	51

Table 3.4 Stiffness, capacity and damping input properties of the SSI macro-element models for pile foundations (units in metres, tonne, kN)

Parameters	Values for Koeriersterweg	Values for Schuitenzandflat 2-56
K_VV	4.78E+007	4.78E+007
K_HH	2.05E+007	2.05E+007
K_MM	8.83E+006	8.83E+006
K_HM	7.86E+006	7.86E+006
K_TT	6.7000E+007	6.7000E+007
QQ_H_MAX	5396	5880
QQ_M_MAX	2.39E+006	4.0E+006
Eplp	6177	6916
C1	121205	121205
C2	34789	34789
C33	5518	5518
CH2M3	10817	10817
Foundation mass	164	164

Chapter 4

Dynamic Analyses of Updated/Additional SDOF Models

Dynamic analyses of the updated/additional SDOF models using hazard-consistent ground motions is undertaken and described herein. These results are directly used for the development of fragility functions, as described further in Chapter 5. As mentioned already, the records are slightly different to those used in the v6 models as the correlation between AvgSa and duration has now been considered when selecting the records, as described below.

4.1 Hazard-Consistent Ground Motions

4.1.1 Database of records

A database of over 4000 accelerograms has been set up for the nonlinear dynamic analyses in previous versions of the fragility functions, by combining recordings from the NGA1 (Chiou et al., 2008), European (Akkar et al., 2014) and Groningen databases (Bommer et al., 2016). The magnitude, epicentral distance and 5-75% significant duration (D_{S5-75}) for each accelerogram have been obtained/calculated, and a smaller database of 3506 records that cover the range of these parameters used in the probabilistic risk assessment for the Groningen field has been extracted. In particular, the magnitude range has been taken to be between 3.5 and 6.5, and epicentral distances up to 60 km have been used.

For the v6 fragility functions, hazard-consistent records selected from the aforementioned database were used, but the duration of these records was not constrained in any way. For the dynamic analyses of the updated/additional SDOF models considered herein, a new set of records have been selected which have the same spectral characteristics of the v6 records, but they also have a distribution of D_{S5-75} that is consistent with the seismic hazard in Groningen.

4.1.2 Disaggregation of v5 hazard model

In November 2018 the v5 hazard model was run under the so-called Bouwstenen Inzet Scenario 1 (2019 - 2024) and the hazard curves at Loppersum (the town with the hightest level of hazard in the field) for spectral ordinates from 0.01 to 1.0s have been produced (Figure 4.1). The average spectral acceleration (AvgSa), defined as the geometric mean of spectral ordinates over a range of periods

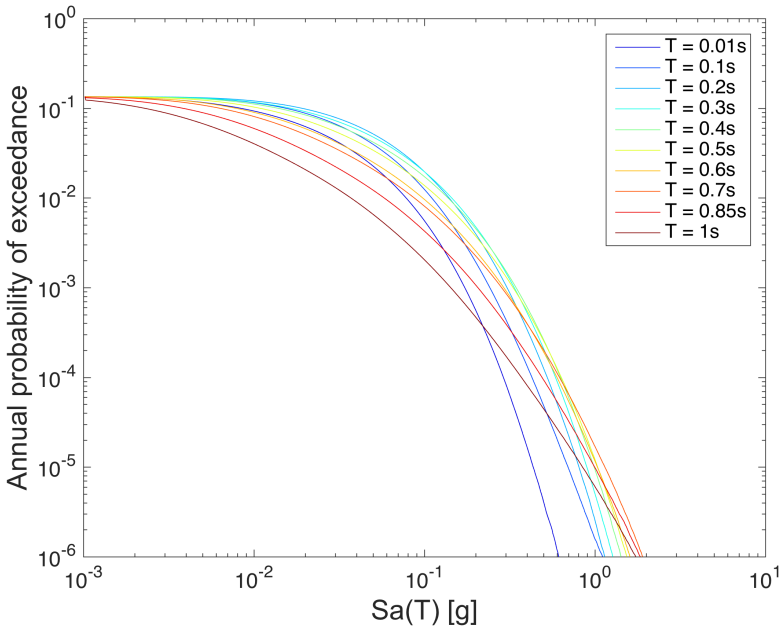

Figure 4.1 Hazard curves at Loppersum for a range of periods, based on v5 hazard model and the Bouwstenen Inzet Scenario 1 (2019 - 2024)

(see e.g. Baker and Cornell, 2006; Bianchini et al., 2009; Eads et al., 2015), at return periods of 50, 500, 2500, 10k, and 100k years has been estimated from the hazard curves and is presented in Table 4.1. The following periods of vibration have been considered for the definition of AvgSa: 0.01, 0.1, 0.2, 0.3, 0.4, 0.5, 0.6, 0.7, 0.85 and 1.0. It is noted that the AvgSa at the aforementioned return periods at Loppersum would ideally be calculated from the hazard engine accounting for period-to-period correlation of the spectral ordinate residuals, but as this was not available at the time of the record selection, the hazard curves have been used and thus full correlation of the spectral ordinate residuals has been assumed.

Disaggregation of AvgSa was not available at the time when the records were being selected, but it was instead available for the spectral ordinates Sa(0.01s), Sa(0.5s) and Sa(1s) at return periods of 50, 500, 2500, 10k, and 100k years. Currently only the marginal distributions of magnitude and distance are available from the disaggregation calculator, rather than the joint distribution of magnitude and distance. Hence, only the mean magnitude and distance contributing to each spectral ordinate has been used to produce hazard-consistent records at this time, using the methodology presented in the next section.

The mean magnitudes and distances contributing to Sa(0.01s), Sa(0.5s) and Sa(1.0s) at each site are presented in Tables 4.2 and 4.3 below. As can be seen, the magnitudes and distances contributing to these spectral ordinates do not vary significantly and it has thus been assumed that the mean values across the three can be used to represent the events contributing to the AvgSa at each return period.

Table 4.1 Estimated values of AvgSa (in g) for five return periods (T) at Loppersum

Return period	AvgSa (g)
T = 50 yrs	0.06
T = 500 yrs	0.20
T = 2500 yrs	0.34
T = 10k yrs	0.50
T = 100k yrs	0.86

Table 4.2 Mean magnitudes contributing to available spectral ordinates for five return periods (T) at Loppersum

Spectral period (s)	T = 50 yrs	T = 500 yrs	T = 2500 yrs	T = 10k yrs	T = 100k yrs
0.01	4.32	4.65	4.81	4.92	5.09
0.5	4.41	4.80	4.98	5.10	5.29
1.0	4.49	4.96	5.22	5.51	6.03

Table 4.3 Mean hypocentral distances contributing to available spectral ordinates for five return periods (T) at Loppersum

Spectral period (s)	T = 50 yrs	T = 500 yrs	T = 2500 yrs	T = 10k yrs	T = 100k yrs
0.01	4.9	4.3	4.1	4.0	3.8
0.5	5.5	4.5	4.2	4.1	3.9
1.0	5.7	4.5	4.2	4.1	4.1

4.1.3 Conditional spectra, duration and record selection

Conditional spectra (Lin and Baker, 2015), conditional on AvgSa and signficant duration for each return period, have been calculated using the mean magnitude and distance from the disaggregation together with the v5 GMPE for spectral ordinates and 5-75% significant duration (Bommer et al., 2017). It is noted that values of epsilon for each aleatory variability component of the v5 GMPE are not available from the disaggregation, and so the logarithmic mean spectral acceleration at the NS_B horizon (see Bommer et al., 2017) based on the mean magntiudes and distances has been used to calculate the amplification factor (for the site zone where Loppersum is located) and the site-to-site variability. The total value of epsilon has then been calculated as the difference between the target AvgSa (Table 4.1) and the AvgSa of the spectrum obtained from the GMPE (calculated using the weighted mean of all logic tree branches).

The methodology presented in Kohrangi et al. (2017) has been followed to define the correlation between ln(AvgSa) and the logarithm of each spectral ordinate, and to calculate the aleatory variability of ln(AvgSa). Instead, to calculate the correlation between ln(AvgSa) and ln(D_{S5-75}), this has been derived from an inter-period correlation model (Baker and Jayaram, 2008) as well as a correlation model for spectral ordinates and significant duration (Bradley, 2011) (Peter Stafford, personal communication).

The ground motion selection procedure that has been used follows the proposal of Baker and Lee (2018), whereby for each statistically simulated spectrum and associated duration, the sum of squared errors (SSE) between the simulated record and each candidate record (taken from the database of 3506 records, as described above, and scaled to match the target AvgSa) is calculated and the record with the lowest SSE is selected. It is noted that a weight of 10 has been given to the significant duration in the sum of squared errors calculation, given that there are 10 spectral ordinates and a similar weight between the spectrum and duration is sought. The selected suite of 50 motions is then compared with the target distribution and the maximum percentage mismatch of the mean and standard deviation of the selected motions' spectra and durations, with respect to their targets, are calculated using the formulae in Baker and Lee (2018). In order to reduce the error, a *greedy optimisation algorithm* is applied to further improve the selection whereby each record within the set is replaced by each of the candidate records, and then for this new set a weighted sum of the squared errors between the selected and target spectra (both mean and standard deviations at each period), plus the selected and target durations (both mean and standard deviation), is calculated. If any of the replaced records reduces the SSE of the set, and has not already been used in the selection, it is retained, and the process is repeated for the next record. The scaling factor applied to all records has been limited to between 0.25 and 3.

Figure 4.2 shows the response spectra of the 50 selected and scaled ground motions with spectra matching the target conditional spectrum for each return period. In this example, the mean and the mean+/- two standard deviations of the target distribution are also shown.

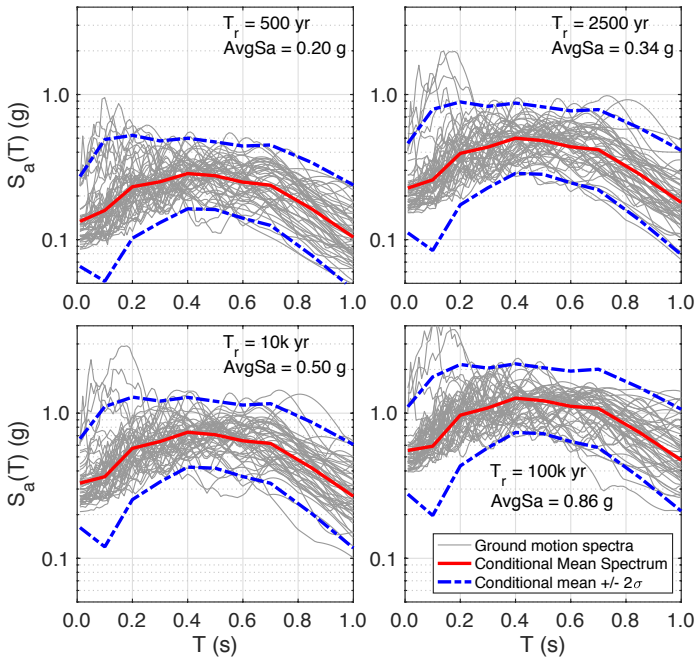

Figure 4.2 Response spectra of 50 selected and scaled ground motions conditional on AvgSa and D_{S5-75} at Loppersum for return periods from 500 to 100k years. The mean and mean +/- two standard deviations of the conditional target spectra are superimposed.

4.2 Nonlinear Dynamic Analysis

For the development of fragility functions, which describe the probability of reaching or exceeding a given damage or collapse state under increasing levels of ground shaking intensity, a model for the probabilistic relationship between ground motion intensity and the nonlinear structural response of the SDOF system is needed. The approaches that are commonly used for estimating this probabilistic relationship include the cloud method (Jalayer, 2003), the multiple-stripe method (Jalayer, 2003) and Incremental Dynamic Analysis (IDA) (Vamvatsikos and Cornell, 2002). Hazard-consistent record selection together with linear regression (typically used in the cloud method) has been used herein. Whilst the selection of records conditional on increasing levels of intensity could allow the multiple-stripe method to be used, whereby the probability of damage/collapse threshold exceedance at each intenasity measure level is calculated from the response data and then maximum likelihood is applied to fit a fragility function to the results, this has not been undertaken herein as the largest selected ground motions do not always lead to suffient numbers of damage exceedance/collapse for many of the vulnerability classes.

The cloud method is typically applied using an assumption of linear variation in the logarithmic space of the structural response with the intensity measure (IM), and homoscedasticity of the residuals (see e.g. Baker, 2007). However, this is not necessarily the case for response quantities that span from pre-yield to collapse. The current fragility input to the risk engine is based on providing a single set of regression parameters to be used for both damage and collapse fragility functions, and given the time constraints to run the v6 hazard and risk engine it has not been possible to

change this input format. For future updates of the risk engine, which may also include DS1 (non-structural) analytical fragility functions, piecewise linear regression may be undertaken. For v6, the response data for the highest four return periods was used to create a set of data which is more adequately represented by a linear response, but for v7 only the two highest return periods have been used in order to ensure a more robust estimate of the collapse capacity (and for comparison with the MDOF models, as described in Chapter 7). This assumption is justified whilst the focus is still on local personal risk, but should the estimation of damage take higher importance in the hazard and risk assessments for the field in the future, the use of piecewise linear regression would be recommended and the engine would need to be adapted to account for this modified input format.

The nonlinear dynamic analyses of each SDOF system have been undertaken in SeismoStruct (Seismosoft, 2020). Once the maximum nonlinear dynamic displacement response of a given SDOF (S_d) is obtained from all n ground-motion records, each response (d_i) is plotted against a scalar/vector intensity measure ($\ln(AvgSa)$ herein) and the statistical parameters corresponding to the lognormal distribution of $S_d \,|\, \ln(AvgSa)$ can be extracted. In particular, the expected value, E[$\ln S_d \,|\, \ln(AvgSa)$], is modelled by a linear regression equation (Equation 4.1) with parameters b_0 and b_1, whilst the standard deviation or dispersion (Equation 4.2) is estimated by the standard error of the regression:

$$E[\ln S_d | \ln(AvgSa)] = \ln \eta_{S_d | \ln(AvgSa)} = b_0 + b_1 \ln(AvgSa) \tag{4.1}$$

$$\beta_{S_d | \ln(AvgSa)} \approx \sqrt{\frac{\sum_i^n (\ln(d_i) - \ln \eta_{S_d | \ln(AvgSa)})^2}{n-2}} \tag{4.2}$$

As mentioned above, the parameters b_0 and b_1 are the estimated regression coefficients obtained by performing a linear regression. In order to correctly treat the results of the nonlinear dynamic analyses where the displacement response exceeds the expected ultimate displacement capacity (and thus these SDOF systems are deemed to have exceeded the collapse limit state and the estimated displacement response is no longer reliable), a censored regression has been undertaken when estimating the coefficients of Equation 4.1 (see Stafford, 2008). In these cases, the value of displacement demand from the nonlinear dynamic analysis is not trusted, but it is known to exceed a given limiting value, and is thus referred to as a censored observation. If all censored observations were set to the limiting value, and a normal linear regression analysis were to be applied as above, the fitted model would be biased. To obtain an unbiased model, maximum likelihood technique is used. The likelihood function for a model with n observations, where $lnS_d | \ln(AvgSa)$ is given by Equation 4.1 is:

$$Likelihood = \prod_i^n \phi\left(\frac{\ln(d_i) - \ln \eta_{S_d | \ln(AvgSa)}}{\beta_{S_d | \ln(AvgSa)}}\right) \tag{4.3}$$

where $\phi(z)$ is the probability density function for the standard normal distribution. However, rather than finding the values of the coefficients of Equation 4.1 that maximize L, it is necessary to minimize the negative of the log-likelihood function, given by:

$$\ln(Likelihood) = \sum_{i}^{n} \ln \phi \left(\frac{\ln(d_i) - \ln \eta_{S_d|\ln(AvgSa)}}{\beta_{S_d|\ln(AvgSa)}} \right) \tag{4.4}$$

With the presence of censored variables the likelihood function becomes:

$$Likelihood = \prod_{j}^{n_c} \left[1 - \Phi \left(\frac{\ln(d_i) - \ln \eta_{S_d|\ln(AvgSa)}}{\beta_{S_d|\ln(AvgSa)}} \right) \right] \prod_{i}^{n_0} \phi \left(\frac{\ln(d_i) - \ln \eta_{S_d|\ln(AvgSa)}}{\beta_{S_d|\ln(AvgSa)}} \right) \tag{4.5}$$

where there are n_c censored observations and n_0 observed (uncensored) values and $n_c + n_0 = n$. The $\Phi(z)$ function is the cumulative standard normal distribution function. Taking the logarithm of this expression, as before, gives:

$$\ln(Likelihood) = \sum_{j}^{n_c} \ln \left[1 - \Phi \left(\frac{\ln(d_i) - \ln \eta_{S_d|\ln(AvgSa)}}{\beta_{S_d|\ln(AvgSa)}} \right) \right] + \sum_{i}^{n_0} \ln \phi \left(\frac{\ln(d_i) - \ln \eta_{S_d|\ln(AvgSa)}}{\beta_{S_d|\ln(AvgSa)}} \right) \tag{4.6}$$

The cloud plots with censored regression for all index buildings are shown in Figure 4.3 and Figure 4.4, where the censored observations have been plotted at the limiting displacement capacity value. The values shown in red are beyond the ultimate collapse displacement and thus were not considered in the regression, and instead a censored regression was undertaken with these points, as described above. The two stripes shown refer to AvgSa values of 0.5g and 0.86g which correspond to return periods of 10k and 100k years, respectively.

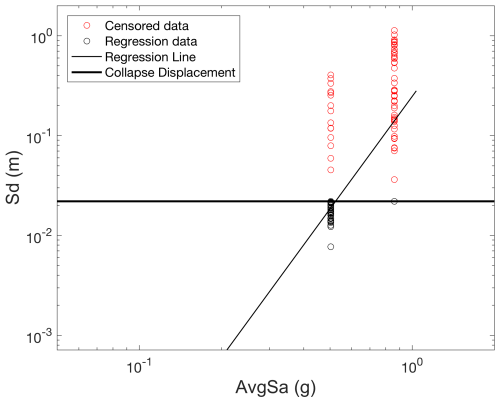

(a) De Haver barn (URM1F_B)

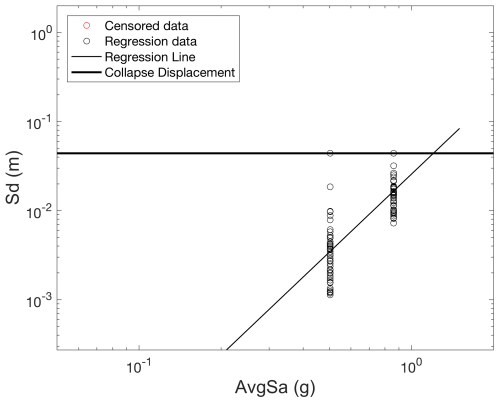

(b) De Haver house (URM1F_HC)

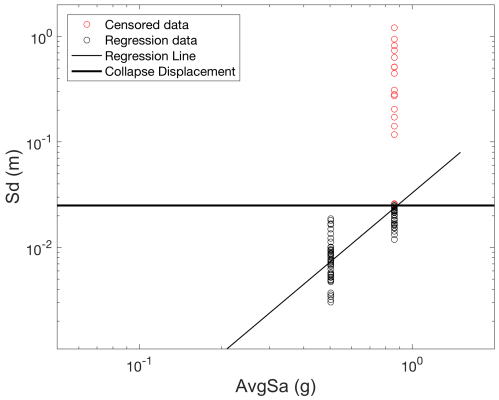

(c) Molenweg 25 barn (URM1F_B)

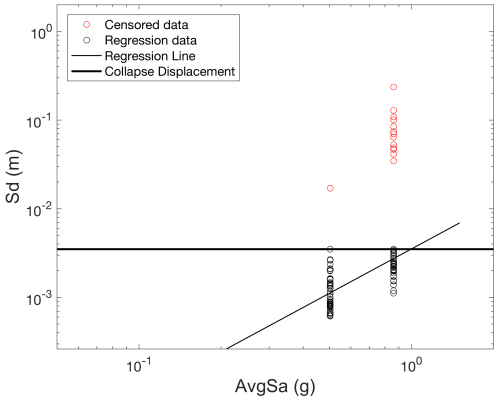

(d) Molenw. 25 house (URM1F_HC)

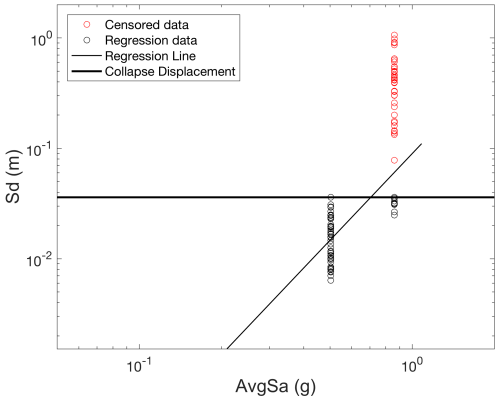

(e) Molenweg 29 barn (URM1F_B)

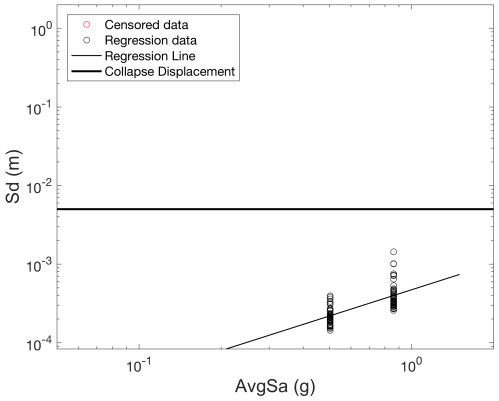

(f) Molenw. 29 house (URM1F_HA)

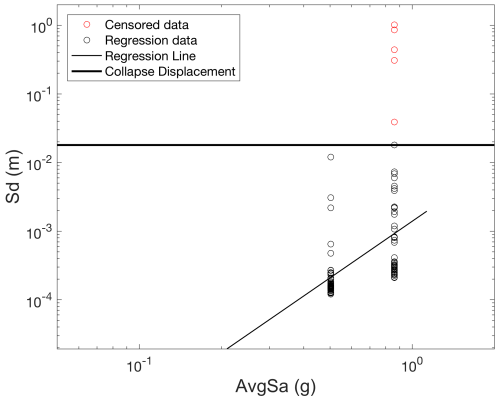

(g) Eestumerw. 51 barn (URM1F_B)

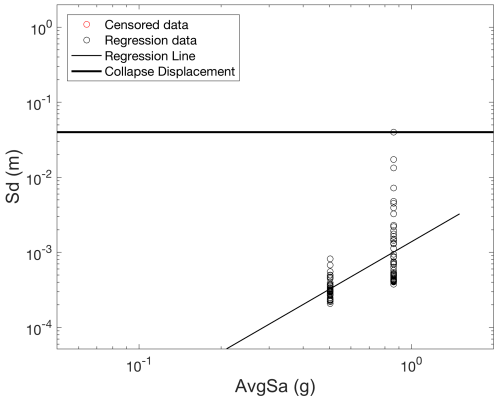

(h) Eestum. 51 house (URM1F_HA)

Figure 4.3 Cloud plots for each index building

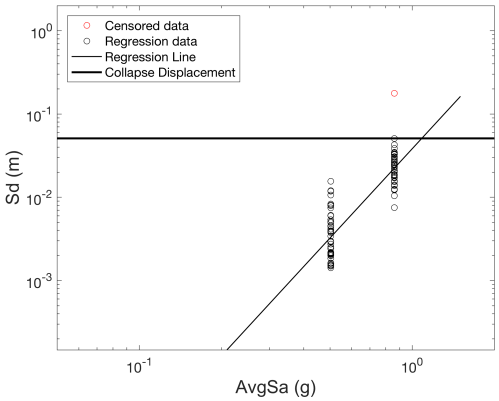

(a) Julianalaan 52 (URM3L)

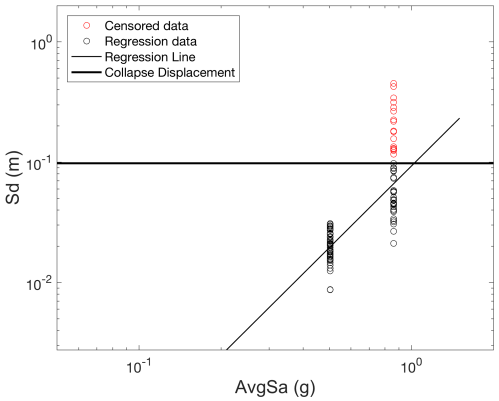

(b) E45 Schildwolde (URM3L)

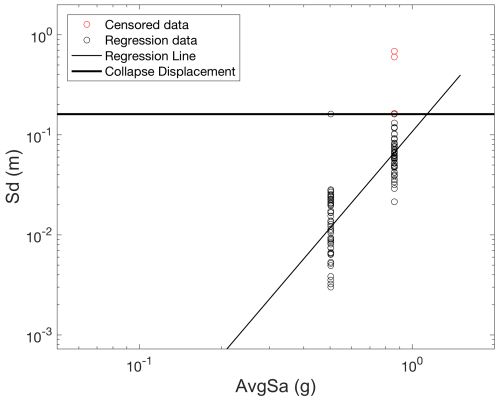

(c) Wilgenbros (URM3L)

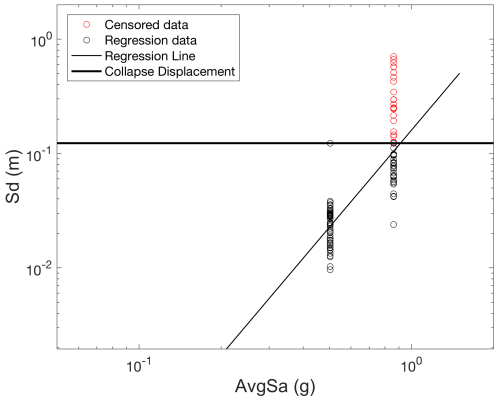

(d) Oostergoweg (URM3L)

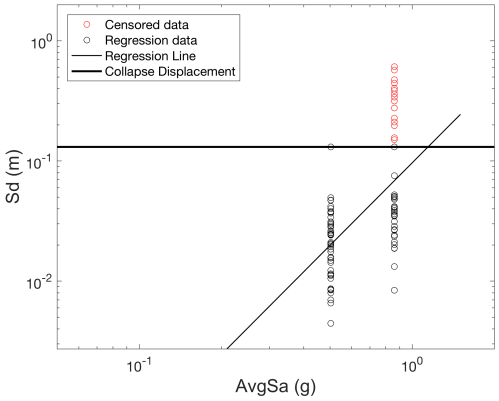

(e) Koeriersterweg (URM3M_U)

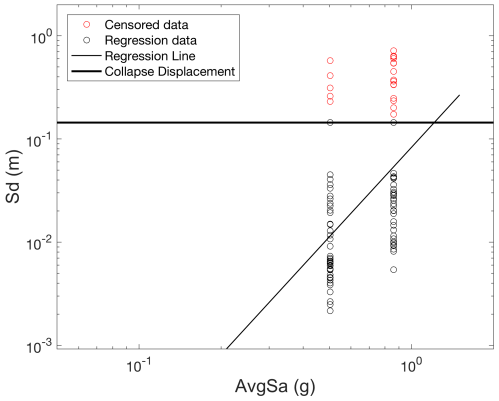

(f) Schuitenzandflat (URM3M_B)

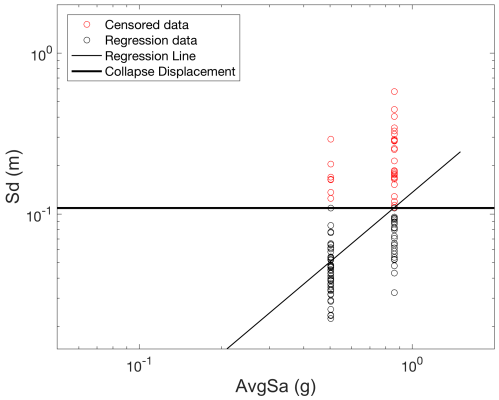

(g) Zijlvest 25 (URM4L)

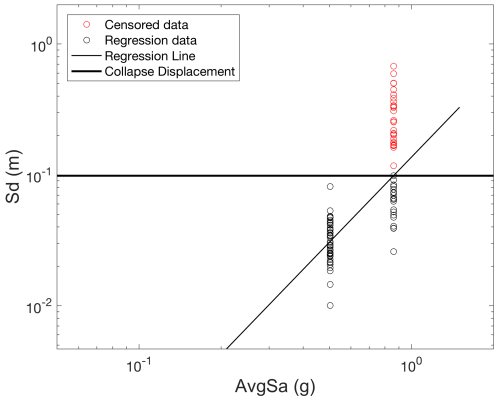

(h) E45 Delfzijl (URM4L)

Figure 4.4 Cloud plots for each index building (cont.)

Chapter 5

Fragility and Fatality Models for Updated/Additional Index Buildings

As already mentioned in the Introduction, this report only provides the results of the updated/additional index buildings and the structural fragility and fatality models that have been developed for these buildings. For this reason chimney fragility functions are not included in this report and the reader is referred to the v6 fragility and consequences report for details on such models (Crowley et al., 2019b).

5.1 Introduction

The regression analyses described in the previous chapter allow equations to be derived that relate the level of shaking with an estimate of the displacement response of an equivalent SDOF system (S_d). By identifying the thresholds to damage or collapse in terms of SDOF displacements (also obtained by multiplying SDOF drifts by the effective height of the SDOF), it is possible to produce fragility functions that describe the probability of exceeding a number of distinct damage/collapse states.

The probability of exceeding the limit displacement to each structural damage or collapse state i under a given level of ground shaking is calculated as follows:

$$P_{eDL_{DSi}} = 1 - \Phi\left(\frac{\ln(DL_{DSi}) - \ln \eta_{S_d|\ln(AvgSa)}}{\sigma_s}\right) \tag{5.1}$$

$$P_{eDL_{CSi}} = 1 - \Phi\left(\frac{\ln(DL_{CSi}) - \ln \eta_{S_d|\ln(AvgSa)}}{\sigma_s}\right) \tag{5.2}$$

where

$$\ln \eta_{S_d|\ln(AvgSa)} = b_0 + b_1 \ln(AvgSa) \tag{5.3}$$

and $\Phi()$ is the cumulative distribution function of the standard normal distribution, b_0 and b_1 are coefficients obtained from the linear regression, DL is the displacement limit of each damage or collapse state (provided in metres), $\ln(AvgSa)$ is the average spectral acceleration (in g), defined as the geometric mean of the spectral ordinates of the GMPE from 0.01 to 1.0 s, as provided by the

hazard calculations of the risk engine, and σ_s is the logarithmic standard deviation due to record-to-record variability, as shown in the cloud plots in Chapter 4. Additional within building and between building variability is explored further in Chapter 6 and is included in the final fragility functions for each vulnerability class.

The damage and collapse states presented herein are sequential. Only the collapse states are used in the fatality risk calculations, whereas damage states DS2 and DS3 are used in the group damage curves. The following two sections present the definition of the damage and collapse states for the index buildings.

5.2 Damage Limit States

The drift levels at which damage occurs in the URM buildings has been informed by the large testing campaign that has been carried out on components and structures that match the construction practices and materials used in the Groningen field. A specific report focusing on the damage observed in the numerous URM tests has been compiled (Graziotti et al., 2017b; Kallioras et al., 2019a), and the results in terms of the damage desriptions and levels of attic displacement have been used to identify SDOF drift limits to damage ($\theta_{SDOF_{DLi}}$). The mean drift limits are 0.13 % and 0.3 % and the CoVs are 62 % and 35 % for DS2 and DS3, respectively.

In order to calculate the threshold SDOF displacements (S_{di}) for each building typology, these average SDOF drift limits have been multiplied by the effective height of each building typology (provided previously in Table **??**).

5.3 Collapse Limit States

A detailed description of the collapse mechanisms (and associate collapse displacement) observed in each of the nonlinear dynamic analyses that have been run in LS-DYNA, described in Chapter 3, has been produced (see Arup 2019b; Arup 2019c, 2019d). It has been possible to identify a weaker direction of the building in all models; this is the direction that has a lower base shear capacity and in which global collapse is initiated. This direction has thus been used for the development of the fragility functions, and so the attic displacement in this weaker direction has been extracted in all cases.

Up to three collapse states per building (with the third being global collapse) have been selected for the development of fragility (and fatality) functions. The collapse states have been assumed to be sequential, with increased consequences from one collapse state to the next (similar to the damage states). The selected partial collapse states (1 and 2) from the LS-DYNA models for each vulnerability model are presented in Table 5.1. It is noted that the displacement values for global callapse obtained from the dynamic analyses of the index buildings might overestimate the actual displacement capacity at global collapse, as only a limited number of records have been used for each structure, and an iterative approach to identify the lowest displacement at which global collapse occurs was not undertaken. In order to attempt to correct for what could be an under- or over-estimation of the global collapse capacity, the SDOF displacement for the global collapse limit state has been calculated using the average of the maximum attic displacement obtained in the records

where global collapse does not occur and the lowest displacement at which global collapse was instead identified.

Table 5.1 Selected partial collapse states from LS-DYNA models

Index Building	Collapse state 1	Collapse state 2
De Haver (barn)	N/A	N/A
De Haver (house)	Roof timber elements and out-of-plane (OOP) failure of internal wall	OOP failure of internal wall and collapse of mezzanine
Molenweg 25 (barn)	OOP failure of a gable wall, roof connection failure	OOP failure of gable walls, internal and external walls and timber floor failure
Molenweg 25 (house)	N/A	N/A
Molenweg 29 (barn)	Partial collapse of roof	Partial collapse of roof (higher debris)
Molenweg 29 (house)	OOP failure of URM outer leaf leading to walkway roof collapse	N/A
Eestumerweg 51 (barn)	Unseating of timber purlin from column	N/A
Eestumerweg 51 (house)	OOP failure of some URM walls	OOP failure of URM outer leaf, attic floor-timber truss connection failure, leading to roof failure
Julianalaan 52	N/A	N/A
E45 Schildwolde	Failure of partition walls at first and ground floor	Failure of partition walls at first and ground floor, local failures of outer and inner leaf at 1st storey
Wilgenbros	Gable and roof party wall failure, roof collapse, outer façade wall collapse OOP	Part wall and chimney failure, collapse of roof outer façade wall collapse OOP
Oostergoweg	Apex of gable and roof party wall fails OOP	Gable wall fails OOP and inner façade and non-loading bearing walls fail
Koeriersterweg	Onset of collapse of chimneys	Overturning of URM walls in roof, roof and chimney collapse, OOP failure of URM outer leaf in all units
Schuitenzandflat 2-56	Local connection failure of roof slab/wall, OOP failure of URM walls on 3rd floor	N/A
Zijlvest 25	Masonry columns collapse outwards and lintel collapse	Masonry columns collapse both inwards and outwards
E45 Delfzijl	Failure of lintels of internal walls	Failure of internal wall lintels, local failure URM walls, OOP failure of inner leaf of gable wall

5.4 Structural Fragility Functions

The strutural fragility functions for each model are calculated using Equations 5.1 and 5.2 and the parameters of the censored linear regression (discussed in Chapter 4), the variability, σ_s, and the displacement limit of each damage or collapse state, as presented in Table 5.2. As the fragility functions are all lognormal distributions in terms of a scalar IM (AvgSa), the median (e^{μ}) and dispersion (β) of each index building fragility function has also been provided in Table 5.3. Figures 5.1 to 5.8 present the fragility functions for all updated/additional index buildings considered in the current model development endeavour.

Table 5.2 Regression parameters for updated/additional index buildings

Index building	b_0	b_1	σ_s	DS2 (m)	DS3 (m)	CS1 (m)	CS2 (m)	CS3 (m)
De Haver barn	-1.399	3.737	0.2570	0.0016	0.0065	0.0220	0.0220	0.0220
De Haver house	-3.662	2.906	0.5606	0.0018	0.0030	0.0030	0.0100	0.0440
Molenweg 25 barn	-3.415	2.177	0.4098	0.0012	0.0049	0.0160	0.0180	0.0250
Molenweg 25 house	-5.649	1.659	0.4068	0.0015	0.0035	0.0035	0.0035	0.0035
Molenweg 29 barn	-2.413	2.605	0.5008	0.0014	0.0056	0.0230	0.0260	0.0360
Molenweg 29 house	-7.660	1.107	0.3222	0.0006	0.0006	0.0006	0.0006	0.0050
Eestumerweg 51 barn	-6.575	2.739	1.0214	0.0010	0.0020	0.0020	0.0180	0.0180
Eestumerweg 51 house	-6.582	2.103	0.7192	0.0013	0.0040	0.0040	0.0060	0.0400
Julianalaan 52	-3.263	3.557	0.5261	0.0019	0.0079	0.0510	0.0510	0.0510
E45 Schildewolde	-2.375	2.251	0.3761	0.0024	0.0098	0.0182	0.0703	0.0980
Wilgenbros	-2.228	3.198	0.5401	0.0018	0.0075	0.0630	0.0890	0.1610
Oostergoweg	-1.834	2.816	0.4406	0.0022	0.0089	0.0160	0.0660	0.1230
Koeriersterweg	-2.350	2.262	0.7272	0.0033	0.0134	0.0230	0.1020	0.1310
Schuitenzandflat 2-56	-2.491	2.876	1.0127	0.0051	0.0210	0.0750	0.1080	0.1440
Zijlvest 25	-1.994	1.431	0.4494	0.0018	0.0074	0.0390	0.0940	0.1090
E45 Delfzij	-1.991	2.159	0.4489	0.0020	0.0080	0.0500	0.0620	0.0990

Table 5.3 Lognormal fragility funcion parameters for the updated/additional index buildings in terms of AvgSa

Index Building	DS2 e^{μ} (g)	DS3 e^{μ} (g)	CS1 e^{μ} (g)	CS2 e^{μ} (g)	CS3 e^{μ} (g)	β
De Haver barn	0.26	0.38	0.52	0.52	0.52	0.07
De Haver house	0.40	0.48	0.48	0.72	1.20	0.19
Molenweg 25 barn	0.22	0.42	0.72	0.76	0.88	0.19
Molenweg 25 house	0.60	1.00	1.00	1.00	1.00	0.25
Molenweg 29 barn	0.20	0.34	0.59	0.62	0.70	0.19
Molenweg 29 house	1.24	1.24	1.24	1.24	8.45	0.29
Eestumerweg 51 25 barn	0.89	1.14	1.14	2.54	2.54	0.37
Eestumerweg 51 house	0.98	1.66	1.66	2.01	4.95	0.34
Julianalaan 52	0.43	0.64	1.08	1.08	1.08	0.15
E45 Schildewolde	0.20	0.37	0.48	0.88	1.02	0.17
Wilgenbros	0.28	0.43	0.85	0.94	1.13	0.17
Oostergoweg	0.22	0.36	0.44	0.73	0.91	0.16
Koeriersterweg	0.23	0.42	0.53	1.03	1.15	0.32
Schuitenzandflat 2-56	0.38	0.62	0.97	1.10	1.21	0.35
Zijlvest 25	0.05	0.13	0.42	0.77	0.86	0.31
E45 Delfzij	0.14	0.27	0.63	0.69	0.86	0.21

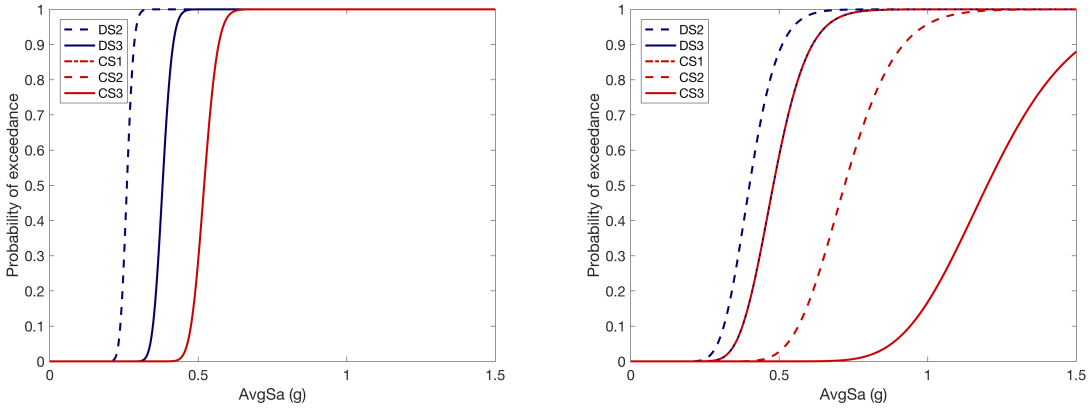

(a) De Haver barn (URM1F_B)

(b) De Haver house (URM1F_HC)

Figure 5.1 Fragility functions for the De Haver barn and house index building models

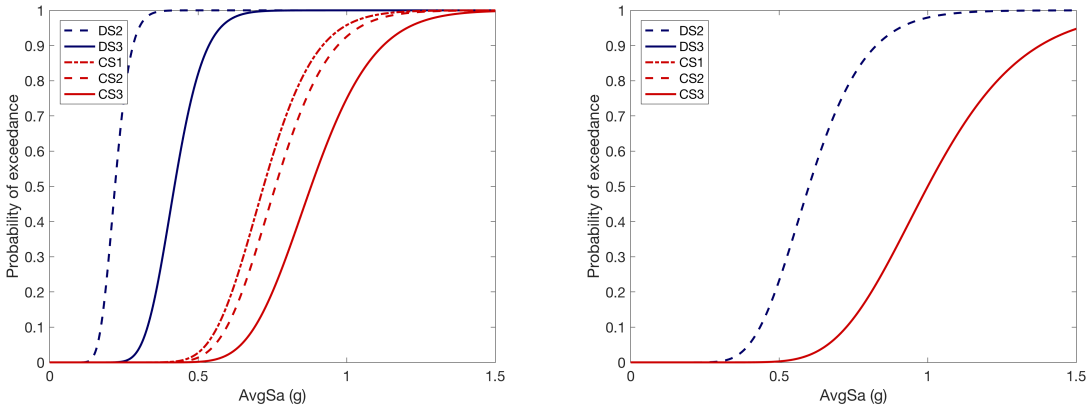

(a) Molenweg 25 barn (URM1F_B) **(b)** Molenweg 25 house (URM1F_HC)

Figure 5.2 Fragility functions for the Molenweg 25 barn and house index building models

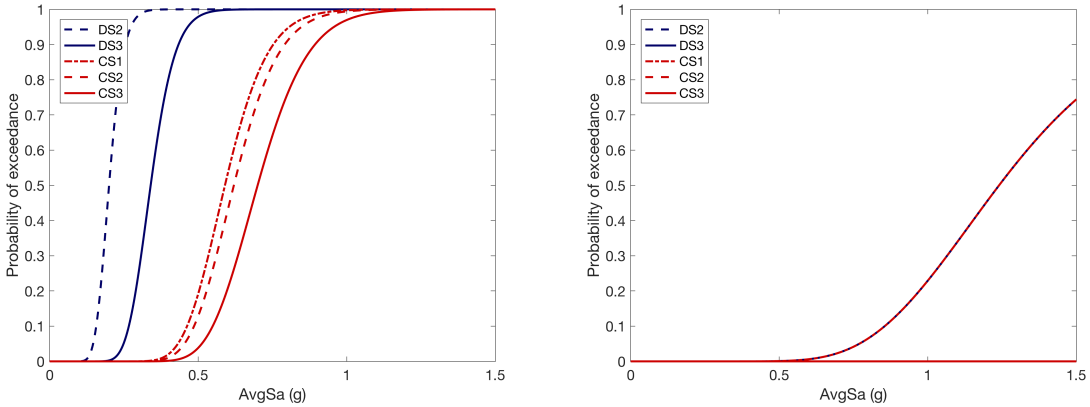

(a) Molenweg 29 barn (URM1F_B) **(b)** Molenw. 29 house (URM1F_HA)

Figure 5.3 Fragility functions for the Molenweg 29 barn and house index building models

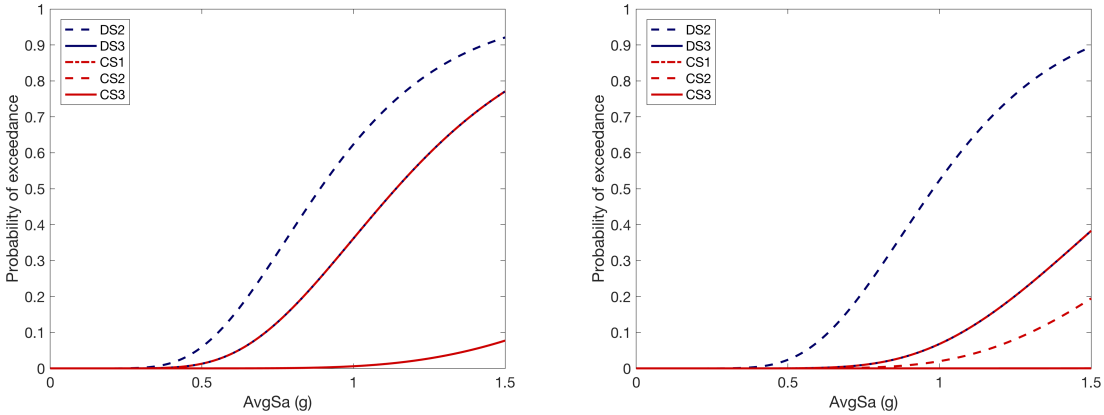

(a) Eestumerweg 51 barn (URM1F_B) **(b)** Eestumerw. 51 house (URM1F_HA)

Figure 5.4 Fragility functions for the Eestumerweg 51 barn and house index building models

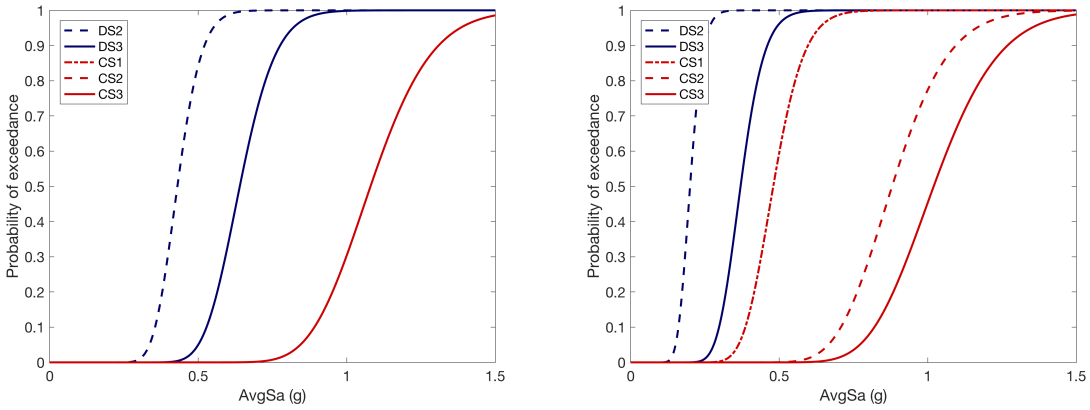

(a) Julianalaan 52 (URM3L) **(b)** E45 Schildwolde (URM3L)

Figure 5.5 Fragility functions for the Julianalaan 52 and E45 Schildwolde index building models

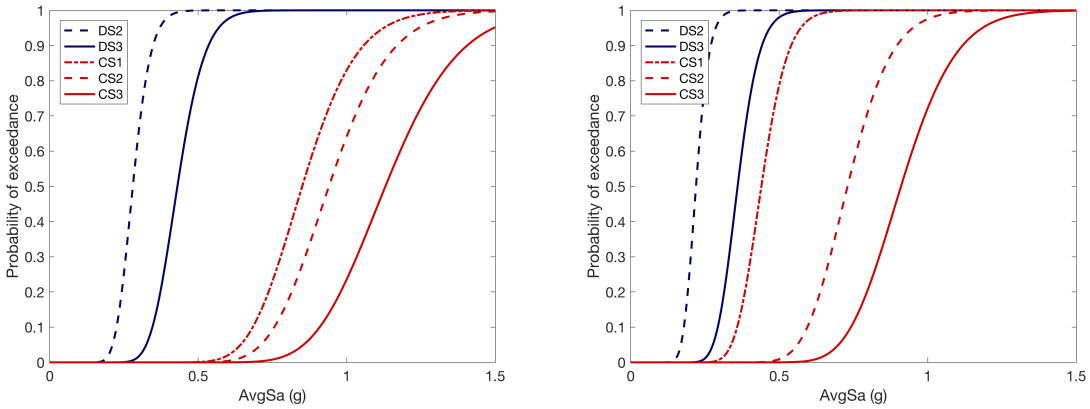

(a) Wilgenbros (URM3L) **(b)** Oostergoweg (URM3L)

Figure 5.6 Fragility functions for the Wilgenbros and Oostergoweg index building models

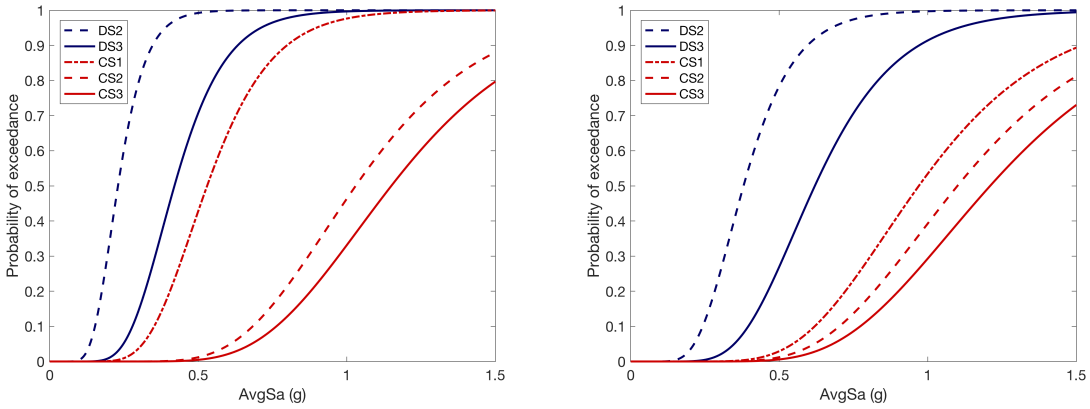

(a) Koeriersterweg (URM3M_U) **(b)** Schuitenzandflat (URM3M_B)

Figure 5.7 Fragility functions for the Koeriersterweg and Schuitenzandflat 2-56 index building models

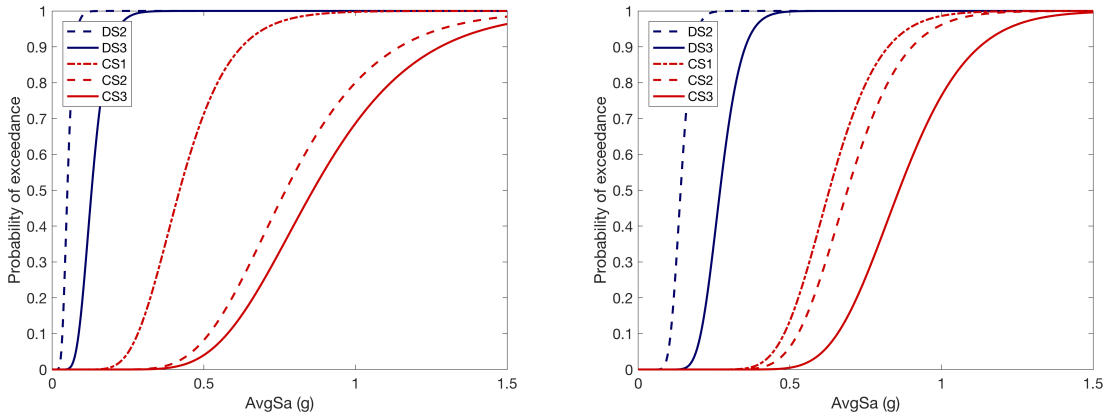

(a) Zijlvest 25 (URM4L)

(b) E45 Delfzijl (URM4L)

Figure 5.8 Fragility functions for the Zijlvest and E45 Delfzijl index building models

5.5 Fatality Models

Readers are referred to the v6 report (Crowley et al. 2019b) for more details on the methodology used to develop the fatality models. Table 5.4 presents the values of inside and outside collapse debris that has been observed/assumed for each of the updated/additional index models.

Table 5.4 Inside and outside collapse debris ratios per collapse state for the updated/additional index buildings

Index Building	M4+M5(1-M4)	α_{inCS1}	α_{inCS2}	α_{inCS3}	α_{outCS1}	α_{outCS2}	α_{outCS3}
De Haver barn	0.315	1.000	1.000	1.000	0.200	0.200	0.200
De Haver house	0.42	0.050	0.125	0.700	0.013	0.031	0.250
Molenweg 25 barn	0.315	0.300	0.500	1.000	0.060	0.100	0.200
Molenweg 25 house	0.42	1.000	1.000	1.000	0.250	0.250	0.250
Molenweg 29 barn	0.315	0.050	0.200	1.000	0.010	0.040	0.200
Molenweg 29 house	0.42	0.300	0.300	0.700	0.075	0.075	0.250
Eestumerweg 51 25 barn	0.315	0.050	1.000	1.000	0.010	0.200	0.200
Eestumerweg 51 house	0.42	0.100	0.600	1.000	0.025	0.150	0.250
Julianalaan	0.42	1.000	1.000	1.000	0.500	0.500	0.500
E45 Schildewolde	0.42	0.150	0.380	1.000	0.075	0.190	0.500
Wilgenbros	0.42	0.300	0.360	1.000	0.150	0.180	0.500
Oostergoweg	0.42	0.040	0.060	1.000	0.020	0.030	0.500
Koeriersterweg	0.42	0.025	0.039	1.000	0.040	0.063	0.670
Schuitenzandflat	0.42	0.004	0.010	1.000	0.002	0.005	0.200
Zijlvest	0.42	0.020	0.050	1.000	0.010	0.025	0.500
E45 Delfzijl	0.42	0.020	0.090	1.000	0.010	0.045	0.500

Chapter 6

Final Fragility and Fatality Models for Vulnerabilty Classes

6.1 Methodology

The previous chapter presented the fragility and consequence models for each of the updated/additional index buildings, however, as described in Chapter 2, in some cases more than one index building represents a vulnerability class. The combination of the results of the index buildings to produce the final fragility and consequence models for the vulnerability classes is described in this section.

6.1.1 Combination of index buildings

For a given vulnerability class, the fatality vulnerability functions (obtained by combining the fragility and fatality ratios for each collapse state) for each index building have been calculated and combined considering the weights of each index building (in the case of more than one index building per class; see Arup 2019a). Maximum likelihood estimation has then been used to fit lognormal parameters to this weighted vulnerability function (see Figure 6.1). However, separate inputs for fragility and fatality functions (rather than vulnerability functions) need to be provided to the risk engine (for damage and collapse results), it has been necessary to back-calculate fragility and fatality models that represent the class. Given that different index buildings within a given class have different collapse states, which increases the complexity of the process, a single collapse state of 100 $\%$ has instead been considered for the vulnerability class, and the corresponding fragility function has been calculated. The cloud regression parameters have then been calculated by assuming that b_0 is given by the average of the b_0 values from the index buildings, and then the b_1 and σ_s values are back-calculated. Table 6.1 shows the collapse (CS3) fragility functions that have been obtained for the updated/additional vulnerabilty classes.

Table 6.1 Collapse (CS3) fragility functions for updated/additional vulnerability classes

Vulnerability Class	Index buildings	e^{μ} (median CS3)	β
URM1F_B	De Haver (25%), Molenweg 25 (34%), Molenweg 29 (23%), Eestumerweg 51 (18%)	0.62	0.155
URM1F_HA	Molenweg 29 (50%), Eestumerweg 51 (50%)	2.58	0.471
URM1F_HC	De Haver (50%), Molenweg 25 (50%)	1.12	0.346
URM3L	Julianalaan 52 (50%), E45 Schildwolde (50%), Wilgenbros (50%), Oostergoweg (50%)	0.99	0.280
URM4L	Zijlvest 25 (50%), E45 Delfzijl (50%)	0.84	0.277
URM3M_B	Sflat (100%)	1.03	0.35
URM3M_U	KFlat (100%)	0.98	0.33

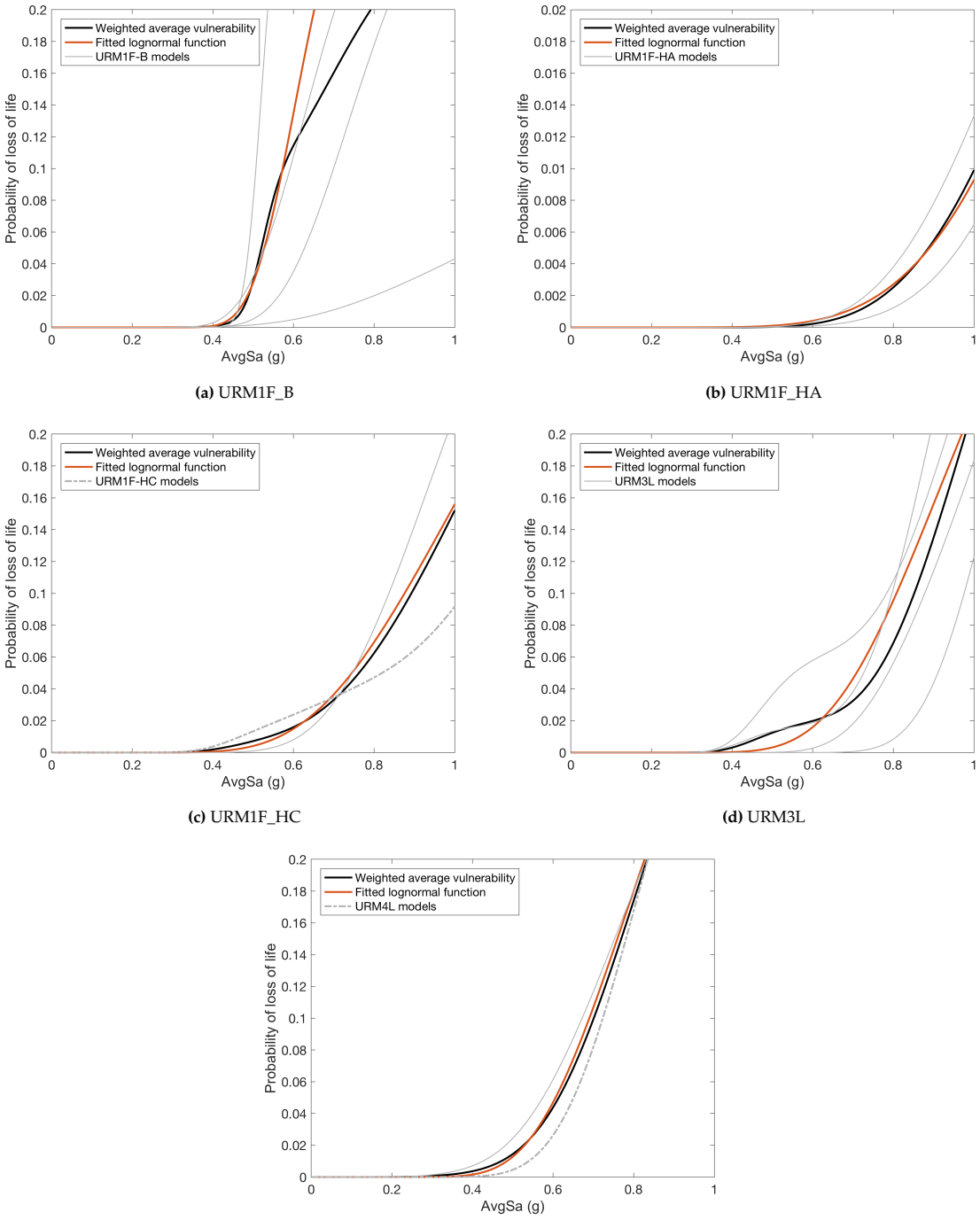

(a) URM1F_B

(b) URM1F_HA

(c) URM1F_HC

(d) URM3L

(e) URM4L

Figure 6.1 Weighted vulnerability functions and corresponding fitted lognormal function for classes with more than one index building, shown up to AvgSa of 1g (which corresponds to a return period of more than 100k years)

6.1.2 Within-building and between-building variability

The fragility functions presented in Table 6.1 have been calculated with deterministic index buildings and thus only include record-to-record variability (β_R). Additional sources of uncertainty that need to be considered are the within building ($\beta_{B-inter}$) and between building ($\beta_{B-intra}$) variability; it is then typically assumed that the total variability in the lognormal fragility functions can be described by the square root sum of squares (SRSS) of these three main components of dispersion:

$$\beta_s = \sqrt{\beta_R^2 + \beta_{B-inter}^2 + \beta_{B-intra}^2} \tag{6.1}$$

A study carried out by Arup (2019e and 2019f) to estimate fragility functions from MDOF models (for buildings falling within the URM3L and URM4L classes) has shown that a disperion of 0.3 can be used to represent the between building variability, whilst the inclusion of the within building variability, on the other hand, was found to lead to only a negligible increase in the total variability. Instead, the parametric study highlighted that when parameter uncertainty is explicitly accounted for, there is a reduction in the median collapse capacity, a result that has also been observed in other endeavours that have looked at the influence of parameter uncertainty on the median collapse intensity (e.g. Gokkaya et al., 2016; Dolsek 2009; Liel et al., 2009, Vamvatsikos and Fragiadakis 2010). Vamvatsikos and Fragiadakis (2010) noted that this is a result of the fact that structures can be considerd as a series system of collapse mechanisms and the weakest link will always cause collapse, and so the possibility of sampling an unusually weak component in the structural system results will lead to a reduction in the median collapse intensity with respect to the deterministic model. Thus, the fragility functions presented in Table 6.1 have been adjusted to account for the parameter uncertainty bias (reduction of 15 % of the median collapse capacity) and additional between building variability (dispersion of 0.3) obtained by Arup, leading to the fragility function parameters given in Table 6.2.

Table 6.2 Final collapse (CS3) fragility functions for updated/additional index buildings

Vulnerability Class	Index buildings	e^{μ} (median CS3)	β
URM1F_B	De Haver (25%), Molenweg 25 (34%), Molenweg 29 (23%), Eestumerweg 51 (18%)	0.52	0.338
URM1F_HA	Molenweg 29 (50%), Eestumerweg 51 (50%)	2.19	0.560
URM1F_HC	De Haver (50%), Molenweg 25 (50%)	0.95	0.460
URM3L	Julianalaan 52 (50%), E45 Schildwolde (50%), Wilgenbros (50%), Oostergoweg (50%)	0.84	0.410
URM4L	Zijlvest 25 (50%), E45 Delfzijl (50%)	0.71	0.410
URM3M_B	Sflat (100%)	1.03	0.46
URM3M_U	KFlat (100%)	0.98	0.44

6.1.3 Model uncertainty

Additional model uncertainty associated with the selected modelling approach (e.g. the uncertainty related to the use of the current version of LS-DYNA to model the collapse capacity of URM structures) also needs to be accounted for in the final set of fragility functions.

In order to account for model uncertainty, the approach adopted in v5 and v6 is being maintained, whereby the recommendations from FEMA P-58 (FEMA, 2012) are used, with a value of dispersion (β_m) equal to 0.27 for URM buidlings and 0.47 for non-URM buildings, given the increased effort placed on calibrating the modelling technique for URM buildings.

However, given that the dispersion in model uncertainty can be correlated for all the buildings belonging to a given vulnerability class, it is not modelled as an aleatory variable in the risk engine, but rather through the use of a logic tree to allow different correlations of this uncertainty to be more easily investigated. For computational efficiency, only three branches have been considered on the logic tree, and hence the model uncertainty dispersion has been modelled as a discrete three-point distribution.

The values of dispersion for URM and non-URM buildings described above have been used to produce a three-point discrete distribution (in terms of number of standard deviations and associated probabilities) following the approach given in Miller and Rice (1983). These three levels

of model uncertainty dispersion (corresponding to standard deviations of -1.73, 0 and 1.73) have then been used to produce lower, middle and upper fragility models with associated weights (w) given by the discrete probabilities of each level (i.e. 0.17, 0.66 and 0.17), as illustrated in Figure 6.2.

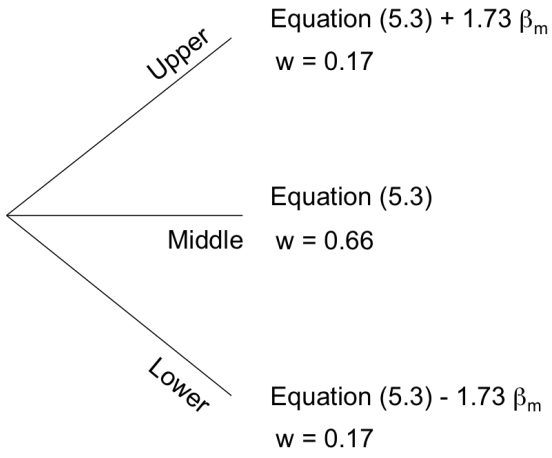

Figure 6.2 Fragility model logic tree used for each vulnerability class

An important consideration has been made when applying the logic tree, which is that the fragility and fatality models obtained for the vulnerability classes using the procedure outlined in this Chapter do not represent the best-estimate models for collapse, but are instead upper bound models. This judgment has been made from our knowledge that numerical models tend to underestimate the ultimate capacity of buildings, as also demonstrated in the many blind prediction exercises that have been carried out (Arup et al., 2015; 2016a; 2016b; 2017). However, for damage assessment such underestimation has not been observed and thus it would appear reasonable to put the damage fragility functions on the best-estimate central branch. Given the limited time available to run the HRA2020 calculations, it has not been possible to provide two different sets of inputs for the damage and collapse fragility, hence a correction has been made to take the mean minus 1 standard deviation drift thresholds (as presented previously in Section 5.2) for the damage fragility functions, to avoid underestimating the probability of damage. These two modelling assumptions have been checked through validation exercises, as presented in Chapter 7.

6.2 Final Fragility and Fatality Models

Table 6.3 presents the input parameters required by the HRA risk engine for all vulnerability classes (with v7 used to identify those updated based on the analyses provided herein), and Tables 6.4, 6.5 and 6.6 present the final fatality model logic tree input parameters.

Table 6.3 Final fragility function inputs for all vulnerability classes in terms of AvgSa

Vulnerability Class	Lower b_0	Middle b_0	Upper b_0	b_1	σ_s	DS2 (m)	DS3 (m)	CS1 (m)	CS2 (m)	CS3 (m)	Version
RC1L	-3.062	-2.249	-1.436	1.195	0.4878	0.0183	0.0293	0.1830	0.1830	0.1830	v6
RC1M	-3.061	-2.248	-1.434	0.931	0.5192	0.0309	0.0492	0.3050	0.3050	0.3050	v6
RC1H	-3.088	-2.275	-1.462	0.801	0.6386	0.0439	0.0702	0.4390	0.4390	0.4390	v6
RC2	-3.094	-2.280	-1.467	0.892	0.5923	0.0260	0.0416	0.2180	0.2180	0.2180	v6
PC2	-3.091	-2.278	-1.465	0.856	0.5919	0.0260	0.0416	0.2180	0.2180	0.2180	v6
RC3L	-2.892	-2.079	-1.266	1.271	0.4780	0.0361	0.0565	0.1236	0.1236	0.2260	v6
RC3M	-2.984	-2.171	-1.358	0.932	0.4997	0.0484	0.0757	0.1802	0.1802	0.3020	v6
RC3H	-2.887	-2.073	-1.260	0.879	0.6489	0.0723	0.1130	0.3624	0.3624	0.4520	v6
PC3L	-3.526	-2.713	-1.899	2.338	0.5003	0.0058	0.0205	0.0711	0.0711	0.1300	v6
PC3M	-3.098	-2.285	-1.472	1.983	0.4645	0.0077	0.0275	0.1032	0.1032	0.1730	v6
PC3H	-2.725	-1.912	-1.096	1.339	0.3329	0.0115	0.0411	0.2085	0.2085	0.2600	v6
W2	-3.055	-2.242	-1.429	1.271	0.4691	0.0176	0.0434	0.3290	0.3290	0.3290	v6
W3	-4.002	-3.189	-2.376	1.694	0.5188	0.0088	0.0217	0.1200	0.1200	0.1200	v6
S1L	-2.725	-1.912	-1.099	0.953	0.6107	0.0301	0.0476	0.4700	0.4700	0.4700	v6
S1H	-2.799	-1.985	-1.172	0.843	0.7889	0.0401	0.0639	0.6280	0.6280	0.6280	v6
S1M	-2.841	-2.028	-1.215	0.929	0.8134	0.0602	0.0953	0.9420	0.9420	0.9420	v6
S2L	-3.051	-2.238	-1.425	1.274	0.4695	0.0219	0.0351	0.2190	0.2190	0.2190	v6
S2H	-3.037	-2.224	-1.411	0.861	0.5091	0.0370	0.0590	0.3660	0.3660	0.3660	v6
S2M	-2.973	-2.159	-1.346	0.778	0.6775	0.0571	0.0913	0.5700	0.5700	0.5700	v6
S3	-5.917	-5.104	-4.291	1.081	0.5736	0.0122	0.0194	0.2950	0.2950	0.2950	v6
URM1F_B	-2.933	-2.466	-1.999	2.815	0.9506	0.0013	0.0053	0.0220	0.0220	0.0220	v7
URM1F_HA	-5.412	-4.945	-4.478	1.605	0.8957	0.0013	0.0053	0.0400	0.0400	0.0400	v7
URM1F_HC	-3.945	-3.478	-3.011	2.283	1.0447	0.0017	0.0067	0.0440	0.0440	0.0440	v7
URM2L	-3.149	-2.682	-2.215	1.462	0.4385	0.0068	0.0164	0.0380	0.0960	0.1230	v6
URM3L	-3.400	-2.933	-2.466	2.956	1.2128	0.0021	0.0085	0.0510	0.0510	0.0510	v7
URM3M_U	-2.922	-2.455	-1.988	2.262	1.0038	0.0033	0.0134	0.0230	0.1020	0.1310	v7
URM3M_D	-2.812	-2.345	-1.878	1.963	0.6633	0.0057	0.0137	0.0770	0.0770	0.0890	v6
URM3M_B	-2.958	-2.491	-2.024	2.873	1.3290	0.0052	0.0210	0.0750	0.1080	0.1440	v7
URM4L	-2.642	-2.175	-1.708	1.795	0.7329	0.0019	0.0077	0.0990	0.0990	0.0990	v7
URM5L	-5.039	-4.572	-4.105	2.159	0.7378	0.0036	0.0087	0.0110	0.0110	0.0170	v6
URM6L	-5.137	-4.670	-4.203	2.466	0.8540	0.0034	0.0083	0.0520	0.0520	0.0520	v6
URM7L	-5.320	-4.853	-4.385	2.376	0.8642	0.0035	0.0080	0.0080	0.0320	0.0560	v6
URM8L	-4.548	-4.081	-3.614	2.037	0.6885	0.0020	0.0020	0.0020	0.0020	0.0200	v6
URM9L	-2.810	-2.342	-1.875	1.491	0.4475	0.0084	0.0204	0.0410	0.1150	0.1540	v6
URM10	-5.137	-4.670	-4.203	2.466	0.8540	0.0034	0.0083	0.0520	0.0520	0.0520	v6

Table 6.4 Final lower branch fatality ratios per collapse state for all vulnerability classes

Vulnerability Class	α_{inCS1}	α_{inCS2}	α_{inCS3}	α_{outCS1}	α_{outCS2}	α_{outCS3}	Version
RC1L	0.0640	0.0640	0.0640	0.0208	0.0208	0.0208	v6
RC1M	0.0492	0.0492	0.0492	0.0160	0.0160	0.0160	v6
RC1H	0.0246	0.0246	0.0246	0.0080	0.0080	0.0080	v6
RC2	0.0640	0.0640	0.0640	0.0208	0.0208	0.0208	v6
PC2	0.0640	0.0640	0.0640	0.0208	0.0208	0.0208	v6
RC3L	0.1082	0.1082	0.4920	0.0352	0.0352	0.1600	v6
RC3M	0.0541	0.0541	0.2460	0.0176	0.0176	0.0800	v6
RC3H	0.0271	0.0271	0.1230	0.0088	0.0088	0.0400	v6
PC3L	0.1082	0.1082	0.4920	0.0352	0.0352	0.1600	v6
PC3M	0.0541	0.0541	0.2460	0.0176	0.0176	0.0800	v6
PC3H	0.0271	0.0271	0.1230	0.0088	0.0088	0.0400	v6
W2	0.0050	0.0050	0.0050	0.0048	0.0048	0.0048	v6
W3	0.0050	0.0050	0.0050	0.0048	0.0048	0.0048	v6
S1L	0.0394	0.0394	0.0394	0.0128	0.0128	0.0128	v6
S1H	0.0246	0.0246	0.0246	0.0080	0.0080	0.0080	v6
S1M	0.0148	0.0148	0.0148	0.0048	0.0048	0.0048	v6
S2L	0.0394	0.0394	0.0394	0.0128	0.0128	0.0128	v6
S2H	0.0246	0.0246	0.0246	0.0080	0.0080	0.0080	v6
S2M	0.0148	0.0148	0.0148	0.0048	0.0048	0.0048	v6
S3	0.0148	0.0148	0.0148	0.0048	0.0048	0.0048	v6
URM1F_B	0.2016	0.2016	0.2016	0.1280	0.1280	0.1280	v7
URM1F_HA	0.2688	0.2688	0.2688	0.1600	0.1600	0.1600	v7
URM1F_HC	0.2688	0.2688	0.2688	0.1600	0.1600	0.1600	v7
URM2L	0.0000	0.0000	0.3360	0.0267	0.0533	0.4000	v6
URM3L	0.2688	0.2688	0.2688	0.3200	0.3200	0.3200	v7
URM3M_U	0.0161	0.0253	0.2688	0.0257	0.0403	0.4288	v7
URM3M_D	0.0202	0.0202	0.3360	0.0320	0.0320	0.5333	v6
URM3M_B	0.0027	0.0070	0.2688	0.0013	0.0033	0.1280	v7
URM4L	0.2688	0.2688	0.2688	0.3200	0.3200	0.3200	v7
URM5L	0.1680	0.1680	0.3360	0.2000	0.2000	0.4000	v6
URM6L	0.3360	0.3360	0.3360	0.2000	0.2000	0.2000	v6
URM7L	0.0000	0.0084	0.3360	0.0080	0.0080	0.2000	v6
URM8L	0.0000	0.0000	0.3360	0.0480	0.0800	0.2000	v6
URM9L	0.0084	0.0168	0.3360	0.0050	0.0100	0.4000	v6
URM10	0.3360	0.3360	0.3360	0.2000	0.2000	0.2000	v6

Table 6.5 Final middle branch fatality ratios per collapse state for all vulnerability classes

Vulnerability Class	α_{inCS1}	α_{inCS2}	α_{inCS3}	α_{outCS1}	α_{outCS2}	α_{outCS3}	Version
RC1L	0.0800	0.0800	0.0800	0.0260	0.0260	0.0260	v6
RC1M	0.0615	0.0615	0.0615	0.0200	0.0200	0.0200	v6
RC1H	0.0308	0.0308	0.0308	0.0100	0.0100	0.0100	v6
RC2	0.0800	0.0800	0.0800	0.0260	0.0260	0.0260	v6
PC2	0.0800	0.0800	0.0800	0.0260	0.0260	0.0260	v6
RC3L	0.1353	0.1353	0.6150	0.0440	0.0440	0.2000	v6
RC3M	0.0677	0.0677	0.3075	0.0220	0.0220	0.1000	v6
RC3H	0.0338	0.0338	0.1538	0.0110	0.0110	0.0500	v6
PC3L	0.1353	0.1353	0.6150	0.0440	0.0440	0.2000	v6
PC3M	0.0677	0.0677	0.3075	0.0220	0.0220	0.1000	v6
PC3H	0.0338	0.0338	0.1538	0.0110	0.0110	0.0500	v6
W2	0.0063	0.0063	0.0063	0.0060	0.0060	0.0060	v6
W3	0.0063	0.0063	0.0063	0.0060	0.0060	0.0060	v6
S1L	0.0492	0.0492	0.0492	0.0160	0.0160	0.0160	v6
S1H	0.0308	0.0308	0.0308	0.0100	0.0100	0.0100	v6
S1M	0.0185	0.0185	0.0185	0.0060	0.0060	0.0060	v6
S2L	0.0492	0.0492	0.0492	0.0160	0.0160	0.0160	v6
S2H	0.0308	0.0308	0.0308	0.0100	0.0100	0.0100	v6
S2M	0.0185	0.0185	0.0185	0.0060	0.0060	0.0060	v6
S3	0.0185	0.0185	0.0185	0.0060	0.0060	0.0060	v6
URM1F_B	0.2520	0.2520	0.2520	0.1600	0.1600	0.1600	v7
URM1F_HA	0.3360	0.3360	0.3360	0.2000	0.2000	0.2000	v7
URM1F_HC	0.3360	0.3360	0.3360	0.2000	0.2000	0.2000	v7
URM2L	0.0000	0.0000	0.4200	0.0333	0.0667	0.5000	v6
URM3L	0.3360	0.3360	0.3360	0.4000	0.4000	0.4000	v7
URM3M_U	0.0202	0.0316	0.3360	0.0322	0.0504	0.5360	v7
URM3M_D	0.0252	0.0252	0.4200	0.0400	0.0400	0.6667	v6
URM3M_B	0.0034	0.0087	0.3360	0.0016	0.0042	0.1600	v7
URM4L	0.3360	0.3360	0.3360	0.4000	0.4000	0.4000	v7
URM5L	0.2100	0.2100	0.4200	0.2500	0.2500	0.5000	v6
URM6L	0.4200	0.4200	0.4200	0.2500	0.2500	0.2500	v6
URM7L	0.0000	0.0105	0.4200	0.0100	0.0100	0.2500	v6
URM8L	0.0000	0.0000	0.4200	0.0600	0.1000	0.2500	v6
URM9L	0.0105	0.0210	0.4200	0.0063	0.0125	0.5000	v6
URM10	0.4200	0.4200	0.4200	0.2500	0.2500	0.2500	v6

Table 6.6 Final upper branch fatality ratios per collapse state for all vulnerability classes

Vulnerability Class	α_{inCS1}	α_{inCS2}	α_{inCS3}	α_{outCS1}	α_{outCS2}	α_{outCS3}	Version
RC1L	0.0959	0.0959	0.0959	0.0312	0.0312	0.0312	v6
RC1M	0.0738	0.0738	0.0738	0.0240	0.0240	0.0240	v6
RC1H	0.0369	0.0369	0.0369	0.0120	0.0120	0.0120	v6
RC2	0.0959	0.0959	0.0959	0.0312	0.0312	0.0312	v6
PC2	0.0959	0.0959	0.0959	0.0312	0.0312	0.0312	v6
RC3L	0.1624	0.1624	0.7380	0.0528	0.0528	0.2400	v6
RC3M	0.0812	0.0812	0.3690	0.0264	0.0264	0.1200	v6
RC3H	0.0406	0.0406	0.1845	0.0132	0.0132	0.0600	v6
PC3L	0.1624	0.1624	0.7380	0.0528	0.0528	0.2400	v6
PC3M	0.0812	0.0812	0.3690	0.0264	0.0264	0.1200	v6
PC3H	0.0406	0.0406	0.1845	0.0132	0.0132	0.0600	v6
W2	0.0076	0.0076	0.0076	0.0072	0.0072	0.0072	v6
W3	0.0076	0.0076	0.0076	0.0072	0.0072	0.0072	v6
S1L	0.0590	0.0590	0.0590	0.0192	0.0192	0.0192	v6
S1H	0.0369	0.0369	0.0369	0.0120	0.0120	0.0120	v6
S1M	0.0221	0.0221	0.0221	0.0072	0.0072	0.0072	v6
S2L	0.0590	0.0590	0.0590	0.0192	0.0192	0.0192	v6
S2H	0.0369	0.0369	0.0369	0.0120	0.0120	0.0120	v6
S2M	0.0221	0.0221	0.0221	0.0072	0.0072	0.0072	v6
S3	0.0221	0.0221	0.0221	0.0072	0.0072	0.0072	v6
URM1F_B	0.3150	0.3150	0.3150	0.2000	0.2000	0.2000	v7
URM1F_HA	0.4200	0.4200	0.4200	0.2500	0.2500	0.2500	v7
URM1F_HC	0.4200	0.4200	0.4200	0.2500	0.2500	0.2500	v7
URM2L	0.0000	0.0000	0.5040	0.0400	0.0800	0.6000	v6
URM3L	0.4200	0.4200	0.4200	0.5000	0.5000	0.5000	v7
URM3M_U	0.0252	0.0395	0.4200	0.0402	0.0630	0.6700	v7
URM3M_D	0.0302	0.0302	0.5040	0.0480	0.0480	0.8000	v6
URM3M_B	0.0042	0.0109	0.4200	0.0020	0.0052	0.2000	v7
URM4L	0.4200	0.4200	0.4200	0.5000	0.5000	0.5000	v7
URM5L	0.2520	0.2520	0.5040	0.3000	0.3000	0.6000	v6
URM6L	0.5040	0.5040	0.5040	0.3000	0.3000	0.3000	v6
URM7L	0.0000	0.0126	0.5040	0.0120	0.0120	0.3000	v6
URM8L	0.0000	0.0000	0.5040	0.0720	0.1200	0.3000	v6
URM9L	0.0126	0.0252	0.5040	0.0075	0.0150	0.6000	v6
URM10	0.4200	0.4200	0.4200	0.5000	0.5000	0.5000	v6

Chapter 7

Validation

7.1 Structural Modelling Software

Before presenting a number of specific verification tests of the models presented herein, it is worth recalling that the software tools that have been used to develop the numerical models of the URM buildings have been validated for seismic analysis of Groningen buildings using the results of a large number of experimental tests (e.g. Graziotti et al., 2016a; 2016b; 2017a; 2017b; 2018; 2019; Tomassetti et al., 2019; Correia et al., 2018; Kallioras et al., 2018; 2019b; Miglietta et al., 2018) as documented in Mosayk (2016; 2017a; 2017b; 2017c; 2017e; 2019a), Malomo et al. (2018; 2019; 2020a; 2020b) and Arup et al. (2015; 2016a; 2016b; 2017).

7.2 Backbone Curves

7.2.1 Experimental Test

The v5 report compared the backbone curves of some of the vulnerability classes with those from experimental tests, and good agreement was found (see Crowley and Pinho, 2017). In the v6 report a blind prediction of the EUC-BUILD6 shaking table test (Miglietta et al., 2018) was undertaken using the URM4L model (based on the Zijlvest index building). Given that this model has been modified in this report and that there are now two URM4L index buildings to represent this class (Zijlvest and E45 Delfzijl), a post-diction has been carried out to ensure that these models still give consistent results with respect to the test. Figure 7.1 shows the results of the post-diction in terms of base shear versus attic displacement and the PGA level versus SDOF displacement (calculated using the transformation method presented in Section 3.1.1) for the two index buildings.

The EUC-BUILD6 shake-table test was run to 0.4g where it reached an attic dispacement of 99 mm and was deemed to be 'near collapse'. In the post-diction the Zijlvest model reached an attic displacement of 73 mm under a PGA of 0.4g, whereas E45 Delfzijl reached 58 mm under the same level of ground shaking. When comparing the results it should be considered that the experimental tests account for cumulative damage whereas this has not been considered with the SDOF models. This can explain why the levels of displacement under each level of PGA are lower than those of the test (as shown in Figure 7.1). The cumulative loading could also have led to a reduction in the maximum base shear observed in the test. The results nevertheless show that the two index

building models bound the results of the test in terms of base shear capacity, and similar (though, as expected, lower) levels of displacement are reached.

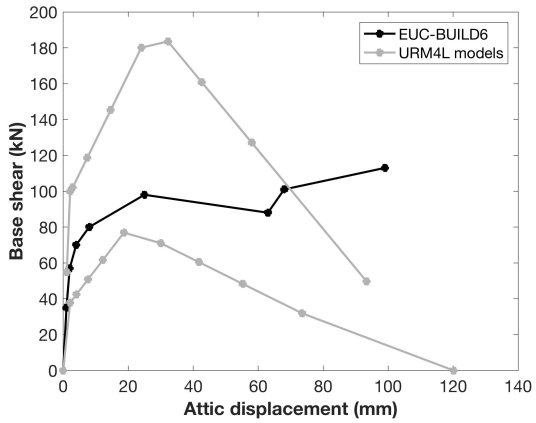

(a) Base shear vs. attic displacement plot

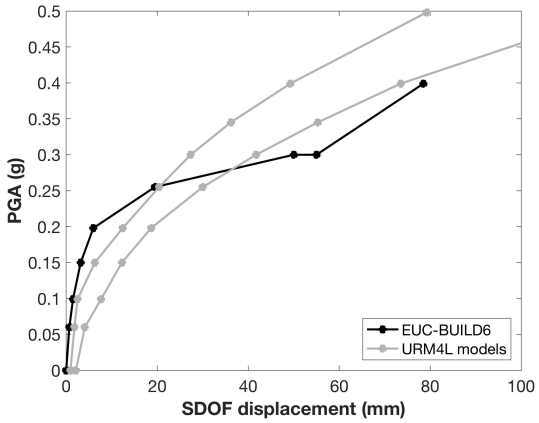

(b) PGA vs. SDOF displacement plot

Figure 7.1 Post-diction of the EUC-BUILD6 shake-table test using URM4L models

7.2.2 Collapse Displacement

The backbone SDOF models have been calibrated using 11 training records that were applied to the MDOF models, as described in Chapter 3. For a number of the MDOF models, the 100 v7 records described in Chapter 4 were applied and so it has been possible to make a comparison between the number of collapses predicted with the SDOF and the MDOF models. The results for three index buildings are presented in Table 7.1 and they show that similar numbers of collapses are predicted, though with a slightly lower prediction with the SDOF model for Zijlvest. These results nevertheless indicate that the backbone curve obtained from the 11 training records appears to be reasonable for the purposes of developing collapse fragility functions.

Table 7.1 Comparison of number of collapses in MDOF and SDOF models

	10k yrs		100k yrs		Total	
Index building	SDOF	MDOF	SDOF	MDOF	SDOF	MDOF
Zijlvest	9	11	30	40	39	51
Wilgenbros	0	0	7	5	7	5
Oostergoweg	0	3	27	27	27	30

7.3 Fragility Functions

7.3.1 MDOF Models

Global collapse fragility functions using the MDOF models have been developed for six index buildings: Zijlvest 25, E45 Schildwolde, E45 Delfzijl, Wilgenbros, Oostergoweg, and Molenweg 29, as described in Arup (2019f). The MDOF and SDOF fragility functions for the index buildings (accounting just for the record-to-record variability) are compared in Figure 7.2. It is noted that the lack of collapses in the Wilgenbros building under the 10k year ground motions (see Table 7.1) meant that it was not possible to derive a fragility function with the deterministic MDOF model,

and so it has not been compared in these figures. These comparisons show very similar median values for all index buildings except E45 Delfzijl (where the SDOF model is more fragile for higher levels of ground motion), but in most cases the dispersion of the SDOF model is lower. However, as mentioned in Chapter 6, the dispersion of the fragility functions for the vulnerability classes is obtained by combining the index buildings and adding an additional component of dispersion to account for between building variability ($\beta_{B-intra}$).

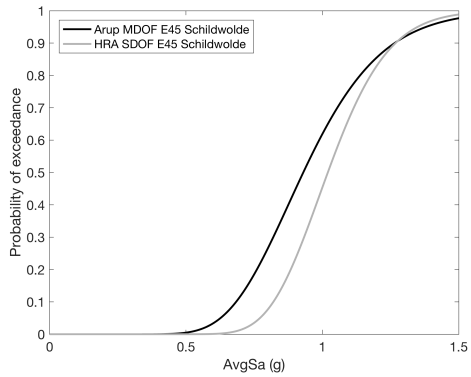

(a) E45 Schildwolde

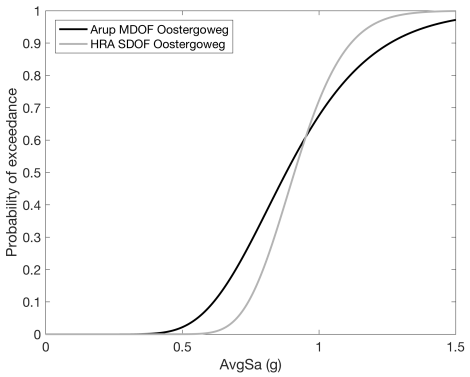

(b) Oostergoweg

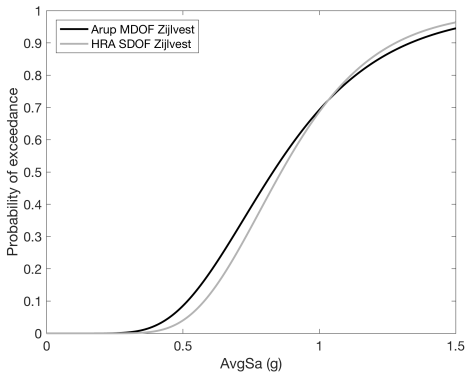

(c) Zijlvest 25

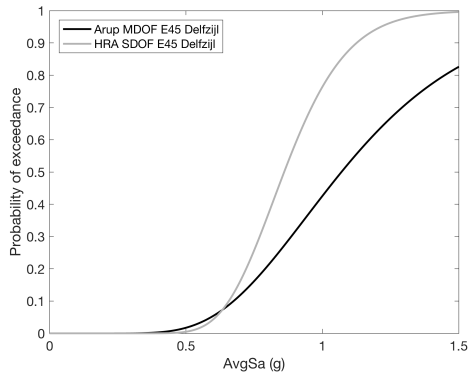

(d) E45 Delfzijl

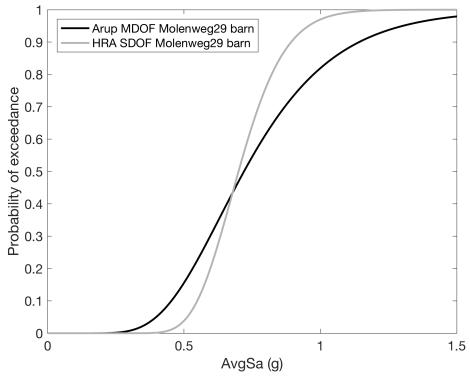

(e) Molenweg 29

Figure 7.2 Comparison of MDOF and SDOF fixed base global collapse fragility functions for deterministic index buildings

In their report, Arup (2019f) also provide combined fragility functions for URM3L and URM4L which account for all sources of uncertainty and are based on combining the fragility functions of the index buildings in each vulnerability class. A comparison of the MDOF and SDOF fragility functions for URM3L and URM4L is thus provided in Table 7.2, which shows that the final functions have similar

levels of dispersion. It is noted that the URM3L SDOF model includes an additional index building (Julianalaan 52) which was not accounted for in the values from Arup, which might explain the larger median value for the SDOF model.

Table 7.2 Comparison of global collapse fragility function parameters for MDOF and SDOF vulnerability classes

	e^{μ}		β	
Vulnerability Class	SDOF	MDOF	SDOF	MDOF
URM3L	0.84	0.71	0.41	0.39
URM4L	0.71	0.64	0.41	0.47

7.3.2 Comparison with published models

The v6 report showed a comparison of the URM fragility functions with models from the literature and similar plots have been obtained when using the updated results of this report, and so this figure has not been repeated herein. An updated comparison with the model from the independent study by Kallioras et al. (2019c) is instead provided, as the results for this vulnerability classes (URM3L) have been extensively updated.

Kallioras et al. (2018b) proposed fragility functions for modern terraced units from the Groningen region, using the experimental test results from EUC-BUILD1 (Graziotti et al., 2016a). The fragility functions for the three branches of the logic tree for URM3L have been converted to PGA by multiplying the AvgSa by 0.65, as this was found to be the ratio between PGA and AvgSa for the selected records used to develop the fragility functions. These are compared with the functions from Kallioris et al. (2019c) in Figure 7.3.

The results show that similar median fragility is obtained for DS2, but a higher dispersion is found in the v7 models. The Kallioras et al. (2019c) DS3 fragility function is more fragile and again has lower dispersion. The third Kallioras et al. (2019c) function refers to near collapse, and thus whilst the level of dispersion is similar, it is expected that they would be more fragile than the global collapse fragility functions. The fact that they are closer to the upper branch of the v7 logic tree for this vulnerablity class provides an initial validation of the choice to place the results from the index buildings obtained herein on the upper branch of the logic tree, rather than the middle branch (see Section 6.1.3).

7.4 History Check on Damage

The v5 and v6 fragility functions were subject to a history check whereby group damage (F-N) curves were calculated using the simulated ground motions from all the events that have occurred in the field with magnitude greater than M_L = 2.5 from 1995 to 2018 (see Crowley et al., 2019a). A repetition of these calculations has been undertaken using the v7 models presented herein. The expected value of each F-N damage curve has been calculated to obtain the average annual number of damaged buildings in each damage/collapse state and this has been multiplied by the number of years considered (in this case 1995 to 2020). The models predict that the average number of buildings with DS2 over this period is just over 8 and is almost 1 for DS3.

It is noted that these numbers are lower than the history check for the v6 models because the vulnerability class with the highest damage fragility (URM4L) has reduced from around 40k in the v6 exposure model to less than 10k in the v7 exposure model (due to a change in the way that

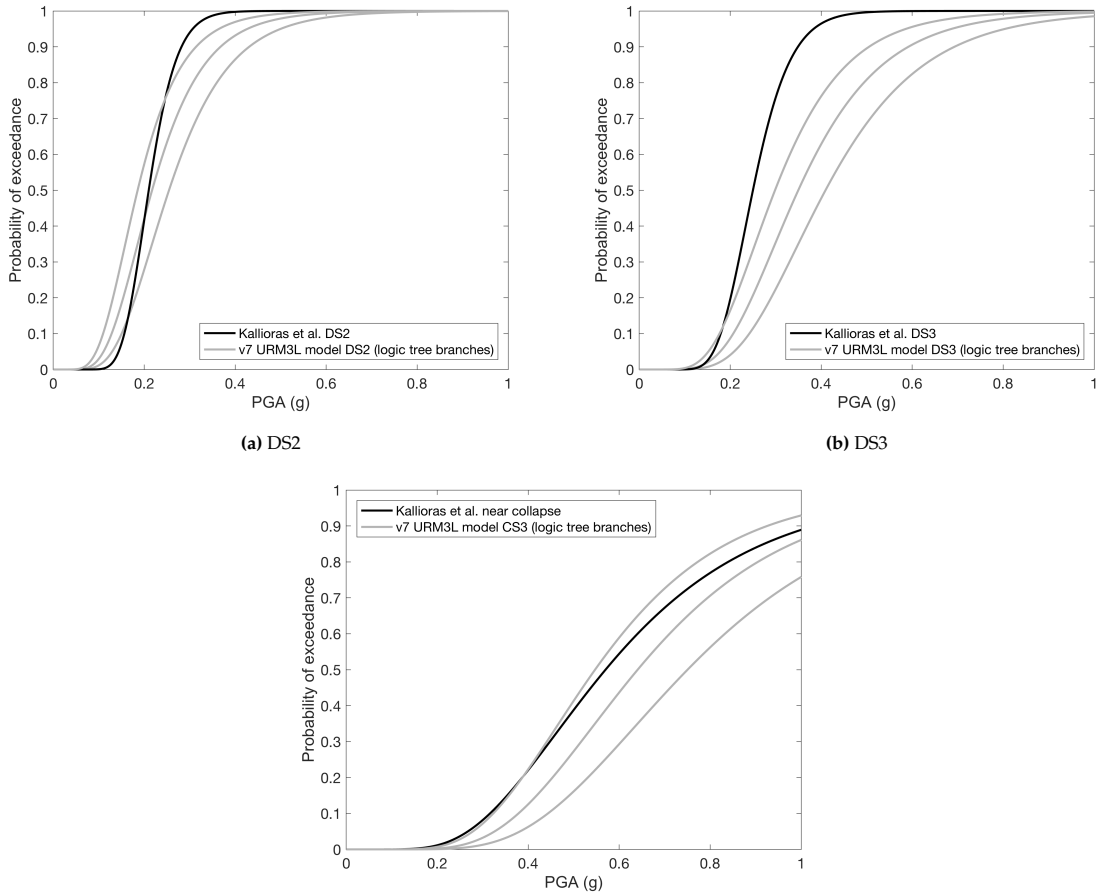

(a) DS2

(b) DS3

(c) Collapse (CS3)

Figure 7.3 Comparison of v7 index building fragility functions with published fragility study for URM3L

buildings with large ground floor openings are being inferred - Arup 2019a). There is limited public data available on the number of buildings that have experienced DS2 and DS3 over the time periods considered in these history checks, but the authors are aware that in the years following the Huizinge earthquake (when the majority of damage claims were submitted) the number of buildings that experienced damage greater than DS1 (i.e. non-structural damage) was less than a few hundred buildings, and thus we would expect an order of magntiude lower for the higher structural damage states.

7.5 Validation of Final Vulnerability Models

As suggested by the international review panel (Baker et al. 2018), a comparison of the proposed vulnerability models with other global models has been made. The empirical vulnerability models developed as part of the PAGER initiative (Jaiswal et al., 2009) for all European countries have thus been selected (i.e. Portugal, Italy, Romania, Greece and Turkey) and the mean of these models has been calculated; it has been necessary to convert MMI to PGA and this has been done using the Caprio et al. (2015) ground motion to intensity conversion equation (GMICE). A weighted mean vulnerability model (weighted by the relative number of buildings of each vulnerability class in the exposure model) for each of the three branches of the v7 logic tree (see Section 6.2) was then

computed and compared in Figure 7.4 with the mean European PAGER vulnerability model (as noted previously, AvgSa has been converted to PGA by multiplying by 0.65).

The figure shows that the mean European PAGER vulnerability model falls within the logic tree and is closer to the lower branch for higher levels of ground shaking. These higher values of vulnerability for Groningen might be explained by the fact that the countries used to develop the mean PAGER model all have a history of earthquakes and seismic design, unlike the Netherlands. The figure also supports the decision to place the models developed herein on the upper branch of the logic tree, as otherwise the PAGER model would not have fallen inside the three branches of the logic tree, indicating that the latter would have been unrealistically conservative.

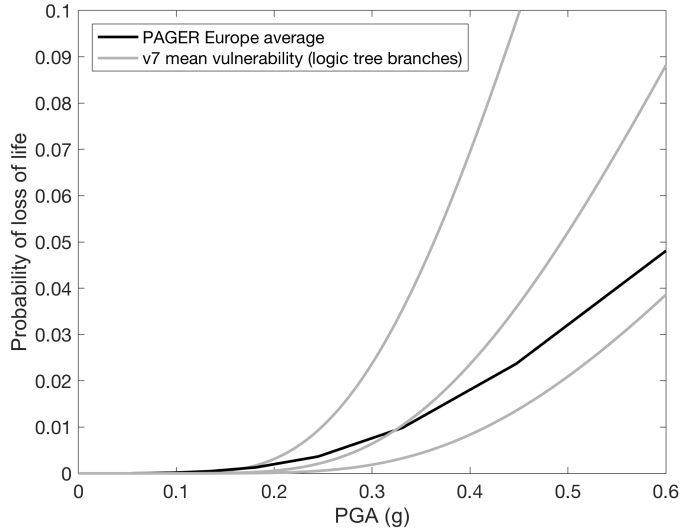

Figure 7.4 Comparison of mean v7 vulnerability model logic tree (in terms of PGA) with a mean European PAGER vulnerability model

Chapter 8

References

Akkar S., Sandıkkaya M.A., Senyurt M., Azari Sisi A., Ay B.O., Traversa P., Douglas J., Cotton F., Luzi L., Hernandez B. and Godey S. (2014) "Reference database for seismic ground-motion in Europe (RESORCE)," Bulletin of Earthquake Engineering, 12, 311-339.

Arup (2017) "Typology modelling: Analysis results in support of fragility functions - 2017 batch results," 229746_031.0_REP2005, November 2017, NAM Platform.

Arup (2019a) "EDB v7 Cover Note," December 2019.

Arup (2019b) "Typology modelling: Analysis results in support of fragility functions - 2018-2019 batch results," June 2019, NAM Platform.

Arup (2019c) "Typology modelling: Analysis results in support of fragility functions - 2019 batch results" December 2019, NAM Platform.

Arup (2019d) "LS-DYNA Masonry Model Recalibration," October 2019, NAM Platform.

Arup (2019e) "Typology modelling: Explicit MDOF validation of fragility functions - URM3L/URM4L" June 2019, NAM Platform.

Arup (2019f) "Typology Modelling: explicit MDOF validation of fragility functions - update" December 2019, NAM Platform.

Arup (2020) "Distance-to-index mapping analysis and feedback v7" January 2020.

Arup, TU Delft, Eucentre (2015) "Eucentre shake-table test of terraced house modelling predictions and analysis cross validation," November 2015, NAM Platform.

Arup, TU Delft, Eucentre and Arcadis (2016a) "EUC-BUILD2: Modelling predictions and analysis cross validation of detached single-storey URM building," September 2016.

Arup, TU Delft and Eucentre (2016b) "Laboratory component testing: Modelling post-test predictions and analysis cross validation," February 2016, NAM Platform.

Arup, TU Delft, Eucentre and Mosayk (2017) "LNEC-BUILD1: Modelling predictions and analysis cross validation," September 2017, NAM Platform.

Baker J.W. (2007) "Probabilistic structural response assessment using vector-valued intensity measures," Earthquake Engineering and Structural Dynamics, 36, pp. 1861-1883.

Baker J.W. and Cornell C.A. (2006) "Spectral shape, epsilon and record selection," Earthquake Engineering and Structural Dynamics, 35(9), pp. 1077-1095.

Baker, J.W. and Jayaram N. (2008) "Correlation of spectral acceleration values from NGA ground motion models," Earthquake Spectra, 24, pp. 299-317.

Baker J.W. and Lee C. (2018) "An improved algorithm for selecting ground motions to match a conditional spectrum," Journal of Earthquake Engineering, 22 (4), pp. 708-723.

Baker J., Engin Bal I., Dolsek M., Franchin P., Hamburger R., Luco N., Schotanus M. and Vamvatsikos D. (2018) "Assurance meeting review report: Exposure, fragility, and fatality models for the Groningen building stock," March 2018, NAM Platform.

Baker J.W., Dolsek M. and Vamvatsikos D. (2019) "Follow-up assurance review of exposure, fragility, and fatality models for the Groningen building stock," December 2019, NAM Platform.

Bianchini M., Diotallevi P.P and Baker J.W. (2009) "Prediction of inelastic structural response using an average of spectrak accelerations," Proceedings of 10th International Conference on Structural Safety and Reliability (ICOSSAR09), Osaka, Japan.

Bommer J.J., Stafford P.J., Edwards B., Dost B., van Dedem E., Rodriguez-Marek A., Kruiver P.P., van Elk J., Doornhof D. and Ntinalexis M. (2016) "Framework for a Ground-Motion Model for Induced Seismic Hazard and Risk Analysis in the Groningen Gas Field, The Netherlands," Earthquake Spectra, 33(2), pp. 481-498.

Bommer J.J., Edwards B., Kruiver P.P., Rodriguez-Marek A., Stafford P.J., Dost B., Ntinalexis M., Ruigrok E. and Spetzler J. (2017) "V5 ground-motion model for the Groningen Field," October 2017.

Bradley B.A. (2011) "Correlation of significant duration with amplitude and cumulative intensity measures and its use in ground motion selection," Journal of Earthquake Engineering, 15, pp. 809-832.

Brzev S., Scawthorn C., Charleson A.W., Allen L., Greene M., Jaiswal K. and Silva V. (2013) "GEM Building Taxonomy Version 2.0," GEM Technical Report 2013-02 V1.0.0, 188 pp., GEM Foundation, Pavia, Italy, DOI: 10.13117/GEM.EXT-MOD.TR2013.02

Calvi G.M., Pinho R., Magenes G., Bommer J.J., Restrepo-Velez L.F. and Crowley H. (2006), "Development of seismic vulnerability assessment methodologies over the past 30 years," ISET Journal of Earthquake Technology, Paper no. 472, 43 (3), pp. 75-104.

Caprio M., Tarigan B., Worden C.B., Wiemer S. and Wald D.J. (2015) "Ground motion to intensity conversion equations (GMICEs): A global relationship and evaluation of regional dependency," Bulletin of Seismological Society of America, 105 (3), pp. 1476-1490.

Casarotti C. and Pinho R. (2007) "An adaptive capacity spectrum method for assessment of bridges subjected to earthquake action," Bulletin of Earthquake Engineering, 5, pp. 377-390.

Cavalieri F., Correia A., Crowley H., Pinho R. (2020a) "Dynamic soil-structure interaction models for fragility characterisation of buildings with shallow foundations," Soil Dynamics and Earthquake Engineering, https://doi.org/10.1016/j.soildyn.2019.106004.

Cavalieri F., Correia A., Crowley H., Pinho R. (2020b) "Seismic fragility analysis of URM buildings founded on piles: influence of dynamic soil-structure interaction models," Bulletin of Earthquake Engineering, in press.

Chiou B., Darragh R., Gregor N. and Silva W. (2008) "NGA Project Strong-Motion Database," Earthquake Spectra, 24(1), pp. 23-44.

Coburn A. and Spence R. (2002) Earthquake Protection, 2nd Edition, John Wiley & Sons Ltd, Chichester.

Coburn A.W., Spence R.J.S. and Pomonis, A. (1992) "Factors Determining Casualty Levels in Earthquakes: Mortality Prediction in Building Collapse," Proceedings of the 10th World Conference on Earthquake Engineering, Madrid, Spain

Correia A.A., Tomassetti U., Penna A., Magenes G., Graziotti F. (2018) "Collapse shake-table test on a URM-timber roof substructure," Proceedings of the 16th European conference on Earthquake Engineering, Thessaloniki, Greece.

Crowley H., Pinho R. (2017) "Report on the v5 fragility and consequence models for the Groningen field," November 2017, NAM Platform.

Crowley H., Pinho R., Polidoro B. and Stafford P. (2015) "Development of v2 partial collapse fragility and consequence functions for the Groningen field," November 2015, NAM Platform.

Crowley H., Polidoro B., Pinho R., van Elk J. (2017) "Framework for developing fragility and consequence models for local personal risk," Earthquake Spectra, 33(4), pp. 1325-1345.

Crowley H., Pinho R., van Elk J., Uilenreef J. (2019a) "Probabilistic damage assessment of buildings due to induced seismicity," Bulletin of Earthquake Engineering, 17, pp. 4495-4516.

Crowley H., Pinho R., Cavalieri F. (2019b) "Report on the v6 Fragility and Consequence Models for the Groningen Field," March 2019, NAM Platform.

D'Ayala D., Meslem A., Vamvatsikos D., Porter K. and Rossetto T. (2014) "Guidelines for analytical vulnerability assessment of low/mid-rise buildings," GEM Technical Report 2014-12, GEM Foundation, Pavia, Italy. DOI: 10.13117/GEM.VULN-MOD.TR2014.12.

Dolsek M. (2009) "Incremental dynamic analysis with consideration of modeling uncertainties," Earthquake Engineering and Structural Dynamics, 38(6), pp. 805-825.

Eads L., Miranda E. and Lignos D. (2015) "Average spectral acceleration as an intensity measure for collapse risk assessment," Earthquake Engineering and Structural Dynamics, 44(12), pp. 2057-2073.

Eucentre, P&P, TU-Delft, TU-Eindhoven (2015) "Material Characterisation," Version 1.3, October 2015.

FEMA (2004) "HAZUS-MH Technical Manual," Federal Emergency Management Agency, Washington D.C.

FEMA (2012) "Seismic performance assessment of buildings. Volume 1 - Methodology," FEMPA P-58-1, Federal Emergency Management Agency, Washington D.C.

Gokkaya B.U., Baker J.W., Deierlein G.G. (2016) "Qualifying the impacts of modeling uncertainties on the seismic drift demands and collapse risk of buildings with implications on seismic design checks," Earthquake Engineering and Structural Dynamics, 45(10), pp. 1661-1683.

Graziotti F., Rossi A., Mandirola M., Penna A., and Magenes G. (2016a) "Experimental characterization of calcium-silicate brick masonry for seismic assessment," Proceedings of the 16th International Brick and Block Masonry Conference (IBMAC), Padua, Italy, 1619-1627.

Graziotti F., Tomassetti U., Penna A., Magenes G. (2016b) "Out-of-plane shaking table tests on URM single leaf and cavity walls," Engineering Structures 125, 455–470.

Graziotti F., Tomassetti U., Kallioras S., Penna A., and Magenes G. (2017a) "Shaking table test on a full scale URM cavity wall building," Bulletin of Earthquake Engineering, 15(12), pp. 5329-5364.

Graziotti F., Tomassetti U., Penna A., Magenes M. (2017b) "Tests on URM clay and calcium-silicate masonry structures: identification of damage states," Eucentre Foundation, Pavia, Italy. Working Version of October 2017, Available from URL: www.eucentre.it/nam-project.

Graziotti F., Tomassetti U., Sharma S., Grottoli L., Magenes G. (2018) "Experimental response of URM single leaf and cavity walls in out-of-plane two-way bending generated by seismic excitation," Construction and Building Materials 195, pp. 650-670

Graziotti F., Penna A., Magenes G. (2019) "A comprehensive in-situ and laboratory testing programme supporting seismic risk analysis of URM buildings subjected to induced earthquakes," Bulletin of Earthquake Engineering, 17, pp. 4575-4599.

Jaiswal K., Wald D.J. and Hearne M. (2009) "Estimating Casualties for Large Worldwide Earthquakes using an Empirical Approach," US Geological Survey Open-File Report 1136

Jalayer F. (2003) "Direct probabilistic seismic analysis: Implementing non-linear dynamic assessments," Ph.D. Dissertation, Stanford University.

Kallioras S., Guerrini G., Tomassetti U., Marchesi B., Penna A., Graziotti F., Magenes G., (2018) "Experimental seismic performance of a full-scale unreinforced clay-masonry building with flexible timber diaphragms," Engineering Structures 161, pp. 231-249

Kallioras S., Grottoli L., Tomassetti U., Miglietta M., Damiani N., Guerrini G., Graziotti F. (2019a) "Experimental seismic performance assessment of Dutch unreinforced masonry buildings: identification of damage limit states," Eucentre Foundation, Pavia, Italy, October 2019, NAM Platform.

Kallioras S., Correia A.A., Graziotti F., Penna A., Magenes G. (2019b) "Experimental seismic performance of a full-scale unreinforced clay-masonry building with flexible timber diaphragms," Engineering Structures, 161, pp. 231-249.

Kallioras S., Graziotti F. and Penna A. (2019c) "Numerical assessment of the dynamic response of a URM terraced house exposed to induced seismicity," Bulletin of Earthquake Engineering, 17, pp. 1521-1552.

Kohrangi M., Bazzurro P., Vamvatsikos D. and Spillatura A. (2017) "Conditional spectrum-based ground motion record selection using average spectral acceleration," Earthquake Engineering and Structural Dynamics, 46(10), pp. 1667-1685

Liel A.B., Haselton C.B., Deierlein G.G. and Baker J.W. (2009) "Incorporating modeling uncertainties in the assessment of seismic collapse risk of buildings," Structural Safety, 31(2), pp. 197.211.

Lin T. and Baker J. (2015) "Conditional Spectra," Encyclopedia of Earthquake Engineering, M. Beer, I.A. Kougioumtzoglou, E. Patelli and I.S.-K. Au, eds., Springer Berlin Heidelberg, 13p.

LSTC - Livermore Software Technology Corporation (2013) LS-DYNA - A general-purpose finite element program capable of simulating complex problems. Livermore, California.

Malomo D., Pinho R., Penna A. (2018) "Using the Applied Element Method for modelling calcium-silicate brick masonry subjected to in-plane cyclic loading," Earthquake Engineering and Structural Dynamics, Vol. 47, pp. 1610–1630.

Malomo D., Pinho R., Penna A. (2019) "Applied Element Modelling of the dynamic response of a full-scale clay brick masonry building specimen with flexible diaphragms," International Journal of Architectural Heritage, published online at: https://doi.org/10.1080/15583058.2019.1616004.

Malomo D., Pinho R., Penna A. (2020a) "Simulating the shake-table response of URM cavity-wall structures tested to collapse or near-collapse conditions," Earthquake Spectra, http://doi.org/10.1177/8755293019891715.

Malomo D., Pinho R., Penna A. (2020b) "Numerical modelling of the out-of-plane response of full-scale brick masonry prototypes subjected to incremental dynamic shake-table tests," Engineering Structures, https://doi.org/10.1016/j.engstruct.2020.110298.

Miglietta M., Mazzella L., Grottoli L., Guerrini G., Graziotti F. (2018) "Full-scale shaking table test on a Dutch URM cavity-wall terraced-house end unit - EUC-BUILD-6" Report n. EUC160/2018U, Eucentre Foundation, Pavia, Italy. Available from URL: www.eucentre.it/nam-project.

Miller A.C. and Rice T.R. (1983) "Discrete approximations of probability distributions," Management Science, 29(3), pp. 352-362

Mosayk (2016) "Using the Applied Element Method to model URM walls subjected to in-plane cyclic shear-compression," December 2016, NAM Platform.

Mosayk (2017a) "Using the Applied Element Method to model the shake-table testing of two full-scale URM houses," October 2017, NAM Platform.

Mosayk (2017b) “Using the Applied Element Method to model the collapse shake-table testing of a URM cavity wall structure,” October 2017, NAM Platform.

Mosayk (2017c) “Using the Applied Element Method to model the collapse shake-table testing of a terraced house roof substructure,” October 2017, NAM Platform.

Mosayk (2017d) "Nonlinear dynamic analysis of index buildings for v5 fragility and consequence models," October 2017, NAM Platform.

Mosayk (2017e) "Using the Applied Element Method to model the shake-table out-of-plane testing of full-scale URM wall specimens subjected to one-way bending," November 2017, NAM Platform.

Mosayk (2019a) “Blind prediction modelling and analysis of EUC-BUILD6 specimen,” January 2019, NAM Platform.

Mosayk (2019b) “Calibration and verification of a nonlinear macro-element for SSI analysis in the Groningen region,” April 2019, NAM Platform.

Samardjieva E. and Badal J. (2002) “Estimation of the expected number of casualties caused by strong earthquakes,” Bulletin of Seismological Society of America, 92, pp. 2310–2322.

Seismosoft (2020) SeismoStruct v2020 - A computer program for static and dynamic nonlinear analysis of framed structures, Available from http://www.seismosoft.com

Sivaselvan M., Reinhorn A.M. (1999) "Hysteretic models for cyclic behavior of deteriorating inelastic structures," Report MCEER-99-0018, MCEER/SUNY/Buffalo.

So E.K.M. and Pomonis A. (2012) “Derivation of globally applicable casualty rates for use in earthquake loss estimation models,” Proceedings of 15th World Conference on Earthquake Engineering, paper 1164.

Stafford P.J. (2008) “Conditional prediction of absolute durations,” Bulletin of Seismological Society of America, 98(3), pp. 1588-1594.

Taig A.R. and Pickup F.E. (2016) “Risk Assessment of Falling Hazards in Earthquakes in the Groningen region,” Arup Report 229746_032.0_REP1008, NAM Platform.

Tomassetti U., Correia A., Candeias P.X., Graziotti F., Campos-Costa A. (2019) "Two-way bending out-of-plane collapse of a full-scale URM building tested on a shake table," Bulletin of Earthquake Engineering, 17(4), pp. 2165–2198.

Vamvatsikos D. and Cornell C.A. (2002) “Incremental dynamic analysis,” Earthquake Engineering and Structural Dynamics, 31(3), pp. 491–514.

Vamvatsikos D. and Fragiadakis M. (2010) "Incremental dynamic analysis for estimating seismic performance sensitivity and uncertainty," Earthquake Engineering and Structural Dynamics, 39(2), pp. 141-163.

van Elk J., Bourne S.J., Oates S.J., Bommer J.J., Pinho R., Crowley H. (2019). “A probabilistic model to evaluate options for mitigating induced seismic risk.” Earthquake Spectra, 35(2), pp.537-564.

Yepes-Estrada C., Silva V., Rossetto T., D’Ayala D., Ioannou I., Meslem A. and Crowley H. (2016) "The Global Earthquake Model Physical Vulnerability Database," Earthquake Spectra, DOI: 10.1193/011816EQS015DP.

Appendix A

Explanation of GEM Taxonomy Codes

The following table explains the GEM Building Taxonomy codes that have been used to describe the structural systems in the EDB v7.

Table A.1 Explanation of GEM Building Taxonomy codes

Attribute	Value	GEM taxonomy code
Material of lateral load-resisting system	Precast concrete	CR+PC
	Cast-in-place concrete	CR+CIP
	Masonry	MUR
	Wood	W
	Steel	S
Type of lateral load-resisting system	No lateral load-resisting system	LN
	Post and beam	LPB
	Moment frame	LFM
	Braced frame	LFBR
	Hybrid lateral load-resisting system	LH
	Walls	LWAL
Presence of exterior wall	No external wall	EWN
	Presence of external wall	EW
Material of floor system	No elevated floor material	FN
	Concrete	FC
	Timber	FW
Height	Range of number of storeys above ground (a = upper bound, b = lower bound)	HBET:a;b
Structural Irregularity	Unknown irregularity	IR99
	Façade openings $\geq 90\%$	IRIR+OPL
	Drive-in building	IRVP+DIB
	Soft storey	IRVP+SOS

Appendix B

Mapping Table for Vulnerability Classes

The following table explains the mapping of each of the 497 structural systems found in the v7 EDB to the 35 vulnerability classes considered in the HRA2020 analyses.

Table B.1 Mapping Table from Structural System to Vulnerability Class

Structural System	Vulnerability Class
B/CR+CIP/LFM/CR+CIP/LFM/EW/FC/HBET:20;3/IR99	RC1
B/CR+CIP/LH/CR+CIP/LH/EW/FC/H99/IR99	RC3M
B/CR+CIP/LH/CR+CIP/LH/EW/FC/HBET:20;3/IR99	RC3M
B/CR+CIP/LH/CR+CIP/LH/EW/FC/HBET:20;3/IRVP+DIB	RC3M
B/CR+CIP/LH/CR+CIP/LH/EW/FC/HBET:20;3/IRVP+SOS	RC3M
B/CR+CIP/LH/CR+CIP/LH/EW/FC/HBET:2;1/IR99	RC3L
B/CR+CIP/LH/CR+CIP/LH/EW/FC/HBET:2;1/IRVP+DIB	RC3L
B/CR+CIP/LWAL/CR+CIP/LN/EW/FC/H99/IR99	RC3M
B/CR+CIP/LWAL/CR+CIP/LN/EW/FC/HBET:20;3/IR99	RC3M
B/CR+CIP/LWAL/CR+CIP/LN/EW/FC/HBET:20;3/IRVP+DIB	RC3M
B/CR+CIP/LWAL/CR+CIP/LN/EW/FC/HBET:20;3/IRVP+SOS	RC3M
B/CR+CIP/LWAL/CR+CIP/LN/EW/FC/HBET:2;1/IR99	RC3L
B/CR+CIP/LWAL/CR+CIP/LN/EW/FC/HBET:2;1/IRVP+DIB	RC3L
B/CR+CIP/LWAL/CR+CIP/LN/EW/FC/HBET:2;1/IRVP+SOS	RC3L
B/CR+CIP/LWAL/CR+CIP/LWAL/EW/FC/H99/IR99	RC3M
B/CR+CIP/LWAL/CR+CIP/LWAL/EW/FC/HBET:20;3/IR99	RC3M
B/CR+CIP/LWAL/CR+CIP/LWAL/EW/FC/HBET:20;3/IRVP+SOS	RC3M
B/CR+CIP/LWAL/CR+CIP/LWAL/EW/FC/HBET:2;1/IR99	RC3L
B/CR+PC/LH/CR+PC/LH/EW/FC/H99/IR99	PC3M
B/CR+PC/LH/CR+PC/LH/EW/FC/HBET:20;3/IR99	PC3M
B/CR+PC/LH/CR+PC/LH/EW/FC/HBET:20;3/IRVP+DIB	PC3M
B/CR+PC/LH/CR+PC/LH/EW/FC/HBET:20;3/IRVP+SOS	PC3M
B/CR+PC/LH/CR+PC/LH/EW/FC/HBET:2;1/IR99	PC3L
B/CR+PC/LH/CR+PC/LH/EW/FC/HBET:2;1/IRVP+DIB	PC3L
B/CR+PC/LWAL/CR+PC/LN/EW/FC/H99/IR99	PC3M
B/CR+PC/LWAL/CR+PC/LN/EW/FC/HBET:20;3/IR99	PC3M
B/CR+PC/LWAL/CR+PC/LN/EW/FC/HBET:20;3/IRVP+DIB	PC3M
B/CR+PC/LWAL/CR+PC/LN/EW/FC/HBET:20;3/IRVP+SOS	PC3M
B/CR+PC/LWAL/CR+PC/LN/EW/FC/HBET:2;1/IR99	PC3L
B/CR+PC/LWAL/CR+PC/LN/EW/FC/HBET:2;1/IRVP+DIB	PC3L
B/CR+PC/LWAL/CR+PC/LWAL/EW/FC/H99/IR99	PC3M
B/CR+PC/LWAL/CR+PC/LWAL/EW/FC/HBET:20;3/IR99	PC3M
B/CR+PC/LWAL/CR+PC/LWAL/EW/FC/HBET:20;3/IRVP+DIB	PC3M
B/CR+PC/LWAL/CR+PC/LWAL/EW/FC/HBET:20;3/IRVP+SOS	PC3M
B/CR+PC/LWAL/CR+PC/LWAL/EW/FC/HBET:2;1/IR99	PC3L
B/CR+PC/LWAL/CR+PC/LWAL/EW/FC/HBET:2;1/IRVP+DIB	PC3L
B/MUR/LH/MUR/LH/EW/FC/H99/IR99	URM9L
B/MUR/LH/MUR/LH/EW/FC/HBET:20;3/IR99	URM3M_B
B/MUR/LH/MUR/LH/EW/FC/HBET:20;3/IRVP+DIB	URM3M_D
B/MUR/LH/MUR/LH/EW/FC/HBET:20;3/IRVP+SOS	URM9L
B/MUR/LH/MUR/LH/EW/FC/HBET:2;1/IR99	URM9L
B/MUR/LH/MUR/LH/EW/FC/HBET:2;1/IRVP+DIB	URM9L
B/MUR/LH/MUR/LH/EW/FC/HBET:2;1/IRVP+SOS	URM9L
B/MUR/LH/MUR/LH/EWN/FM/H99/IR99	URM9L
B/MUR/LH/MUR/LH/EWN/FM/HBET:20;3/IR99	URM9L
B/MUR/LH/MUR/LH/EWN/FM/HBET:2;1/IR99	URM9L
B/MUR/LH/MUR/LH/EWN/FM/HBET:2;1/IRVP+DIB	URM9L
B/MUR/LH/MUR/LH/EWN/FM/HBET:2;1/IRVP+SOS	URM9L
B/MUR/LH/MUR/LH/EWN/FN/H99/IR99	URM9L
B/MUR/LH/MUR/LH/EWN/FN/HBET:20;1/IR99	URM9L
B/MUR/LH/MUR/LH/EWN/FN/HBET:2;1/IR99	URM9L
B/MUR/LH/MUR/LH/EWN/FN/HBET:2;1/IRVP+DIB	URM9L
B/MUR/LH/MUR/LH/EWN/FN/HBET:2;1/IRVP+SOS	URM9L
B/MUR/LH/MUR/LH/EWN/FW/H99/IR99	URM9L
B/MUR/LH/MUR/LH/EWN/FW/HBET:20;3/IR99	URM9L
B/MUR/LH/MUR/LH/EWN/FW/HBET:20;3/IRVP+SOS	URM9L
B/MUR/LH/MUR/LH/EWN/FW/HBET:2;1/IR99	URM9L
B/MUR/LH/MUR/LH/EWN/FW/HBET:2;1/IRVP+DIB	URM9L
B/MUR/LH/MUR/LH/EWN/FW/HBET:2;1/IRVP+SOS	URM9L
B/MUR/LWAL/MUR/LN/EW/FC/H99/IR99	URM3M_B
B/MUR/LWAL/MUR/LN/EW/FC/HBET:20;3/IR99	URM3M_B
B/MUR/LWAL/MUR/LN/EW/FC/HBET:20;3/IRVP+DIB	URM3M_D
B/MUR/LWAL/MUR/LN/EW/FC/HBET:20;3/IRVP+SOS	URM3M_D
B/MUR/LWAL/MUR/LN/EW/FC/HBET:2;1/IR99	URM3L
B/MUR/LWAL/MUR/LN/EW/FC/HBET:2;1/IRVP+DIB	URM3M_D
B/MUR/LWAL/MUR/LN/EW/FC/HBET:2;1/IRVP+SOS	URM4L
B/MUR/LWAL/MUR/LN/EWN/FW/H99/IR99	URM3M_B
B/MUR/LWAL/MUR/LN/EWN/FW/HBET:20;3/IR99	URM3M_B
B/MUR/LWAL/MUR/LN/EWN/FW/HBET:2;1/IR99	URM2L
B/MUR/LWAL/MUR/LN/EWN/FW/HBET:2;1/IRVP+DIB	URM3M_D
B/MUR/LWAL/MUR/LN/EWN/FW/HBET:2;1/IRVP+SOS	URM2L
B/MUR/LWAL/MUR/LWAL/EW/FC/H99/IR99	URM3M_B
B/MUR/LWAL/MUR/LWAL/EW/FC/HBET:20;3/IR99	URM3M_B
B/MUR/LWAL/MUR/LWAL/EW/FC/HBET:20;3/IRVP+DIB	URM3M_D
B/MUR/LWAL/MUR/LWAL/EW/FC/HBET:20;3/IRVP+SOS	URM3M_B
B/MUR/LWAL/MUR/LWAL/EW/FC/HBET:2;1/IR99	URM7L
B/MUR/LWAL/MUR/LWAL/EW/FC/HBET:2;1/IRVP+DIB	URM3M_D
B/MUR/LWAL/MUR/LWAL/EW/FC/HBET:2;1/IRVP+SOS	URM7L
B/MUR/LWAL/MUR/LWAL/EW/FM/H99/IR99	URM3M_B
B/MUR/LWAL/MUR/LWAL/EW/FM/HBET:20;3/IR99	URM3M_B
B/MUR/LWAL/MUR/LWAL/EW/FM/HBET:2;1/IR99	URM7L
B/MUR/LWAL/MUR/LWAL/EW/FM/HBET:2;1/IRVP+SOS	URM7L
B/MUR/LWAL/MUR/LWAL/EW/FN/HBET:20;1/IR99	URM3M_B
B/MUR/LWAL/MUR/LWAL/EW/FN/HBET:2;1/IR99	URM7L
B/MUR/LWAL/MUR/LWAL/EW/FO/HBET:20;3/IR99	URM3M_B
B/MUR/LWAL/MUR/LWAL/EW/FO/HBET:2;1/IR99	URM7L
B/MUR/LWAL/MUR/LWAL/EW/FO/HBET:2;1/IRVP+SOS	URM7L

Table B.2 Mapping Table from Structural System to Vulnerability Class (cont.)

Structural System	Vulnerability Class
B/MUR/LWAL/MUR/LWAL/EW/FW/H99/IR99	URM3M_B
B/MUR/LWAL/MUR/LWAL/EW/FW/HBET:20;3/IR99	URM3M_B
B/MUR/LWAL/MUR/LWAL/EW/FW/HBET:2;1/IR99	URM8L
B/MUR/LWAL/MUR/LWAL/EW/FW/HBET:2;1/IRVP+DIB	URM3M_D
B/MUR/LWAL/MUR/LWAL/EW/FW/HBET:2;1/IRVP+SOS	URM8L
B/MUR/LWAL/MUR/LWAL/EWN/FN/H99/IR99	URM3M_B
B/MUR/LWAL/MUR/LWAL/EWN/FN/HBET:20;1/IR99	URM3M_B
B/MUR/LWAL/MUR/LWAL/EWN/FN/HBET:2;1/IR99	URM6L
B/MUR/LWAL/MUR/LWAL/EWN/FN/HBET:2;1/IRVP+DIB	URM3M_D
B/MUR/LWAL/MUR/LWAL/EWN/FN/HBET:2;1/IRVP+SOS	URM6L
B/MUR/LWAL/MUR/LWAL/EWN/FW/H99/IR99	URM6L
B/MUR/LWAL/MUR/LWAL/EWN/FW/HBET:20;3/IR99	URM3M_B
B/MUR/LWAL/MUR/LWAL/EWN/FW/HBET:20;3/IRVP+SOS	URM3M_B
B/MUR/LWAL/MUR/LWAL/EWN/FW/HBET:2;1/IR99	URM6L
B/MUR/LWAL/MUR/LWAL/EWN/FW/HBET:2;1/IRVP+DIB	URM3M_D
B/MUR/LWAL/MUR/LWAL/EWN/FW/HBET:2;1/IRVP+SOS	URM6L
B/S/LFBR/S/LFBR/EW/FC/H99/IR99	S2M
B/S/LFBR/S/LFBR/EW/FC/HBET:20;3/IR99	S2M
B/S/LFBR/S/LFBR/EW/FC/HBET:20;3/IRVP+DIB	S2M
B/S/LFBR/S/LFBR/EW/FC/HBET:20;3/IRVP+SOS	S2M
B/S/LFBR/S/LFBR/EW/FC/HBET:2;1/IR99	S2L
B/S/LFBR/S/LFBR/EW/FC/HBET:2;1/IRVP+DIB	S2L
B/S/LFM/S/LFM/EW/FC/H99/IR99	S1M
B/S/LFM/S/LFM/EW/FC/HBET:20;3/IR99	S1M
B/S/LFM/S/LFM/EW/FC/HBET:2;1/IR99	S1L
B/S/LFM/S/LFM/EW/FC/HBET:2;1/IRVP+DIB	S1L
B/S/LFM/S/LFM/EW/FN/HBET:20;1/IR99	S1M
B/S/LFM/S/LFM/EW/FN/HBET:2;1/IR99	S1L
S/MAT99/LN/MAT99/LN/EW99/F99/H99/IR99	URM10
S/MAT99/LN/MAT99/LN/EW99/F99/HBET:20;1/IR99	URM10
S/MUR/LWAL/MUR/LN/EW/FC/HBET:20;1/IR99	URM10
S/MUR/LWAL/MUR/LWAL/EWN/FN/HBET:20;1/IR99	URM10
S/W/LN/W/LN/EWN/FN/HBET:20;1/IR99	URM10
T/CR+CIP/LFM/CR+CIP/LFM/EW/FC/HBET:20;1/IR99	RC1H
T/CR+CIP/LH/CR+CIP/LH/EW/FC/HBET:20;1/IR99	RC3H
T/CR+CIP/LWAL/CR+CIP/LN/EW/FC/HBET:20;1/IR99	RC3H
T/CR+CIP/LWAL/CR+CIP/LN/EW/FC/HBET:20;1/IRVP+SOS	RC3H
T/CR+CIP/LWAL/CR+CIP/LWAL/EW/FC/HBET:20;1/IR99	RC3H
T/CR+PC/LH/CR+PC/LH/EW/FC/HBET:20;1/IR99	PC3H
T/CR+PC/LWAL/CR+PC/LWAL/EW/FC/HBET:20;1/IR99	PC3H
T/CR+PC/LWAL/CR+PC/LWAL/EW/FC/HBET:20;1/IRVP+SOS	PC3H
T/MUR/LH/MUR/LH/EW/FC/HBET:20;1/IR99	URM9L
T/MUR/LWAL/MUR/LN/EW/FC/HBET:20;1/IR99	URM3L
T/MUR/LWAL/MUR/LN/EW/FC/HBET:20;1/IRVP+SOS	URM4L
T/MUR/LWAL/MUR/LWAL/EW/FC/HBET:20;1/IR99	URM7L
T/MUR/LWAL/MUR/LWAL/EWN/FW/HBET:20;1/IR99	URM6L
T/S/LFBR/S/LFBR/EW/FC/HBET:20;1/IR99	S2H
T/S/LFM/S/LFM/EW/FC/HBET:20;1/IR99	S1H
U/CR+CIP/LFM/CR+CIP/LFM/EW/FC/HBET:20;3/IRVP+SOS	RC1M
U/CR+CIP/LFM/CR+CIP/LFM/EW/FC/HBET:2;1/IR99	RC1L
U/CR+CIP/LFM/CR+CIP/LFM/EW/FC/HBET:2;1/IRVP+SOS	RC1L
U/CR+CIP/LFM/CR+CIP/LFM/EWN/FO/HBET:2;1/IR99	RC1L
U/CR+CIP/LFM/CR+CIP/LFM/EWN/FO/HBET:2;1/IRVP+SOS	RC1L
U/CR+CIP/LH/CR+CIP/LH/EW/FC/HBET:2;1/IR99	RC3L
U/CR+CIP/LH/CR+CIP/LH/EW/FC/HBET:2;1/IRVP+SOS	RC3L
U/CR+CIP/LWAL/CR+CIP/LN/EW/FC/H99/IR99	RC3L
U/CR+CIP/LWAL/CR+CIP/LN/EW/FC/H99/IRVP+OPL	RC3L
U/CR+CIP/LWAL/CR+CIP/LN/EW/FC/HBET:20;3/IR99	RC3M
U/CR+CIP/LWAL/CR+CIP/LN/EW/FC/HBET:20;3/IRVP+DIB	RC3M
U/CR+CIP/LWAL/CR+CIP/LN/EW/FC/HBET:20;3/IRVP+OPL	RC3M
U/CR+CIP/LWAL/CR+CIP/LN/EW/FC/HBET:20;3/IRVP+SOS	RC3M
U/CR+CIP/LWAL/CR+CIP/LN/EW/FC/HBET:2;1/IR99	RC3L
U/CR+CIP/LWAL/CR+CIP/LN/EW/FC/HBET:2;1/IRVP+DIB	RC3L
U/CR+CIP/LWAL/CR+CIP/LN/EW/FC/HBET:2;1/IRVP+OPL	RC3L
U/CR+CIP/LWAL/CR+CIP/LN/EW/FC/HBET:2;1/IRVP+SOS	RC3L
U/CR+CIP/LWAL/CR+CIP/LN/EW/FW/HBET:2;1/IR99	RC3L
U/CR+CIP/LWAL/CR+CIP/LWAL/EW/FC/H99/IR99	RC3L
U/CR+CIP/LWAL/CR+CIP/LWAL/EW/FC/HBET:20;3/IR99	RC3M
U/CR+CIP/LWAL/CR+CIP/LWAL/EW/FC/HBET:20;3/IRVP+DIB	RC3M
U/CR+CIP/LWAL/CR+CIP/LWAL/EW/FC/HBET:20;3/IRVP+SOS	RC3M
U/CR+CIP/LWAL/CR+CIP/LWAL/EW/FC/HBET:2;1/IR99	RC3L
U/CR+CIP/LWAL/CR+CIP/LWAL/EW/FC/HBET:2;1/IRVP+DIB	RC3L
U/CR+CIP/LWAL/CR+CIP/LWAL/EW/FC/HBET:2;1/IRVP+SOS	RC3L
U/CR+PC/LH/CR+PC/LH/EW/FC/HBET:2;1/IRVP+SOS	PC3L
U/CR+PC/LWAL/CR+PC/LN/EW/FC/H99/IR99	PC3L
U/CR+PC/LWAL/CR+PC/LN/EW/FC/HBET:20;3/IR99	PC3M
U/CR+PC/LWAL/CR+PC/LN/EW/FC/HBET:20;3/IRVP+DIB	PC3M
U/CR+PC/LWAL/CR+PC/LN/EW/FC/HBET:20;3/IRVP+OPL	PC3M
U/CR+PC/LWAL/CR+PC/LN/EW/FC/HBET:20;3/IRVP+SOS	PC3M
U/CR+PC/LWAL/CR+PC/LN/EW/FC/HBET:2;1/IR99	PC3L
U/CR+PC/LWAL/CR+PC/LN/EW/FC/HBET:2;1/IRVP+DIB	PC3L
U/CR+PC/LWAL/CR+PC/LN/EW/FC/HBET:2;1/IRVP+OPL	PC3L
U/CR+PC/LWAL/CR+PC/LN/EW/FC/HBET:2;1/IRVP+SOS	PC3L
U/CR+PC/LWAL/CR+PC/LN/EWN/FC/HBET:2;1/IR99	PC3L
U/CR+PC/LWAL/CR+PC/LN/EWN/FC/HBET:2;1/IRVP+OPL	PC3L
U/CR+PC/LWAL/CR+PC/LWAL/EW/FC/H99/IR99	PC3L
U/CR+PC/LWAL/CR+PC/LWAL/EW/FC/HBET:20;3/IR99	PC3M

Table B.3 Mapping Table from Structural System to Vulnerability Class (cont.)

Structural System	Vulnerability Class
U/CR+PC/LWAL/CR+PC/LWAL/EW/FC/HBET:20;3/IRVP+DIB	PC3M
U/CR+PC/LWAL/CR+PC/LWAL/EW/FC/HBET:20;3/IRVP+SOS	PC3M
U/CR+PC/LWAL/CR+PC/LWAL/EW/FC/HBET:2;1/IR99	PC3L
U/CR+PC/LWAL/CR+PC/LWAL/EW/FC/HBET:2;1/IRVP+DIB	PC3L
U/CR+PC/LWAL/CR+PC/LWAL/EW/FC/HBET:2;1/IRVP+OPL	PC3L
U/CR+PC/LWAL/CR+PC/LWAL/EW/FC/HBET:2;1/IRVP+SOS	PC3L
U/MUR/LFM/MUR/LFM/EW/FO/HBET:2;1/IR99	URM3L
U/MUR/LH/MUR/LH/EW/FC/H99/IR99	URM9L
U/MUR/LH/MUR/LH/EW/FC/HBET:20;3/IR99	URM9L
U/MUR/LH/MUR/LH/EW/FC/HBET:20;3/IRVP+DIB	URM3M_D
U/MUR/LH/MUR/LH/EW/FC/HBET:20;3/IRVP+SOS	URM9L
U/MUR/LH/MUR/LH/EW/FC/HBET:2;1/IR99	URM9L
U/MUR/LH/MUR/LH/EW/FC/HBET:2;1/IRVP+DIB	URM3M_D
U/MUR/LH/MUR/LH/EW/FC/HBET:2;1/IRVP+SOS	URM9L
U/MUR/LH/MUR/LH/EW/FM/HBET:2;1/IR99	URM9L
U/MUR/LH/MUR/LH/EW/FN/HBET:2;1/IR99	URM9L
U/MUR/LH/MUR/LH/EW/FN/HBET:2;1/IRVP+SOS	URM9L
U/MUR/LH/MUR/LH/EW/FW/H99/IR99	URM9L
U/MUR/LH/MUR/LH/EW/FW/HBET:20;3/IR99	URM9L
U/MUR/LH/MUR/LH/EW/FW/HBET:20;3/IRVP+DIB	URM3M_D
U/MUR/LH/MUR/LH/EW/FW/HBET:20;3/IRVP+SOS	URM9L
U/MUR/LH/MUR/LH/EW/FW/HBET:2;1/IR99	URM9L
U/MUR/LH/MUR/LH/EW/FW/HBET:2;1/IRVP+DIB	URM3M_D
U/MUR/LH/MUR/LH/EW/FW/HBET:2;1/IRVP+SOS	URM9L
U/MUR/LH/MUR/LH/EWN/FC/H99/IR99	URM9L
U/MUR/LH/MUR/LH/EWN/FC/HBET:2;1/IR99	URM9L
U/MUR/LH/MUR/LH/EWN/FC/HBET:2;1/IRVP+SOS	URM9L
U/MUR/LH/MUR/LH/EWN/FW/H99/IR99	URM9L
U/MUR/LH/MUR/LH/EWN/FW/HBET:20;3/IR99	URM9L
U/MUR/LH/MUR/LH/EWN/FW/HBET:20;3/IRVP+DIB	URM3M_D
U/MUR/LH/MUR/LH/EWN/FW/HBET:20;3/IRVP+SOS	URM9L
U/MUR/LH/MUR/LH/EWN/FW/HBET:2;1/IR99	URM9L
U/MUR/LH/MUR/LH/EWN/FW/HBET:2;1/IRVP+DIB	URM3M_D
U/MUR/LH/MUR/LH/EWN/FW/HBET:2;1/IRVP+OPL	URM9L
U/MUR/LH/MUR/LH/EWN/FW/HBET:2;1/IRVP+SOS	URM9L
U/MUR/LN/MUR/LN/EWN/FW/HBET:2;1/IR99	URM4L
U/MUR/LWAL/MUR/LH/EW/FN/HBET:2;1/IR99	URM5L
U/MUR/LWAL/MUR/LH/EWN/FW/HBET:2;1/IR99	URM2L
U/MUR/LWAL/MUR/LN/EW/FC/H99/IR99	URM3L
U/MUR/LWAL/MUR/LN/EW/FC/H99/IRVP+OPL	URM4L
U/MUR/LWAL/MUR/LN/EW/FC/HBET:20;3/IR99	URM3M_U
U/MUR/LWAL/MUR/LN/EW/FC/HBET:20;3/IRVP+DIB	URM3M_D
U/MUR/LWAL/MUR/LN/EW/FC/HBET:20;3/IRVP+OPL	URM3M_D
U/MUR/LWAL/MUR/LN/EW/FC/HBET:20;3/IRVP+SOS	URM3M_D
U/MUR/LWAL/MUR/LN/EW/FC/HBET:2;1/IR99	URM3L
U/MUR/LWAL/MUR/LN/EW/FC/HBET:2;1/IRVP+DIB	URM3M_D
U/MUR/LWAL/MUR/LN/EW/FC/HBET:2;1/IRVP+OPL	URM4L
U/MUR/LWAL/MUR/LN/EW/FC/HBET:2;1/IRVP+SOS	URM4L
U/MUR/LWAL/MUR/LN/EW/FM/HBET:2;1/IR99	URM3L
U/MUR/LWAL/MUR/LN/EW/FM/HBET:2;1/IRVP+OPL	URM4L
U/MUR/LWAL/MUR/LN/EW/FW/H99/IR99	URM5L
U/MUR/LWAL/MUR/LN/EW/FW/H99/IRVP+OPL	URM5L
U/MUR/LWAL/MUR/LN/EW/FW/HBET:20;3/IR99	URM3M_U
U/MUR/LWAL/MUR/LN/EW/FW/HBET:20;3/IRVP+DIB	URM3M_D
U/MUR/LWAL/MUR/LN/EW/FW/HBET:20;3/IRVP+OPL	URM3M_U
U/MUR/LWAL/MUR/LN/EW/FW/HBET:20;3/IRVP+SOS	URM3M_D
U/MUR/LWAL/MUR/LN/EW/FW/HBET:2;1/IR99	URM5L
U/MUR/LWAL/MUR/LN/EW/FW/HBET:2;1/IRVP+DIB	URM3M_D
U/MUR/LWAL/MUR/LN/EW/FW/HBET:2;1/IRVP+OPL	URM5L
U/MUR/LWAL/MUR/LN/EW/FW/HBET:2;1/IRVP+SOS	URM5L
U/MUR/LWAL/MUR/LN/EWN/FW/H99/IR99	URM2L
U/MUR/LWAL/MUR/LN/EWN/FW/H99/IRVP+OPL	URM3M_U
U/MUR/LWAL/MUR/LN/EWN/FW/HBET:20;3/IR99	URM3M_U
U/MUR/LWAL/MUR/LN/EWN/FW/HBET:20;3/IRVP+DIB	URM3M_D
U/MUR/LWAL/MUR/LN/EWN/FW/HBET:20;3/IRVP+OPL	URM3M_U
U/MUR/LWAL/MUR/LN/EWN/FW/HBET:20;3/IRVP+SOS	URM3M_D
U/MUR/LWAL/MUR/LN/EWN/FW/HBET:2;1/IR99	URM2L
U/MUR/LWAL/MUR/LN/EWN/FW/HBET:2;1/IRVP+DIB	URM3M_D
U/MUR/LWAL/MUR/LN/EWN/FW/HBET:2;1/IRVP+OPL	URM2L
U/MUR/LWAL/MUR/LN/EWN/FW/HBET:2;1/IRVP+SOS	URM2L
U/MUR/LWAL/MUR/LWAL/EW/FC/H99/IR99	URM7L
U/MUR/LWAL/MUR/LWAL/EW/FC/H99/IRVP+OPL	URM7L
U/MUR/LWAL/MUR/LWAL/EW/FC/HBET:20;3/IR99	URM3M_U
U/MUR/LWAL/MUR/LWAL/EW/FC/HBET:20;3/IRVP+DIB	URM3M_D
U/MUR/LWAL/MUR/LWAL/EW/FC/HBET:20;3/IRVP+OPL	URM3M_D
U/MUR/LWAL/MUR/LWAL/EW/FC/HBET:20;3/IRVP+SOS	URM3M_D
U/MUR/LWAL/MUR/LWAL/EW/FC/HBET:2;1/IR99	URM7L
U/MUR/LWAL/MUR/LWAL/EW/FC/HBET:2;1/IRVP+DIB	URM3M_D
U/MUR/LWAL/MUR/LWAL/EW/FC/HBET:2;1/IRVP+OPL	URM4L
U/MUR/LWAL/MUR/LWAL/EW/FC/HBET:2;1/IRVP+SOS	URM7L
U/MUR/LWAL/MUR/LWAL/EW/FM/H99/IR99	URM7L
U/MUR/LWAL/MUR/LWAL/EW/FM/HBET:20;3/IR99	URM3M_U
U/MUR/LWAL/MUR/LWAL/EW/FM/HBET:20;3/IRVP+DIB	URM3M_D
U/MUR/LWAL/MUR/LWAL/EW/FM/HBET:2;1/IR99	URM7L
U/MUR/LWAL/MUR/LWAL/EW/FM/HBET:2;1/IRVP+DIB	URM3M_D
U/MUR/LWAL/MUR/LWAL/EW/FM/HBET:2;1/IRVP+OPL	URM4L
U/MUR/LWAL/MUR/LWAL/EW/FM/HBET:2;1/IRVP+SOS	URM7L

Table B.4 Mapping Table from Structural System to Vulnerability Class (cont.)

Structural System	Vulnerability Class
U/MUR/LWAL/MUR/LWAL/EW/FN/H99/IR99	URM7L
U/MUR/LWAL/MUR/LWAL/EW/FN/HBET:20;1/IR99	URM7L
U/MUR/LWAL/MUR/LWAL/EW/FN/HBET:2;1/IR99	URM7L
U/MUR/LWAL/MUR/LWAL/EW/FN/HBET:2;1/IRVP+SOS	URM7L
U/MUR/LWAL/MUR/LWAL/EW/FO/HBET:20;3/IR99	URM7L
U/MUR/LWAL/MUR/LWAL/EW/FO/HBET:2;1/IR99	URM7L
U/MUR/LWAL/MUR/LWAL/EW/FO/HBET:2;1/IRVP+OPL	URM7L
U/MUR/LWAL/MUR/LWAL/EW/FW/H99/IR99	URM8L
U/MUR/LWAL/MUR/LWAL/EW/FW/HBET:20;3/IR99	URM3M_U
U/MUR/LWAL/MUR/LWAL/EW/FW/HBET:20;3/IRVP+DIB	URM3M_D
U/MUR/LWAL/MUR/LWAL/EW/FW/HBET:20;3/IRVP+SOS	URM3M_D
U/MUR/LWAL/MUR/LWAL/EW/FW/HBET:2;1/IR99	URM8L
U/MUR/LWAL/MUR/LWAL/EW/FW/HBET:2;1/IRVP+DIB	URM3M_D
U/MUR/LWAL/MUR/LWAL/EW/FW/HBET:2;1/IRVP+OPL	URM8L
U/MUR/LWAL/MUR/LWAL/EW/FW/HBET:2;1/IRVP+SOS	URM8L
U/MUR/LWAL/MUR/LWAL/EWN/FC/H99/IR99	URM3M_U
U/MUR/LWAL/MUR/LWAL/EWN/FC/HBET:20;3/IR99	URM3M_U
U/MUR/LWAL/MUR/LWAL/EWN/FC/HBET:2;1/IR99	URM6L
U/MUR/LWAL/MUR/LWAL/EWN/FN/HBET:2;1/IR99	URM6L
U/MUR/LWAL/MUR/LWAL/EWN/FO/HBET:2;1/IR99	URM6L
U/MUR/LWAL/MUR/LWAL/EWN/FO/HBET:2;1/IRVP+SOS	URM6L
U/MUR/LWAL/MUR/LWAL/EWN/FW/H99/IR99	URM6L
U/MUR/LWAL/MUR/LWAL/EWN/FW/HBET:20;3/IR99	URM3M_U
U/MUR/LWAL/MUR/LWAL/EWN/FW/HBET:20;3/IRVP+DIB	URM3M_D
U/MUR/LWAL/MUR/LWAL/EWN/FW/HBET:20;3/IRVP+OPL	URM3M_D
U/MUR/LWAL/MUR/LWAL/EWN/FW/HBET:20;3/IRVP+SOS	URM3M_D
U/MUR/LWAL/MUR/LWAL/EWN/FW/HBET:2;1/IR99	URM6L
U/MUR/LWAL/MUR/LWAL/EWN/FW/HBET:2;1/IRVP+DIB	URM3M_D
U/MUR/LWAL/MUR/LWAL/EWN/FW/HBET:2;1/IRVP+OPL	URM6L
U/MUR/LWAL/MUR/LWAL/EWN/FW/HBET:2;1/IRVP+SOS	URM6L
U/MUR/LWAL/S/LFM/EW/FW/HBET:2;1/IR99	URM9L
U/S/LFBR/S/LFBR/EW/FC/H99/IR99	S2L
U/S/LFBR/S/LFBR/EW/FC/HBET:20;3/IR99	S2M
U/S/LFBR/S/LFBR/EW/FC/HBET:2;1/IR99	S2L
U/S/LFBR/S/LN/EWN/FN/HBET:2;1/IR99	S2L
U/S/LFM/S/LFBR/EW/FN/HBET:2;1/IR99	S2L
U/S/LFM/S/LFM/EW/FC/HBET:2;1/IR99	S1L
U/S/LFM/S/LN/EW/FW/HBET:2;1/IR99	S1L
U/S/LH/MUR/LWAL/EWN/FO/HBET:2;1/IR99	S1L
U/S/LPB/S/LFBR/EW/FN/HBET:2;1/IR99	S3
U/S/LPB/S/LN/EW/FN/HBET:2;1/IR99	S3
U/S/LPB/S/LPB/EW/FC/HBET:2;1/IR99	S3
U/W/LFBR/W/LFBR/EWN/FW/HBET:2;1/IR99	W2
U/W/LFM/W/LN/EWN/FW/HBET:2;1/IR99	URM1F_B
U/W/LH/W/LH/EW/FC/HBET:2;1/IR99	W3
U/W/LH/W/LH/EW/FN/HBET:2;1/IR99	W3
U/W/LH/W/LH/EW/FW/HBET:20;3/IR99	W3
U/W/LH/W/LH/EW/FW/HBET:2;1/IR99	W3
U/W/LH/W/LH/EWN/FW/HBET:2;1/IR99	W3
U/W/LPB/W/LPB/EW/FW/HBET:2;1/IR99	URM1F_B
U/W/LWAL/W/LN/EW/FW/H99/IR99	W3
U/W/LWAL/W/LN/EW/FW/HBET:20;3/IR99	W3
U/W/LWAL/W/LN/EW/FW/HBET:20;3/IRVP+DIB	W3
U/W/LWAL/W/LN/EW/FW/HBET:2;1/IR99	W3
U/W/LWAL/W/LN/EW/FW/HBET:2;1/IRVP+DIB	W3
U/W/LWAL/W/LN/EW/FW/HBET:2;1/IRVP+OPL	W3
U/W/LWAL/W/LWAL/EW/FC/HBET:2;1/IR99	W3
U/W/LWAL/W/LWAL/EW/FN/HBET:2;1/IR99	W3
U/W/LWAL/W/LWAL/EW/FO/HBET:2;1/IR99	W3
U/W/LWAL/W/LWAL/EW/FW/H99/IR99	W3
U/W/LWAL/W/LWAL/EW/FW/HBET:20;3/IR99	W3
U/W/LWAL/W/LWAL/EW/FW/HBET:20;3/IRVP+DIB	W3
U/W/LWAL/W/LWAL/EW/FW/HBET:2;1/IR99	W3
U/W/LWAL/W/LWAL/EW/FW/HBET:2;1/IRVP+DIB	W3
U/W/LWAL/W/LWAL/EW/FW/HBET:2;1/IRVP+OPL	W3
U/W/LWAL/W/LWAL/EW/FW/HBET:2;1/IRVP+SOS	W3
U/W/LWAL/W/LWAL/EWN/FW/HBET:20;3/IR99	W3
U/W/LWAL/W/LWAL/EWN/FW/HBET:2;1/IR99	W3
WA/CR+CIP/LWAL/CR+CIP/LWAL/EW/FC/HBET:20;1/IR99	URM1F_HA
WA/MUR/LH/MUR/LH/EW/FC/H99/IR99	URM1F_HA
WA/MUR/LH/MUR/LH/EW/FC/HBET:20;1/IR99	URM1F_HA
WA/MUR/LH/MUR/LH/EW/FC/HBET:20;1/IRVP+SOS	URM1F_HA
WA/MUR/LH/MUR/LH/EW/FM/HBET:20;1/IR99	URM1F_HA
WA/MUR/LH/MUR/LH/EW/FM/HBET:20;1/IRVP+SOS	URM1F_HA
WA/MUR/LH/MUR/LH/EW/FN/HBET:20;1/IR99	URM1F_HA
WA/MUR/LH/MUR/LH/EW/FW/H99/IR99	URM1F_HA
WA/MUR/LH/MUR/LH/EW/FW/HBET:20;1/IR99	URM1F_HA
WA/MUR/LH/MUR/LH/EW/FW/HBET:20;1/IRVP+SOS	URM1F_HA
WA/MUR/LH/MUR/LH/EWN/FC/HBET:20;1/IR99	URM1F_HA
WA/MUR/LH/MUR/LH/EWN/FW/H99/IR99	URM1F_HA
WA/MUR/LH/MUR/LH/EWN/FW/HBET:20;1/IR99	URM1F_HA
WA/MUR/LH/MUR/LH/EWN/FW/HBET:20;1/IRVP+SOS	URM1F_HA
WA/MUR/LH/MUR/LWAL/EWN/FW/HBET:20;1/IR99	URM1F_HA
WA/MUR/LWAL/MUR/LWAL/EW/FC/H99/IR99	URM1F_HA
WA/MUR/LWAL/MUR/LWAL/EW/FC/HBET:20;1/IR99	URM1F_HA
WA/MUR/LWAL/MUR/LWAL/EW/FC/HBET:20;1/IRVP+SOS	URM1F_HA
WA/MUR/LWAL/MUR/LWAL/EW/FN/HBET:20;1/IR99	URM1F_HA

Table B.5 Mapping Table from Structural System to Vulnerability Class (cont.)

Structural System	Vunerability Class
WA/MUR/LWAL/MUR/LWAL/EW/FO/HBET:20;1/IR99	URM1F_HA
WA/MUR/LWAL/MUR/LWAL/EW/FW/HBET:20;1/IR99	URM1F_HA
WA/MUR/LWAL/MUR/LWAL/EW/FW/HBET:20;1/IRVP+SOS	URM1F_HA
WA/MUR/LWAL/MUR/LWAL/EWN/FC/HBET:20;1/IR99	URM1F_HA
WA/MUR/LWAL/MUR/LWAL/EWN/FM/HBET:20;1/IR99	URM1F_HA
WA/MUR/LWAL/MUR/LWAL/EWN/FO/HBET:20;1/IR99	URM1F_HA
WA/MUR/LWAL/MUR/LWAL/EWN/FW/H99/IR99	URM1F_HA
WA/MUR/LWAL/MUR/LWAL/EWN/FW/HBET:20;1/IR99	URM1F_HA
WA/MUR/LWAL/MUR/LWAL/EWN/FW/HBET:20;1/IRVP+SOS	URM1F_HA
WA/S/LFM/S/LFBR/EWN/FW/H99/IR99	URM1F_HA
WA/S/LFM/S/LFBR/EWN/FW/HBET:20;1/IR99	URM1F_HA
WA/S/LPB/S/LPB/EW/FW/HBET:20;1/IR99	URM1F_HA
WA/W/LH/W/LH/EW/FC/HBET:20;1/IR99	URM1F_HA
WA/W/LH/W/LH/EW/FW/HBET:20;1/IR99	URM1F_HA
WA/W/LPB/W/LPB/EW/FM/HBET:20;1/IR99	URM1F_HA
WA/W/LPB/W/LPB/EW/FN/HBET:20;1/IR99	URM1F_HA
WA/W/LPB/W/LPB/EW/FW/HBET:20;1/IR99	URM1F_HA
WC/CR+CIP/LWAL/CR+CIP/LWAL/EW/FC/HBET:20;1/IR99	URM1F_HC
WC/MUR/LH/MUR/LH/EW/FC/H99/IR99	URM1F_HC
WC/MUR/LH/MUR/LH/EW/FC/HBET:20;1/IR99	URM1F_HC
WC/MUR/LH/MUR/LH/EW/FC/HBET:20;1/IRVP+SOS	URM1F_HC
WC/MUR/LH/MUR/LH/EW/FM/HBET:20;1/IR99	URM1F_HC
WC/MUR/LH/MUR/LH/EW/FM/HBET:20;1/IRVP+SOS	URM1F_HC
WC/MUR/LH/MUR/LH/EW/FN/HBET:20;1/IR99	URM1F_HC
WC/MUR/LH/MUR/LH/EW/FW/H99/IR99	URM1F_HC
WC/MUR/LH/MUR/LH/EW/FW/HBET:20;1/IR99	URM1F_HC
WC/MUR/LH/MUR/LH/EW/FW/HBET:20;1/IRVP+SOS	URM1F_HC
WC/MUR/LH/MUR/LH/EWN/FC/HBET:20;1/IR99	URM1F_HC
WC/MUR/LH/MUR/LH/EWN/FW/H99/IR99	URM1F_HC
WC/MUR/LH/MUR/LH/EWN/FW/HBET:20;1/IR99	URM1F_HC
WC/MUR/LH/MUR/LWAL/EWN/FW/HBET:20;1/IR99	URM1F_HC
WC/MUR/LWAL/MUR/LWAL/EW/FC/H99/IR99	URM1F_HC
WC/MUR/LWAL/MUR/LWAL/EW/FC/HBET:20;1/IR99	URM1F_HC
WC/MUR/LWAL/MUR/LWAL/EW/FC/HBET:20;1/IRVP+SOS	URM1F_HC
WC/MUR/LWAL/MUR/LWAL/EW/FN/HBET:20;1/IR99	URM1F_HC
WC/MUR/LWAL/MUR/LWAL/EW/FO/HBET:20;1/IR99	URM1F_HC
WC/MUR/LWAL/MUR/LWAL/EW/FO/HBET:20;1/IRVP+SOS	URM1F_HC
WC/MUR/LWAL/MUR/LWAL/EW/FW/HBET:20;1/IR99	URM1F_HC
WC/MUR/LWAL/MUR/LWAL/EW/FW/HBET:20;1/IRVP+SOS	URM1F_HC
WC/MUR/LWAL/MUR/LWAL/EWN/FC/HBET:20;1/IR99	URM1F_HC
WC/MUR/LWAL/MUR/LWAL/EWN/FM/HBET:20;1/IR99	URM1F_HC
WC/MUR/LWAL/MUR/LWAL/EWN/FO/HBET:20;1/IR99	URM1F_HC
WC/MUR/LWAL/MUR/LWAL/EWN/FW/H99/IR99	URM1F_HC
WC/MUR/LWAL/MUR/LWAL/EWN/FW/HBET:20;1/IR99	URM1F_HC
W/CR+CIP/LFM/CR+CIP/LFM/EW/FM/HBET:20;1/IR99	RC1L
W/CR+CIP/LFM/CR+CIP/LH/EW/FW/HBET:20;1/IR99	RC1L
W/CR+CIP/LH/CR+CIP/LH/EW/FC/HBET:20;1/IR99	RC3L
W/CR+CIP/LH/CR+CIP/LH/EW/FC/HBET:20;1/IRVP+SOS	RC3L
W/CR+CIP/LPB/CR+CIP/LPB/EW/FN/H99/IR99	RC2
W/CR+CIP/LPB/CR+CIP/LPB/EW/FN/HBET:20;1/IR99	RC2
W/CR+CIP/LWAL/CR+CIP/LWAL/EW/FC/HBET:20;1/IR99	RC3L
W/CR+CIP/LWAL/CR+CIP/LWAL/EW/FC/HBET:20;1/IRVP+SOS	RC3L
W/CR+PC/LH/CR+PC/LH/EWN/FO/HBET:20;1/IR99	PC2
W/CR+PC/LPB/CR+PC/LPB/EW/FN/H99/IR99	PC2
W/CR+PC/LPB/CR+PC/LPB/EW/FN/HBET:20;1/IR99	PC2
W/CR+PC/LWAL/CR+PC/LWAL/EW/FN/H99/IR99	PC3L
W/CR+PC/LWAL/CR+PC/LWAL/EW/FN/HBET:20;1/IR99	PC3L
WC/S/LFM/S/LFBR/EWN/FW/H99/IR99	URM1F_HC
WC/S/LFM/S/LFBR/EWN/FW/HBET:20;1/IR99	URM1F_HC
WC/S/LPB/S/LPB/EW/FW/HBET:20;1/IR99	URM1F_HC
WC/W/LH/W/LH/EW/FC/HBET:20;1/IR99	URM1F_HC
WC/W/LH/W/LH/EW/FW/HBET:20;1/IR99	URM1F_HC
WC/W/LPB/W/LPB/EW/FM/HBET:20;1/IR99	URM1F_HC
WC/W/LPB/W/LPB/EW/FN/HBET:20;1/IR99	URM1F_HC
WC/W/LPB/W/LPB/EW/FW/HBET:20;1/IR99	URM1F_HC
W/MUR/LFBR/MUR/LFBR/EWN/FO/HBET:20;1/IR99	URM9L
W/MUR/LH/MUR/LH/EW/FC/H99/IR99	URM9L
W/MUR/LH/MUR/LH/EW/FC/HBET:20;1/IR99	URM9L
W/MUR/LH/MUR/LH/EW/FC/HBET:20;1/IRVP+SOS	URM9L
W/MUR/LH/MUR/LH/EW/FN/H99/IR99	URM9L
W/MUR/LH/MUR/LH/EW/FN/HBET:20;1/IR99	URM9L
W/MUR/LH/MUR/LH/EW/FN/HBET:20;1/IRVP+SOS	URM9L
W/MUR/LH/MUR/LH/EW/FW/H99/IR99	URM9L
W/MUR/LH/MUR/LH/EW/FW/HBET:20;1/IR99	URM9L
W/MUR/LH/MUR/LH/EW/FW/HBET:20;1/IRVP+SOS	URM9L
W/MUR/LH/MUR/LH/EWN/FW/H99/IR99	URM9L
W/MUR/LH/MUR/LH/EWN/FW/HBET:20;1/IR99	URM9L
W/MUR/LH/MUR/LWAL/EW/FW/HBET:20;1/IR99	URM5L
W/MUR/LH/MUR/LWAL/EW/FW/HBET:20;1/IRVP+SOS	URM5L
W/MUR/LWAL/MUR/LN/EW/FC/HBET:20;1/IR99	URM3L
W/MUR/LWAL/MUR/LN/EW/FC/HBET:20;1/IRVP+SOS	URM4L
W/MUR/LWAL/MUR/LN/EW/FN/HBET:20;1/IR99	URM5L
W/MUR/LWAL/MUR/LWAL/EW/FC/H99/IR99	URM7L
W/MUR/LWAL/MUR/LWAL/EW/FC/HBET:20;1/IR99	URM7L
W/MUR/LWAL/MUR/LWAL/EW/FC/HBET:20;1/IRVP+SOS	URM7L
W/MUR/LWAL/MUR/LWAL/EW/FN/H99/IR99	URM8L
W/MUR/LWAL/MUR/LWAL/EW/FN/HBET:20;1/IR99	URM9L

Table B.6 Mapping Table from Structural System to Vulnerability Class (cont.)

Structural System	Vunerability Class
W/MUR/LWAL/MUR/LWAL/EW/FN/HBET:20;1/IRVP+SOS	URM8L
W/MUR/LWAL/MUR/LWAL/EW/FW/H99/IR99	URM8L
W/MUR/LWAL/MUR/LWAL/EW/FW/HBET:20;1/IR99	URM8L
W/MUR/LWAL/MUR/LWAL/EW/FW/HBET:20;1/IRVP+SOS	URM8L
W/MUR/LWAL/MUR/LWAL/EWN/FN/H99/IR99	URM6L
W/MUR/LWAL/MUR/LWAL/EWN/FN/HBET:20;1/IR99	URM9L
W/MUR/LWAL/MUR/LWAL/EWN/FN/HBET:20;1/IRVP+SOS	URM6L
W/MUR/LWAL/MUR/LWAL/EWN/FW/H99/IR99	URM6L
W/MUR/LWAL/MUR/LWAL/EWN/FW/HBET:20;1/IR99	URM6L
W/MUR/LWAL/MUR/LWAL/EWN/FW/HBET:20;1/IRVP+SOS	URM6L
W/S/LFBR/S/LFBR/EW/FC/H99/IR99	S2L
W/S/LFBR/S/LFBR/EW/FC/HBET:20;1/IR99	S2L
W/S/LFBR/S/LFBR/EW/FC/HBET:20;1/IRVP+SOS	S2L
W/S/LFBR/S/LFBR/EW/FN/H99/IR99	S2L
W/S/LFBR/S/LFBR/EW/FN/HBET:20;1/IR99	S2L
W/S/LFBR/S/LFBR/EW/FN/HBET:20;1/IRVP+SOS	S2L
W/S/LFBR/S/LFBR/EWN/FN/HBET:20;1/IR99	S2L
W/S/LFBR/S/LFBR/EWN/FN/HBET:20;1/IRVP+SOS	S2L
W/S/LFBR/S/LFM/EWN/FN/HBET:20;1/IR99	S2L
W/S/LFBR/S/LFM/EWN/FN/HBET:20;1/IRVP+SOS	S2L
W/S/LFBR/S/LN/EW/FN/HBET:20;1/IR99	S2L
W/S/LFBR/S/LN/EW/FN/HBET:20;1/IRVP+SOS	S2L
W/S/LFM/S/LFBR/EW/FN/HBET:20;1/IR99	S1L
W/S/LFM/S/LFBR/EW/FN/HBET:20;1/IRVP+SOS	S2L
W/S/LFM/S/LFBR/EWN/FN/H99/IR99	S2L
W/S/LFM/S/LFBR/EWN/FN/HBET:20;1/IR99	S2L
W/S/LFM/S/LFBR/EWN/FN/HBET:20;1/IRVP+SOS	S2L
W/S/LFM/S/LFM/EW/FW/HBET:20;1/IR99	S1L
W/S/LFM/S/LFM/EW/FW/HBET:20;1/IRVP+SOS	S1L
W/S/LFM/S/LFM/EWN/FN/H99/IR99	S1L
W/S/LFM/S/LFM/EWN/FN/HBET:20;1/IR99	S1L
W/S/LFM/S/LFM/EWN/FN/HBET:20;1/IRVP+SOS	S1L
W/S/LFM/S/LN/EW/FN/H99/IR99	S1L
W/S/LFM/S/LN/EW/FN/HBET:20;1/IR99	S1L
W/S/LFM/S/LN/EW/FN/HBET:20;1/IRVP+SOS	S1L
W/S/LFM/S/LN/EWN/FN/H99/IR99	S1L
W/S/LFM/S/LN/EWN/FN/HBET:20;1/IR99	S1L
W/S/LFM/S/LN/EWN/FN/HBET:20;1/IRVP+SOS	S1L
W/S/LPB/S/LFBR/EW/FN/H99/IR99	S3
W/S/LPB/S/LFBR/EW/FN/HBET:20;1/IR99	S3
W/S/LPB/S/LFBR/EW/FN/HBET:20;1/IRVP+SOS	S3
W/S/LPB/S/LN/EW/FN/HBET:20;1/IR99	S3
W/S/LPB/S/LPB/EW/FN/H99/IR99	S3
W/S/LPB/S/LPB/EW/FN/HBET:20;1/IR99	S3
W/S/LPB/S/LPB/EW/FN/HBET:20;1/IRVP+SOS	S3
W/S/LPB/S/LPB/EW/FW/HBET:20;1/IR99	S3
W/S/LPB/S/LPB/EW/FW/HBET:20;1/IRVP+SOS	S3
W/S/LPB/S/LPB/EWN/FME/HBET:20;1/IR99	S3
W/S/LPB/S/LPB/EWN/FME/HBET:20;1/IRVP+SOS	S3
W/W/LH/W/LH/EW/FN/HBET:20;1/IR99	W3
W/W/LPB/MUR/LWAL/EW/FN/H99/IR99	W2
W/W/LPB/MUR/LWAL/EW/FN/HBET:20;1/IR99	W2
W/W/LPB/S/LFBR/EW/FN/H99/IR99	W2
W/W/LPB/S/LFBR/EW/FN/HBET:20;1/IR99	W2
W/W/LPB/W/LPB/EW/FN/H99/IR99	URM1F_B
W/W/LPB/W/LPB/EW/FN/HBET:20;1/IR99	URM1F_B
W/W/LPB/W/LPB/EW/FW/HBET:20;1/IR99	URM1F_B
W/W/LWAL/W/LWAL/EW/FN/HBET:20;1/IR99	W3
W/W/LWAL/W/LWAL/EWN/FN/HBET:20;1/IR99	W3
W/W/LWAL/W/LWAL/EWN/FW/HBET:20;1/IR99	W3
WA/BARN	URM1F_B
WC/BARN	URM1F_B

Appendix C

Structural Fragility Functions

The following plots illustrate the damage and collapse state fragility functions for all 35 vulnerability classes considered in the HRA2020 analyses.

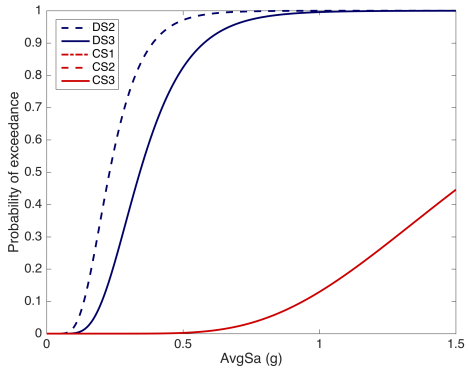

(a) RC1L

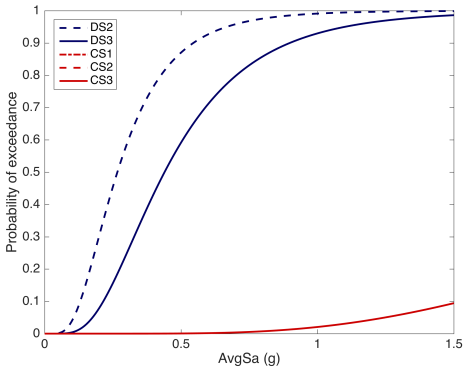

(b) RC1M

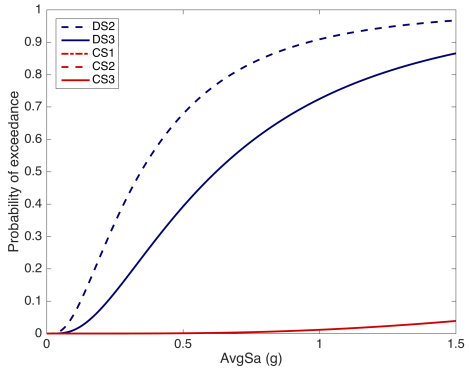

(c) RC1H

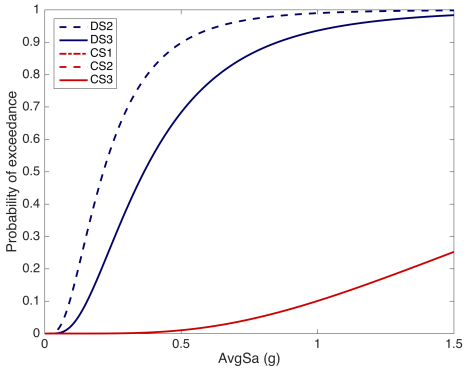

(d) RC2

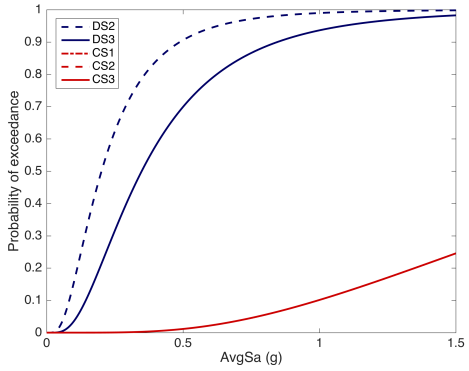

(e) PC2

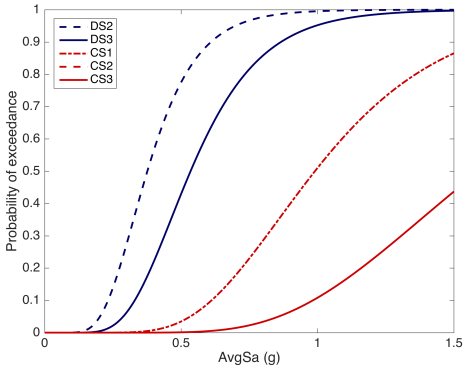

(f) RC3L

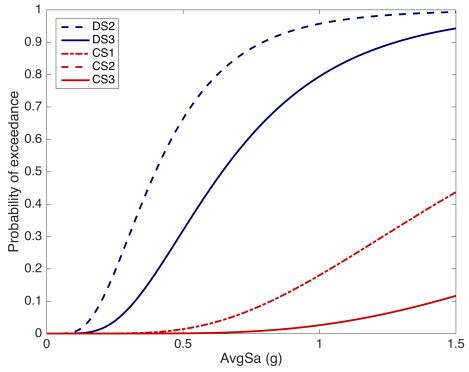

(g) RC3M

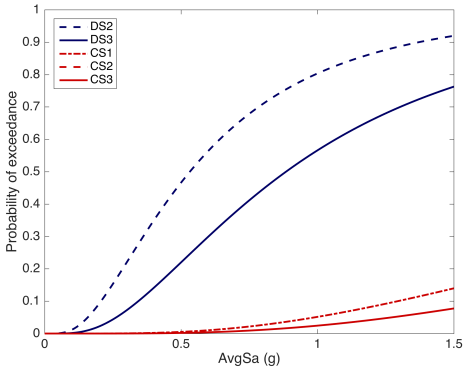

(h) RC3H

Figure C.1 Fragility functions for each vulnerability class

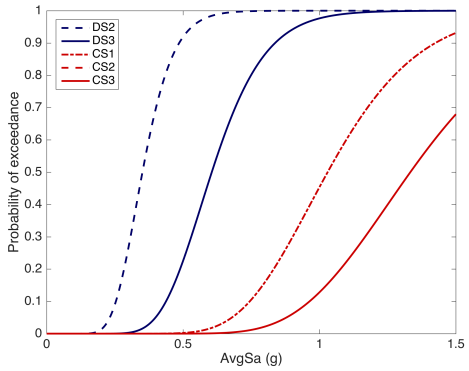

(a) PC3L

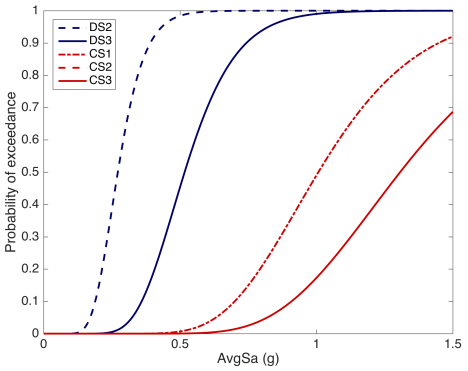

(b) PC3M

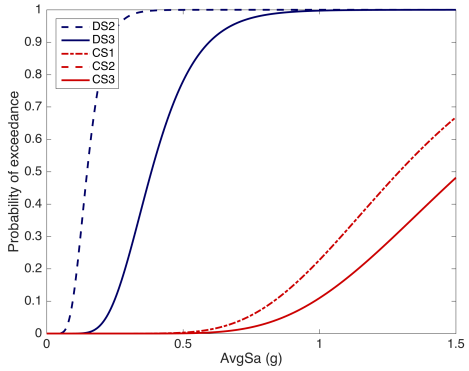

(c) PC3H

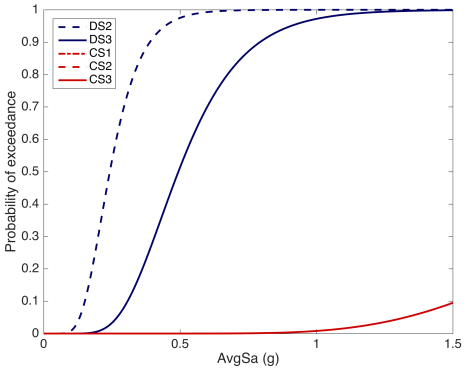

(d) W2

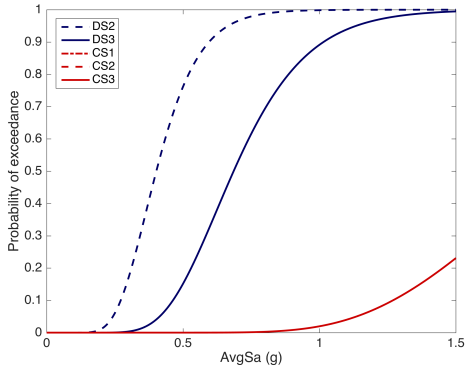

(e) W3

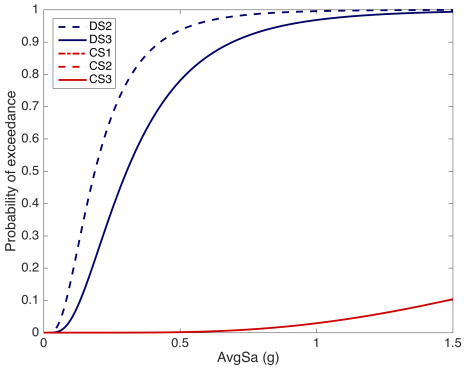

(f) S1L

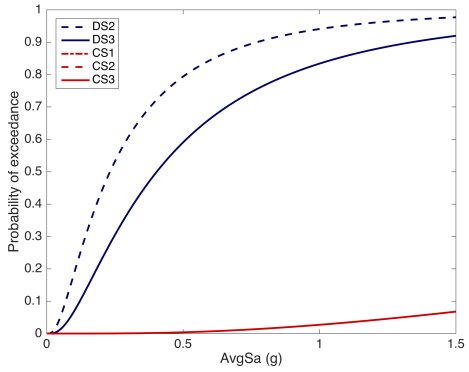

(g) S1M

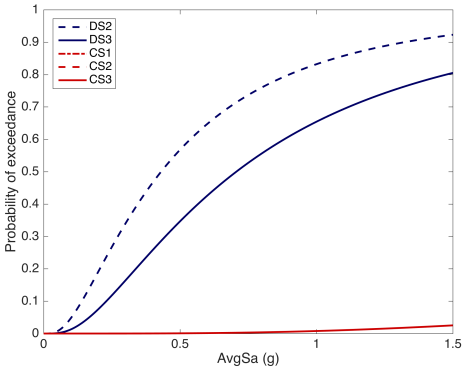

(h) S1H

Figure C.2 Fragility functions for each vulnerability class (cont.)

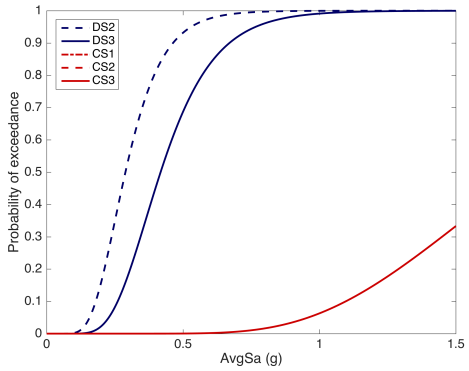

(a) S2L

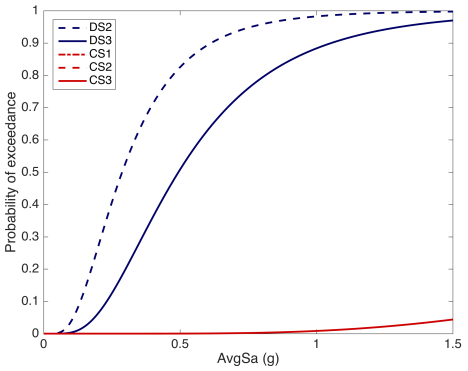

(b) S2M

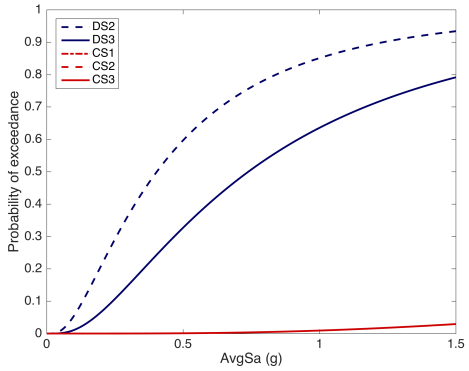

(c) S2H

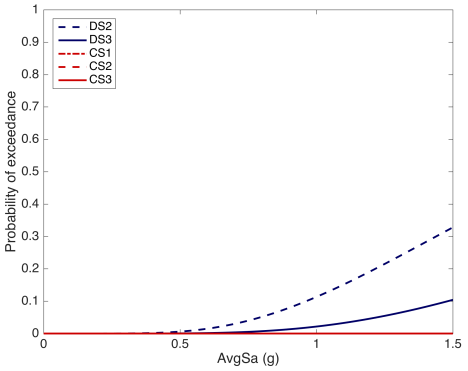

(d) S3

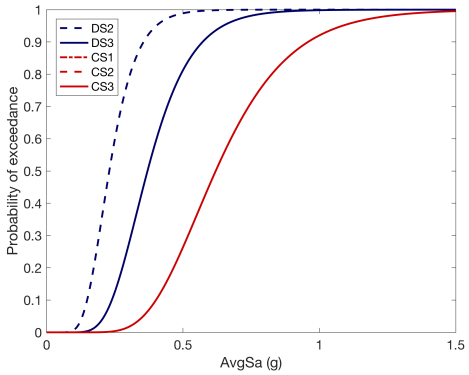

(e) URM1F_B

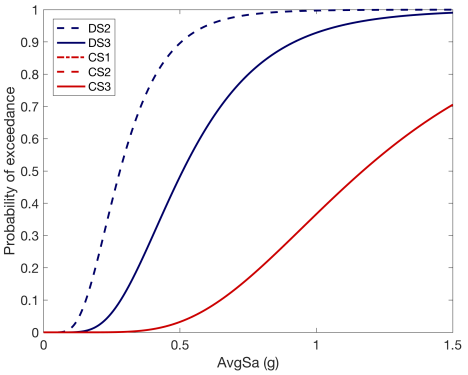

(f) URM1F_HC

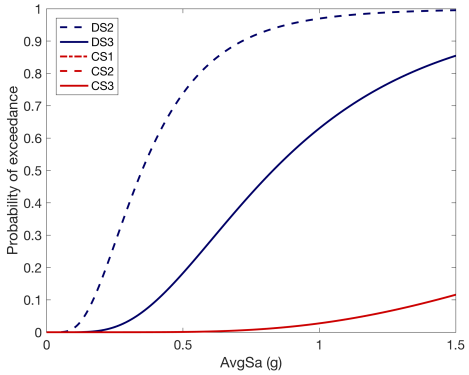

(g) URM1F_HA

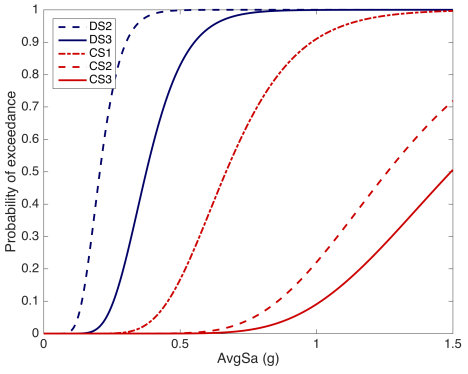

(h) URM2L

Figure C.3 Fragility functions for each vulnerability class (cont.)

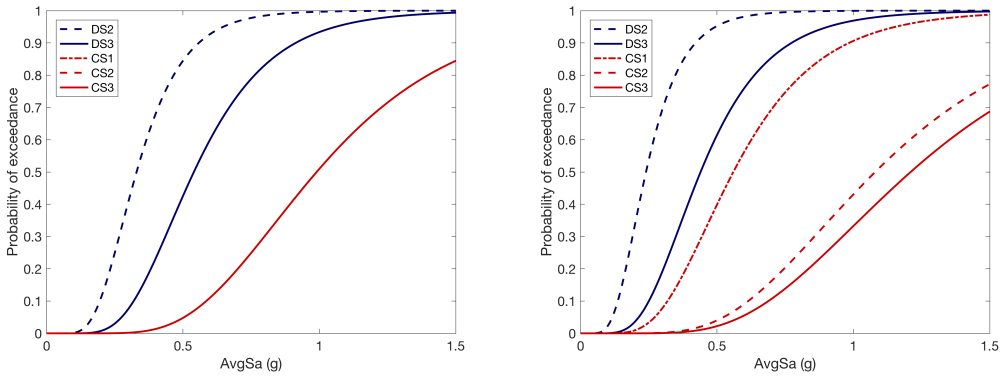

(a) URM3L

(b) URM3M_U

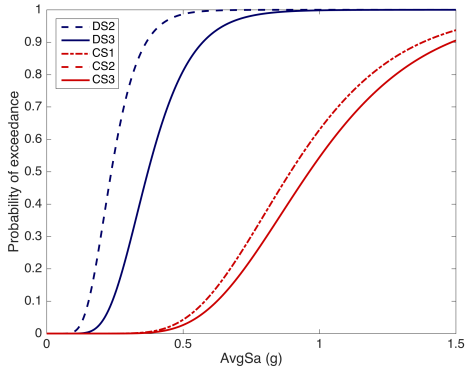

(c) URM3M_D

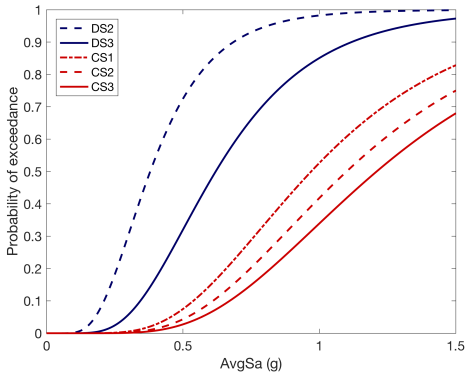

(d) URM3M_B

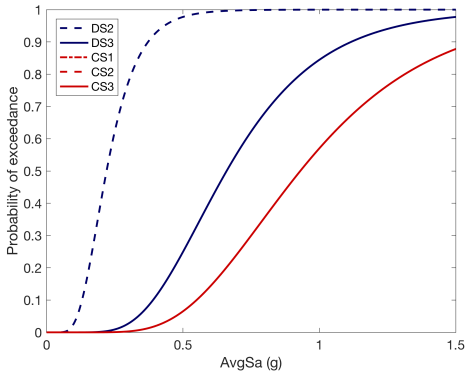

(e) URM4L

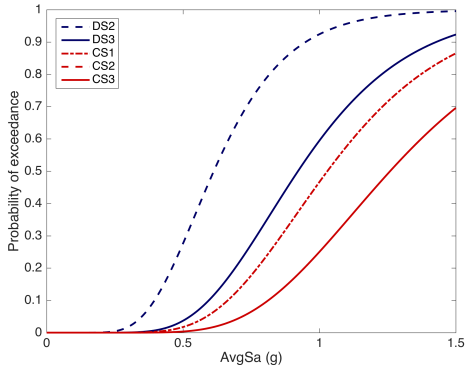

(f) URM5L

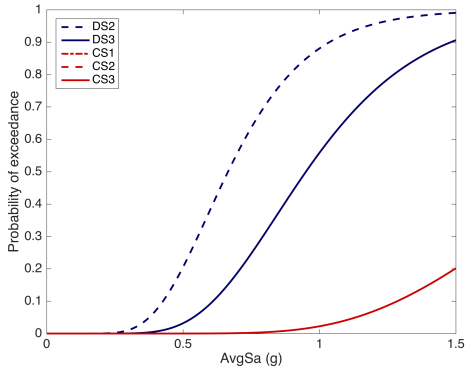

(g) URM6L and URM10L

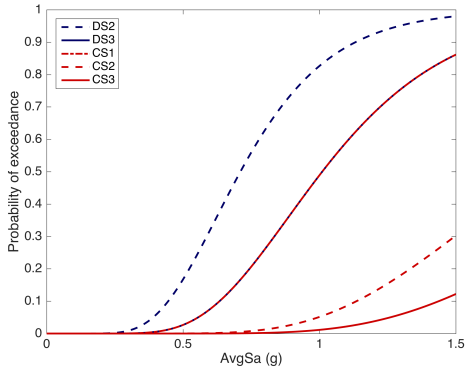

(h) URM7L

Figure C.4 Fragility functions for each vulnerability class (cont.)

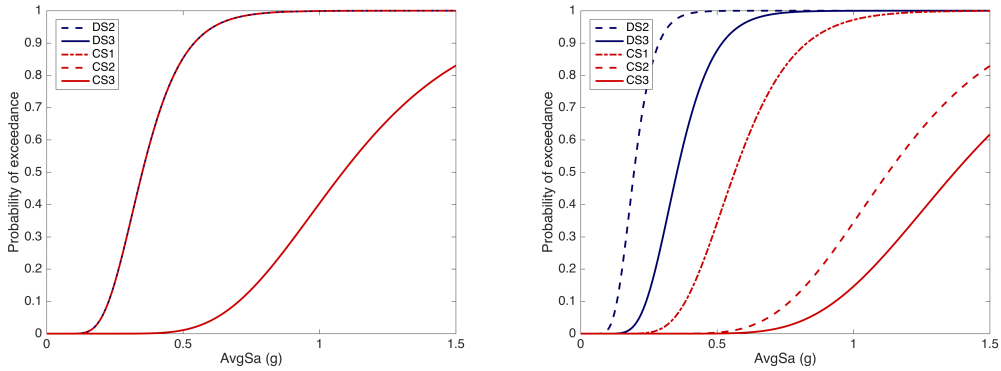

(a) URM8L **(b)** URM9L

Figure C.5 Fragility functions for each vulnerability class (cont.)